

Computational Mathematics and Information Technologies

Computational
Mathematics

Mathematical
Modelling

Information
Technologies





Computational Mathematics and Information Technologies

Peer-reviewed scientific and theoretical journal

eISSN 2587–8999

Published since 2017

Periodicity — 4 issues per year

DOI: 10.23947/2587–8999

Founder and Publisher — Don State Technical University (DSTU), Rostov-on-Don, Russian Federation

The journal “Computational Mathematics and Information Technologies” publishes reviews, original articles and short reports on mathematical modeling, numerical methods and information technologies for solving complex and topical problems of science and modern technology. Research areas include continuum mechanics, fluid dynamics, Earth sciences, chemistry, biology, image processing and pattern recognition, parallel computing theory and its applications, big database and artificial intelligence technologies, etc.

The journal “Computational Mathematics and Information Technologies” accepts scientific and review articles for publication in accordance with the sections:

1. Computational Mathematics
2. Mathematical Modelling
3. Information Technologies

Registration: Mass media registration certificate ЭЛ № ФС 77–66529 dated July 21, 2016 issued by the Federal Service for Supervision of Communications, Information Technology and Mass Media

Indexing and Archiving: RISC, Crossref, Cyberleninka

Website: <https://cmit-journal.ru>

Address of the Editorial Office: 1, Gagarin sq., Rostov-on-Don, 344003, Russian Federation

E-mail: CMIT-EJ@yandex.ru

Telephone: +7 (863) 273–85–14

Date of publication 31.03.2025

No. 1, 2025:





Computational Mathematics and Information Technologies

Рецензируемый научно-теоретический журнал

eISSN 2587–8999

Издается с 2017 года

Периодичность — 4 выпуска в год

DOI: 10.23947/2587–8999

Учредитель и издатель — Федеральное государственное бюджетное образовательное учреждение высшего образования «Донской государственный технический университет» (ДГТУ), г. Ростов-на-Дону, Российская Федерация

Журнал «Computational Mathematics and Information Technologies» публикует обзоры, оригинальные статьи и краткие сообщения, посвященные математическому моделированию, численным методам и информационным технологиям для решения сложных и актуальных проблем науки и современной технологии. Область применения исследований — это механика сплошных сред, гидроаэродинамика, науки о Земле, химия, биология, обработка изображений и распознавание образов, теория параллельных вычислений и ее приложения, технологии больших баз данных и искусственного интеллекта и т. д.

Журнал «Computational Mathematics and Information Technologies» принимает к публикации научные и обзорные статьи в соответствии с разделами:

1. Вычислительная математика
2. Математическое моделирование
3. Информационные технологии

<i>Регистрация:</i>	Свидетельство о регистрации средства массовой информации ЭЛ № ФС 77 – 66529 от 21 июля 2016 г., выдано Федеральной службой по надзору в сфере связи, информационных технологий и массовых коммуникаций
<i>Индексация и архивация:</i>	РИНЦ, CrossRef, CyberLeninka
<i>Сайт:</i>	https://cmit-journal.ru
<i>Адрес редакции:</i>	344003, Российская Федерация, г. Ростов-на-Дону, пл. Гагарина, 1
<i>E-mail:</i>	CMIT-EJ@yandex.ru
<i>Телефон:</i>	+7 (863) 273–85–14
<i>Дата выхода</i> <i>№ 1, 2025 в свет:</i>	31.03.2025



Editorial Board

Editor-in-Chief, Alexander I. Sukhinov, Corresponding member of RAS, Dr.Sci. (Phys.-Math.), Professor, Don State Technical University (Rostov-on-Don, Russian Federation), [Scopus](#), [ResearcherID](#), [MathSciNet](#), [SPIN-code](#), [ORCID](#), sukhinov@gmail.com, spu-40.4@donstu.ru

Deputy Chief Editor, Mikhail V. Yakobovski, Corresponding Member of RAS, Dr.Sci. (Phys.-Math.), Professor, Keldysh Institute of Applied Mathematics, Russian Academy of Sciences (Moscow, Russian Federation), [Scopus](#), [SPIN-code](#), [ORCID](#)

Executive Secretary, Alexander P. Petrov Dr.Sci. (Phys.-Math.), Leading Research Fellow, Institute of Control Sciences RAS (Moscow, Russian Federation), [Scopus](#), [ResearcherID](#), [SPIN-code](#), [ORCID](#), [Istina](#)

Elena V. Aleksenko, Ph.D., Candidate of Physical and Mathematical Sciences, Professor, University of Littoral Opal Coast (Boulogne-sur-Mer, France), [Scopus](#), [ResearcherID](#), [ORCID](#)

Vladimir V. Voevodin, Corresponding Member of RAS, Dr.Sci. (Phys.-Math.), Professor, Lomonosov Moscow State University (Moscow, Russian Federation), [Scopus](#), [ResearcherID](#), [ORCID](#)

Vladimir A. Gasilov, Dr.Sci. (Phys.-Math.), Professor, Keldysh Institute of Applied Mathematics, Russian Academy of Sciences (Moscow, Russian Federation), [Scopus](#), [ResearcherID](#), [SPIN-code](#), [ORCID](#)

Valentin A. Gushchin, Corresponding Member of RAS, Dr.Sci. (Phys.-Math.), Professor, Institute of Computer Aided Design, Russian Academy of Sciences (Moscow, Russian Federation), [Scopus](#), [SPIN-code](#), [ORCID](#)

Galina G. Lazareva, Corresponding member of RAS, Dr. Sci. (Phys.-Math), Professor of RAS, RUDN University, (Moscow, Russian Federation), [Scopus](#), [SPIN-code](#), [ORCID](#)

Igor B. Petrov, Corresponding Member of RAS, Dr.Sci. (Phys.-Math.), Professor, Moscow Institute of Physics and Technology (State University) (Moscow, Russian Federation), [Scopus](#), [SPIN-code](#)

Sergey V. Polyakov, Dr.Sci. (Phys.-Math.), Professor, Keldysh Institute of Applied Mathematics, Russian Academy of Sciences (Moscow, Russian Federation), [Scopus](#), [SPIN-code](#), [ORCID](#)

Vladimir F. Tishkin, Corresponding Member of RAS, Dr.Sci. (Phys.-Math.), Professor, Keldysh Institute of Applied Mathematics, Russian Academy of Sciences (Moscow, Russian Federation), [Scopus](#), [ResearcherID](#), [SPIN-code](#)

Boris N. Chetverushkin, Academician of RAS, Dr.Sci. (Phys.-Math.), Professor, Keldysh Institute of Applied Mathematics, Russian Academy of Sciences (Moscow, Russian Federation), [Scopus](#), [ResearcherID](#), [SPIN-code](#), [ORCID](#)

Konstantin A. Chekhonin, Dr.Sci. (Phys.-Math.), Associate Professor, Deputy Director of the Institute for Applied Mathematics, Director of the Khabarovsk Branch of the Institute for Applied Mathematics, Far Eastern Branch of the Russian Academy of Sciences (Khabarovsk, Russian Federation), [Scopus](#), [ResearcherID](#), [SPIN-code](#), [ORCID](#)

Alexander E. Chistyakov, Dr.Sci. (Phys.-Math.), Professor, Don State Technical University (Rostov-on-Don, Russian Federation), [Scopus](#), [ResearcherID](#), [SPIN-code](#), [ORCID](#)

Редакционная коллегия

Главный редактор, Сухинов Александр Иванович, член-корреспондент РАН, доктор физико-математических наук, профессор, Донской государственный технический университет (Ростов-на-Дону, Российская Федерация), [Scopus](#), [ResearcherID](#), [MathSciNet](#), [SPIN-код](#), [ORCID](#), sukhinov@gmail.com, spu-40.4@donstu.ru

Заместитель главного редактора, Якобовский Михаил Владимирович, член-корреспондент РАН, доктор физико-математических наук, профессор, Институт прикладной математики им. М.В. Келдыша РАН (Москва, Российская Федерация), [Scopus](#), [SPIN-код](#), [ORCID](#)

Ответственный секретарь, Петров Александр Пхоун Чжо, доктор физико-математических наук, главный научный сотрудник, Институт проблем управления им. В.А. Трапезникова РАН (Москва, Российская Федерация), [Scopus](#), [ResearcherID](#), [SPIN-код](#), [ORCID](#), [ИСТИНА](#)

Алексеев Елена В., кандидат физико-математических наук, PhD, профессор, Университет Литораль Кот д'Опаль, (Булонь-сюр-Мер, Франция), [Scopus](#), [ResearcherID](#), [ORCID](#)

Воеводин Владимир Валентинович, член-корреспондент РАН, доктор физико-математических наук, профессор, Московский государственный университет им. М.В. Ломоносова (Москва, Российская Федерация), [Scopus](#), [ResearcherID](#), [SPIN-код](#), [ORCID](#)

Гасилов Владимир Анатольевич, доктор физико-математических наук, профессор, Институт прикладной математики им. М.В. Келдыша РАН (Москва, Российская Федерация), [Scopus](#), [ResearcherID](#), [SPIN-код](#), [ORCID](#)

Гущин Валентин Анатольевич, член-корреспондент РАН, доктор физико-математических наук, профессор, Институт автоматизации проектирования РАН (Москва, Российская Федерация), [Scopus](#), [SPIN-код](#), [ORCID](#)

Лазарева Галина Геннадьевна, член-корреспондент РАН, доктор физико-математических наук, профессор РАН, Российский университет дружбы народов (Москва, Российская Федерация), [Scopus](#), [SPIN-код](#), [ORCID](#)

Петров Игорь Борисович, член-корреспондент РАН, доктор физико-математических наук, профессор, Московский физико-технический институт (государственный университет) (Москва, Российская Федерация), [Scopus](#), [SPIN-код](#)

Поляков Сергей Владимирович, доктор физико-математических наук, старший научный сотрудник, Институт прикладной математики им. М.В. Келдыша РАН (Москва, Российская Федерация), [Scopus](#), [SPIN-код](#), [ORCID](#)

Тишкин Владимир Федорович, член-корреспондент РАН, доктор физико-математических наук, профессор, Институт прикладной математики им. М.В. Келдыша РАН (Москва, Российская Федерация), [Scopus](#), [ResearcherID](#), [SPIN-код](#)

Четверушкин Борис Николаевич, академик РАН, доктор физико-математических наук, профессор, научный руководитель Института прикладной математики им. М.В. Келдыша РАН (Москва, Российская Федерация), [Scopus](#), [ResearcherID](#), [SPIN-код](#), [ORCID](#)

Чехонин Константин Александрович, доктор физико-математических наук, доцент, зам. директора Института прикладной математики ДВО РАН, руководитель (директор) Хабаровского отделения ИПМ ДВО РАН (Хабаровск, Российская Федерация), [Scopus](#), [ResearcherID](#), [SPIN-код](#), [ORCID](#)

Чистяков Александр Евгеньевич, доктор физико-математических наук, профессор, Донской государственный технический университет (Ростов-на-Дону, Российская Федерация), [Scopus](#), [ResearcherID](#), [SPIN-код](#), [ORCID](#)

Contents

COMPUTATIONAL MATHEMATICS

- Solution of Boundary Value Problems for Certain Nonlinear Differential Equations Using the Bubnov-Galerkin Method** 7
Natalya K. Volosova, Konstantin A. Volosov, Aleksandra K. Volosova, Mikhail I. Karlov, Dmitriy F. Pastukhov, Yuriy F. Pastukhov
- Sufficient Conditions for the Convergence of Solutions of the Linearized Problem to the Solution of the Original Nonlinear Problem of Multifractional Sediment Transport in Shallow Water** 20
Valentina V. Sidoryakina

MATHEMATICAL MODELLING

- Accuracy Assessment of Sentinel-3 Satellite Altimetry in the Coastal Areas of the Azov Sea** 31
Sofya V. Protsenko, Elena A. Protsenko, Anton V. Kharchenko
- Estimation of the Unidirectional Traffic Flow Velocity Limit with High Computational Efficiency** 39
Ivan A. Kuteynikov

INFORMATION TECHNOLOGIES

- Automatic Depth Value Recognition on Pilot Charts Using Deep Learning Methods** 52
Elena O. Rakhimbaeva, Tajaddin A. Alyshov, Yulia V. Belova

Содержание

ВЫЧИСЛИТЕЛЬНАЯ МАТЕМАТИКА

- Решение краевых задач для некоторых нелинейных дифференциальных уравнений методом Бубнова-Галеркина 7**
Н.К. Волосова, К.А. Волосов, А.К. Волосова, Д.Ф. Пастухов, Ю.Ф. Пастухов
- Достаточные условия сходимости решений линеаризованной задачи к решению исходной нелинейной задачи транспорта многофракционных наносов в зоне мелководья 20**
В.В. Сидорякина

МАТЕМАТИЧЕСКОЕ МОДЕЛИРОВАНИЕ

- Оценка точности спутниковой альтиметрии Sentinel-3 в прибрежных районах Азовского моря 31**
С.В. Проценко, Е.А. Проценко, А.В. Харченко
- Оценка предельной скорости однонаправленного транспортного потока с высокой вычислительной эффективностью 39**
И.А. Кутейников

ИНФОРМАЦИОННЫЕ ТЕХНОЛОГИИ

- Автоматическое распознавание значений глубины на лоцманских картах с использованием методов глубокого обучения 52**
Е.О. Рахимбаева, Т.А. Альшов, Ю.В. Белова

COMPUTATIONAL MATHEMATICS ВЫЧИСЛИТЕЛЬНАЯ МАТЕМАТИКА



UDC 519.6

Original Theoretical Research

<https://doi.org/10.23947/2587-8999-2025-9-1-7-19>



Solution of Boundary Value Problems for Certain Nonlinear Differential Equations Using the Bubnov-Galerkin Method

Natalya K. Volosova¹, Konstantin A. Volosov², Aleksandra K. Volosova², Mikhail I. Karlov³,
Dmitriy F. Pastukhov⁴✉, Yuriy F. Pastukhov⁴

¹ MGTU named after. N.E. Bauman, Moscow, Russian Federation

² Russian University of Transport, Moscow, Russian Federation

³ Moscow Institute of Physics and Technology (National Research University), Dolgoprudny, Russian Federation

⁴ Polotsk State University named after Euphrosyne of Polotsk, Novopolotsk, Republic of Belarus

✉ dmitrij.pastuhov@mail.ru

Abstract

Introduction. This study investigates the possibility of numerically solving a boundary value problem with a nonlinear differential equation, continuous coefficients, and a right-hand side using the modified Bubnov-Galerkin method. In the problem formulation, the partial derivatives of the equation's coefficients are continuous functions of all arguments. The order of the nonlinear differential equation n is strictly less than the number of coordinate functions m .

Materials and Methods. To numerically solve the nonlinear boundary value problem, the modified Petrov-Galerkin method and the uniqueness property of decomposing a smooth function into a system of linearly independent polynomial basis functions on the interval $[-1, 1]$ with a unit Chebyshev norm for each function in the system are used. The system of linear algebraic equations includes linearly independent boundary conditions. The matrix elements and the right-hand side of the system depend on the simple iteration index s . The coefficient vector of the solution decomposition into basis functions also depends on the index s . The inverse matrix of the system was computed using the Msimsl linear algebra library in Fortran.

Results. Sufficient conditions for the existence and uniqueness of the solution to the boundary value problem with a nonlinear differential equation using the simple iteration method have been formulated. When the sufficient conditions are met, the decomposition coefficients decrease absolutely as the basis function index increases.

Discussion and Conclusion. Three boundary value problems with a second-order nonlinear equation and one problem with a third-order equation were solved exactly. The analytical solutions were compared with numerical solutions, with the uniform norm of the difference having an order of 10^{-13} , 10^{-11} , 10^{-10} , 10^{-10} , respectively. The modified Bubnov-Galerkin method allows for solving each branch of a multivalued function in boundary value problems with nonlinear differential equations.

Keywords: hydrodynamics, mechanics, numerical methods, nonlinear differential equations, boundary value problems, Galerkin method

For Citation. Volosova N.K., Volosov K.A., Volosova A.K., Karlov M.I., Pastukhov D.F., Pastukhov Yu.F. Solution of Boundary Value Problems for Certain Nonlinear Differential Equations Using the Bubnov-Galerkin Method. *Computation Mathematics and Information Technologies*. 2025;9(1):7–19. <https://doi.org/10.23947/2587-8999-2025-9-1-7-19>

Решение краевых задач с нелинейными дифференциальными уравнениями методом Бубнова-Галеркина

Н.К. Волосова¹ , К.А. Волосов² , А.К. Волосова² , М.И. Карлов³,
Д.Ф. Пастухов⁴  , Ю.Ф. Пастухов⁴ 

¹ Московский государственный технический университет им. Н.Э. Баумана, г. Москва, Российская Федерация

² Российский университет транспорта, г. Москва, Российская Федерация

³ Московский физико-технический институт (национальный исследовательский университет),
г. Долгопрудный, Российская Федерация

⁴ Полоцкий государственный университет им. Евфросинии Полоцкой, г. Новополоцк, Республика Беларусь

✉ dmitrij.pastuhov@mail.ru

Аннотация

Введение. Исследуется возможность численного решения модифицированным методом Бубнова-Галеркина краевой задачи с нелинейным дифференциальным уравнением, непрерывными коэффициентами и правой частью. В постановке задачи частные производные коэффициентов уравнения являются непрерывными функциями по всем аргументам. Порядок нелинейного дифференциального уравнения n строго меньше числа координатных функций m .

Материалы и методы. Для численного решения нелинейной краевой задачи использован модифицированный метод Петрова-Галеркина и идея единственности разложения гладкой функции по системе линейно независимых базисных функций степенного вида на отрезке $[-1, 1]$ с единичной нормой Чебышева для каждой функции системы. В систему линейных алгебраических уравнений включены линейно независимые краевые условия. При этом элементы матрицы и правая часть системы зависят от индекса простой итерации s . От индекса s зависит и вектор коэффициентов разложения решения по базисным функциям. Обратная матрица системы находилась библиотекой линейной алгебры Msimsl на языке Fortran.

Результаты исследования. Сформулированы достаточные условия существования и единственности решения краевой задачи с нелинейным дифференциальным уравнением методом простой итерации. При выполнении достаточных условий коэффициенты разложения абсолютно уменьшаются с ростом номера базисной функции.

Обсуждение и заключение. Точно решены три краевых задачи с нелинейным уравнением второго порядка и одна задача с уравнением третьего порядка. Аналитические решения сравнены с численными решениями, равномерная норма разности имеет порядок 10^{-13} , 10^{-11} , 10^{-10} , 10^{-10} соответственно. Модифицированный метод Бубнова-Галеркина позволяет находить решение каждой ветви многозначной функции в краевых задачах с нелинейными дифференциальными уравнениями.

Ключевые слова: гидродинамика, механика, численные методы, нелинейные дифференциальные уравнения, краевые задачи, метод Галеркина

Для цитирования. Волосова Н.К., Волосов К.А., Волосова А.К., Карлов М.И., Пастухов Д.Ф., Пастухов Ю.Ф. Решение краевых задач для некоторых нелинейных дифференциальных уравнений методом Бубнова-Галеркина. *Computational Mathematics and Information Technologies*. 2025;9(1):7–19. <https://doi.org/10.23947/2587-8999-2025-9-1-7-19>

Introduction. Various methods are known for solving boundary value problems on an interval with a nonlinear differential equation, such as Newton's method [1, p. 460]. Methods for solving boundary value problems in hydrodynamics and mechanics are also presented in [2, 3]. The methods for solving nonlinear boundary value problems share many similarities with those used for linear problems [1, p. 458]. In this study, the modified Bubnov-Galerkin method, previously proposed in [4, 5] for solving boundary value problems with linear differential equations, has been extended to the case of boundary value problems with nonlinear differential equations.

In this work, any branch (graph) of a smooth solution of a nonlinear differential equation is represented as a linear combination of polynomial-type basis functions (i. e., the numerical solution is expressed in functional form). All basis functions are defined on the interval $[-1, 1]$ with a unit Chebyshev norm.

The solution of the nonlinear boundary value problem is reduced to the simple iteration method. At each iteration, a system of linear algebraic equations (SLAE) is solved, where the matrix elements and the right-hand side coefficients depend on the iteration index s . For a third-order equation, the SLAE includes $n-1$ linearly independent boundary conditions and $m-n+1$ orthogonality conditions for the residual of the differential equation to the basis functions [1, 6] (n is the order of the ODE, m is the number of basis functions).

New results and ideas for solving boundary value problems, including high-accuracy solutions and problems in complex domains, have been obtained in [7–10].

Materials and Methods

Problem Statement. Let the unknown function $u(x)$, belonging to the class of functions that are n -times continuously differentiable on the interval $C^n[a, b]$, be the solution of a boundary value problem with a nonlinear differential equation of order n with variable coefficients $g_i(x, u(x), u'(x), \dots, u^{(i)}(x)) \in C[a, b], i = \overline{0, n}$

$$\begin{cases} L[u(x)] = f(x, u(x)), x \in (a, b), u(x) \in (c, d) \\ L[u(x)] \equiv \left(\sum_{i=0}^n g_i(x, u(x), u'(x), \dots, u^{(i)}(x)) \frac{d^i}{dx^i} \right) u(x), \end{cases} \quad (1)$$

$$\sum_{i=0}^{n-1} (\alpha_\mu^i u^{(i)}(a) + \beta_\mu^i u^{(i)}(b)) = \gamma_\mu, \mu = \overline{1, n}. \quad (2)$$

In the boundary value problem (1)–(2), the given functions $g_i(x, u(x), u'(x), \dots, u^{(i)}(x)) \in C[a, b], i = \overline{0, n}$ are continuous on the interval $[a, b]$ with respect to all arguments. Each term of the nonlinear equation (1) can be expressed such that the coefficient $g_i(x, u(x), u'(x), \dots, u^{(i)}(x)), i = \overline{0, n}$, multiplying the derivative $\frac{d^i u(x)}{dx^i}$, depends only on derivatives of the function $u^{(p)}(x), p = 0, i$ up to order i at most.

For simplicity, the boundary conditions (2) at the points $x=a, x=b$ are given as linear forms with respect to the function and its derivatives up to order $n-1$ similar to a linear boundary value problem. To ensure the well-posedness of problem (1), the total number of boundary conditions must be equal to n . The coefficient matrices $\alpha_\mu^i, \beta_\mu^i, i = \overline{0, n-1}, \mu = 1, n$, as well as the values of $\gamma_\mu, \mu = 1, n$ are predefined. To uniquely determine a specific branch of the nonlinear solution of equation (1), one or more additional conditions can be imposed on the boundary conditions of type (2).

Assume that the coefficients $g_i(x, u(x), u'(x), \dots, u^{(i)}(x)) \in C[a, b], i = \overline{0, n}$ are continuously differentiable with respect to their variables $u^{(p)}$, i. e. $\frac{\partial g_i}{\partial u^{(p)}} \in C[c_i, d_i], p = \overline{0, i}$.

We generalize the Bubnov-Galerkin method, proposed in [4, 5] for solving boundary value problems with linear ordinary differential equations, to the case of a nonlinear differential equation. Suppose that any smooth function $u(x)$ or its specific branch (a solution of equation (1)) can be uniquely represented as a linear combination of polynomial basis functions [4, 5]:

$$\{\phi_i(x)\}_{i=0}^m = \left\{ \left(\frac{2x-a-b}{b-a} \right)^i, x \in [a, b], i = \overline{0, m} \right\}, \|\phi_i(x)\|_C = \max_{x \in [a, b]} |\phi_i(x)| = 1 \forall i = \overline{0, m}, \quad (3)$$

$$u(x) = u(c) + \sum_{j=1}^m \phi_j(x) D_j = u(c) + \sum_{j=1}^m \left(\frac{2(x-c)}{b-a} \right)^j D_j, c = \frac{a+b}{2}. \quad (4)$$

The goal of the numerical algorithm is to determine the decomposition vector D_j for solving the boundary value problem (1)–(2) using the basis functions $\phi_j(x)$. We define the residual of the nonlinear equation (1) and take into account the representation of its solution using formula (4):

$$\begin{aligned} R(u(x)) &= L[u(x)] - f(x, u(x)) = \left(\sum_{i=0}^n g_i(x, u(x), u'(x), \dots, u^{(i)}(x)) \frac{d^i}{dx^i} \right) u(x) - f(x, u(x)) = \\ &= \sum_{j=1}^m D_j \sum_{i=1}^n g_i(x, u(x), u'(x), \dots, u^{(i)}(x)) \frac{d^i \phi_j(x)}{dx^i} + g_0(x, u(x)) \cdot u(x) - f(x, u(x)) = \\ &= \sum_{j=1}^m D_j \sum_{i=1}^n g_i(x, u(x), u'(x), \dots, u^{(i)}(x)) \frac{d^i \phi_j(x)}{dx^i} - \overline{f(x, u(x))}, \overline{f(x, u(x))} = f(x, u(x)) - g_0(x, u(x)) \cdot u(x). \end{aligned} \quad (5)$$

We require [1, 4–6] that the residual $R(u(x))$ be orthogonal to the maximum number of $m-n+1$ basis functions (where m is the number of basis coordinate functions and n is the order of the differential equation):

$$\langle R(u(x)), \phi_k(x) \rangle = 0 \Leftrightarrow k = \overline{0, m-n},$$

$$\left\langle \sum_{j=1}^m D_j \sum_{i=1}^n g_i(x, u(x), u'(x), \dots, u^{(i)}(x)) \frac{d^i \phi_j(x)}{dx^i} - \overline{f(x, u(x))}, \phi_k(x) \right\rangle = 0 \forall k = \overline{0, m-n} \Leftrightarrow$$

$$\begin{cases} \sum_{j=1}^m A_{k,j} D_j = F_k, F_k = \left\langle \overline{f(x, u(x))}, \phi_k(x) \right\rangle \\ A_{k,j} = \left\langle \sum_{i=1}^n g_i(x, u(x), u'(x), \dots, u^{(i)}(x)) \frac{d^i \phi_j(x)}{dx^i}, \phi_k(x) \right\rangle, k = \overline{0, m-n}. \end{cases}$$

Other linearly independent boundary conditions (2) for the system of linear algebraic equations (5) should be selected from the set of admissible functions of the original boundary problem (1) [11].

We will solve the system of linear algebraic equations (5), where the matrix coefficients and the coefficients of the right-hand side depend implicitly on the solution, using the simple iteration method. To do this, we will consider the implicit dependence of the solution on the decomposition vector $D_j^s, s = 0, 1, 2, \dots, j = \overline{1, m}$, (4) by the system of basis functions with iteration number s .

From (5) we obtain:

$$A_{k,j} = A_{k,j}(u^s) = A_{k,j}(u(D^s)), F_k = F_k(u^s) = F_k(u(D^s)), D = D^{s+1},$$

$$\sum_{j=1}^m A_{k,j}(D^s) \cdot D_j^{s+1} = F_k(D^s), j = \overline{1, m}, k = \overline{0, m-n}, D^{s+1} = A^{-1}(D^s) \cdot F(D^s), s = 0, 1, 2, \dots \quad (6)$$

Let us denote the limiting values

$$\lim_{s \rightarrow \infty} A(D^s) = A^*, \lim_{s \rightarrow \infty} F(D^s) = F^*, \lim_{s \rightarrow \infty} D^s = D^*.$$

We will write the limiting form of equation (6):

$$A^* D^* = F^*. \quad (7)$$

Theorem 1 (sufficient conditions for the existence and uniqueness of the solution D^* of equation (7) in the simple iteration (6)).

Let the coefficients of equation (1) be continuous $g_i(x, u(x), u'(x), \dots, u^{(i)}(x)) \in C[a, b], i = \overline{0, n}$ and continuously differentiable with respect to all arguments, starting from the second $\frac{\partial g_i}{\partial u^{(p)}} \in C[c_p, d_p], p = \overline{0, i}, i = \overline{1, n}$. Let the limiting matrix A^* in (7), computed according to formulas (5), be non-singular. Let the conditions for a contraction mapping

$q = \left\| A^{-1} \cdot G \right\| < 1$ be satisfied. Then, in the boundary value problem (1) with boundary conditions (2), there exists a unique solution. The residual norm decreases according to the formula $\left\| \delta D^s \right\| \leq \left\| \delta D^0 \right\| q^s / (1 - q)$, where s is the iteration number in the algorithm (6).

Proof. Consider the increment of equation (6) in the vicinity of all its limiting values:

$$A^* D^* = F^* \Rightarrow \delta A D^* + A^* \delta D^* = \delta F^*,$$

where $\delta A^s = A^s - A^*$ is the increment of the matrix of dimension $m \times m$; A^* is the matrix of dimension $m \times m$; $\delta D^{s+1} = D^{s+1} - D^*$ is the increment of the vector of dimension m ; $\delta F^s = F^s - F^*$ is the increment of the vector of dimension m . Introduce an integer index $t = \overline{1, m}$ and consider the increment of the specified quantities $\delta A^s, \delta F^s$ as a function of the increment of the component of the vector δD^s , using formula (5): $\delta D_t^s = D_t^s - D_t^*$:

$$\delta A_{k,j}(\delta D_t^s) D^* = \left\langle \sum_{j=1}^m D_j \sum_{i=1}^n \sum_{p=0}^i \frac{\partial g_i}{\partial u^{(p)}} \cdot \phi_j^{(p)}(x) \cdot \phi_j^{(i)}(x), \phi_k(x) \right\rangle \delta D_t^s, u_p \equiv u^{(p)}(x) \quad t = \overline{1, m}, k = \overline{0, n-m}, j = \overline{1, m}.$$

In the last formula, summation over the index p , has been added because the coefficients of the nonlinear ODE $g_i(x, u(x), u'(x), \dots, u^{(i)}(x))$ depend on the function and its derivatives up to the i -th order, inclusively. The effective right-hand side of the nonlinear equation $\overline{f(x, u(x))} = f(x, u(x)) - g_0(x, u(x)) \cdot u(x)$ depends only on the function $u(x)$:

$$\delta F_k(\delta D_t^s) = \left\langle \frac{\partial \overline{f(x, u(x))}}{\partial u} \phi_t(x), \phi_k(x) \right\rangle \delta D_t^s, t = \overline{1, m}.$$

We obtain $\delta D^{s+1} = A^{*-1} (\delta F^s - \delta A^s D^*)$ and replace the last equation with a similar equation of simple iteration

$$\delta D^{s+1} = (A^s)^{-1} (\delta F^s - \delta A^s D^s) = (A^s)^{-1} G^s \delta D^s. \tag{8}$$

In equation (8)

$$A^s_{k,j} = \left\langle \sum_{i=1}^n g_i(x, u^s(x), u'^s(x), \dots, u^{(i)s}(x)) \frac{d^i \phi_j(x)}{dx^i}, \phi_k(x) \right\rangle, k = \overline{0, m-n}, j = \overline{1, m}, \tag{9}$$

$$G^s_{k,t} = \left\langle \frac{\partial f(x, u(x))}{\partial u} \phi_t(x), \phi_k(x) \right\rangle - \left\langle \sum_{j=1}^m D_j^s \sum_{i=1}^n \sum_{p=0}^i \frac{\partial g_i^s}{\partial u_p} \cdot \phi_t^{(p)}(x) \cdot \phi_j^{(i)}(x), \phi_k(x) \right\rangle, k = \overline{0, m-n}, t = \overline{1, m}, \tag{10}$$

$\delta D_t^{s+1} = \delta D_t^s = 0, t = \overline{m-n+1, m}$ the last rows of the matrix coefficients and the coefficients of the right-hand side in equation (5) are determined by the boundary conditions and are constant numbers. In formula (10), $\phi_t^{(p)}$ denotes the p-th order derivative of the basis coordinate function with index t. Similarly, for $\phi_j^{(i)}(x)$. Explicit formulas $\phi_j^{(i)}(x)$ are provided in [4, 5].

Let us estimate the right and left sides of equation (8)

$$\|\delta D^{s+1}\| \leq \left\| (A^s)^{-1} \right\| \|G^s\| \|\delta D^s\| = q \|\delta D^s\|, q^s = \left\| (A^s)^{-1} \right\| \|G^s\| \leq \left\| (A^*)^{-1} \right\| \|G^*\|. \tag{11}$$

by the norm in complete metric spaces [12]. If the compression parameter

$$q_s = \left\| (A^s)^{-1} \right\| \|G^s\| \leq q = \left\| (A^*)^{-1} \right\| \|G^*\| < 1, s = 0, 1, 2, \dots$$

for the mapping $\delta D^s \rightarrow \delta D^{s+1} = (A^s)^{-1} G^s \delta D^s$ is less than one, the solution to the boundary value problem (1)–(2) exists and is unique.

According to the work of A.N. Kolmogorov and S.V. Fomin [12, p. 87], the residual norm decreases according to the formula $\|\delta D^s\| \leq \|\delta D^0\| q^s / (1-q), \|\delta D^s\| = \|D^s - D^*\| = \rho(D^s, D^*)$.

Theorem 1 is proved.

Let us consider three examples of solving a nonlinear boundary value problem with a second-order equation and one example with a third-order equation.

Example 1.

$$\begin{cases} u \cdot u''(x) - u' \cdot u'(x) = u^2(x) = f(x, u), \\ u(0) = 1, u(1) = e^{1/2}, x \in [0, 1]. \end{cases} \tag{12}$$

The exact solution of the problem was obtained by considering the transformations:

$$u \cdot u''(x) - u' \cdot u'(x) = u^2(x) \Leftrightarrow \left(\frac{u'}{u} \right)' = (\ln(u(x)))' = \frac{uu'' - (u')^2}{u^2} = 1 \Leftrightarrow$$

$$\ln(u(x)) = \frac{x^2}{2} + C_1x + C_2 \Leftrightarrow u(x) = \overline{C_2} e^{\frac{x^2}{2} + C_1x}, u(0) = 1 \Leftrightarrow \overline{C_2} = 1, u(1) = e^{1/2} \Leftrightarrow \frac{1}{2} + C_1 = \frac{1}{2} \Rightarrow C_1 = 0.$$

As a result, the exact solution of Example (1) is of the form $u(x) = e^{\frac{x^2}{2}}$.

Let us convert the condition of the example to a numerical algorithm (5)–(6). It is also necessary to specify the initial function — a solution that satisfies the Dirichlet boundary conditions, i. e., the given values of the function at the boundaries of the interval.

We obtain that

$$u^0(x) = \frac{u_0 + u_n}{2} + \phi_1(x) D_1^0 = \frac{u_0 + u_n}{2} + \phi_1(x) \left(\frac{u_n - u_0}{2} \right), D_2^0 = \dots = D_n^0 = 0, \tag{13}$$

since

$$\phi_1(a) = -1, \phi_1(b) = 1, u^0(a) = \frac{u_0 + u_n}{2} - \left(\frac{u_n - u_0}{2} \right) = u_0, u^0(b) = \frac{u_0 + u_n}{2} + \left(\frac{u_n - u_0}{2} \right) = u_n$$

and the boundary conditions for the initial function $u^0(x)$ are satisfied. The coefficients and the right-hand side in Example 1 are as follows:

$$g_2(x, u, u', u'') = u, g_1(x, u, u') = -u', g_0(x, u) = 0, f(x, u) = u^2(x).$$

In the numerical algorithm, in addition to formulas (5)–(6), we use the detailed formulas from the work [5], which account for the Dirichlet boundary conditions for the second-order linear differential equation:

$$\sum_{j=1}^m a^s_{i,j} D_j^{s+1} = \overline{f_i^s}, i = \overline{0, m-1}. \tag{14}$$

Here, the elements of the matrix $a_{i,j}, i = \overline{0, m-1}, j = \overline{1, m}$ and the coefficients of the right-hand side $\overline{f_i^s}$ of the system of equations (14) are:

$$a^s_{i,j} = \begin{cases} \langle L^s \phi_j, \phi_i \rangle, j \equiv 1 \pmod{2}, i = \overline{0, m-2}, \\ \langle L^s (\phi_j - 1), \phi_i \rangle, j \equiv 0 \pmod{2}, i = \overline{0, m-2}, \\ 1, i = m-1, j \equiv 1 \pmod{2}, \\ 0, i = m-1, j \equiv 0 \pmod{2}, \end{cases}$$

$$\overline{f_i^s} = \begin{cases} \langle f(x, u^s) - L^s \left(\frac{u_a + u_b}{2} \right), \phi_i(x) \rangle, i = \overline{0, m-2}, \\ \frac{u_b - u_a}{2}, i = m-1. \end{cases}$$

However, the operator $L^s \phi_j$ for the matrix coefficients $a^s_{i,j}$ in (14) is nonlinear and is computed using formula (1), unlike in [5]. The absolute and relative Chebyshev vector norm of the residual for the problem:

$$\|u^{num} - u^{exact}\|_c = 1.072313895664201E - 013, \frac{\|u^{num} - u^{exact}\|_c}{\|u^{exact}\|_c} = 6.503912545562317E - 014.$$

The number of intervals for calculating the scalar product of two functions in (14) is $n_1=20$, the number of coordinate functions $m=15$, and the number of iterations $n_1=30$.

The scalar product of functions was computed using the formulas from [5]:

$$\langle y_1, y_2 \rangle = \int_a^b y_1(x)y_2(x)dx = 10h \sum_{i=0}^{n_1} y_1(x_i)y_2(x_i)C_i + O(h^{22}), n_1 = 20s, h = \frac{b-a}{n_1}, s \in N, \tag{15}$$

$$C_i = \begin{cases} \frac{1145302367137}{48426042384720}, \text{ if } i = 0 \text{ or } i = n_1, \\ \frac{1145302367137}{24213021192360}, \text{ if } (i \equiv 0 \pmod{20}) \text{ and } (0 < i < n_1), \\ \frac{335582304250}{1470076286679}, \text{ if } (i \equiv 1 \pmod{20}) \text{ or } (i \equiv 19 \pmod{20}), \\ \frac{-19467909708875}{41162136027012}, \text{ if } (i \equiv 2 \pmod{20}) \text{ or } (i \equiv 18 \pmod{20}), \\ \frac{8274871497250}{3430178002251}, \text{ if } (i \equiv 3 \pmod{20}) \text{ or } (i \equiv 17 \pmod{20}), \\ \frac{-413929922392625}{54882848036016}, \text{ if } (i \equiv 4 \pmod{20}) \text{ or } (i \equiv 16 \pmod{20}), \\ \frac{50652939811064}{2450127144465}, \text{ if } (i \equiv 5 \pmod{20}) \text{ or } (i \equiv 15 \pmod{20}), \\ \frac{-155790561130375}{3430178002251}, \text{ if } (i \equiv 6 \pmod{20}) \text{ or } (i \equiv 14 \pmod{20}), \\ \frac{286955364893000}{3430178002251}, \text{ if } (i \equiv 7 \pmod{20}) \text{ or } (i \equiv 13 \pmod{20}), \\ \frac{-502376261017625}{3920203431144}, \text{ if } (i \equiv 8 \pmod{20}) \text{ or } (i \equiv 12 \pmod{20}), \\ \frac{1704056522480500}{10290534006753}, \text{ if } (i \equiv 9 \pmod{20}) \text{ or } (i \equiv 11 \pmod{20}), \\ \frac{-1684005984173647}{9355030915230}, \text{ if } i \equiv 10 \pmod{20}. \end{cases} \tag{16}$$

The results of the program (Example 1) are presented in Table 1.

Table 1

Numerical $u_i^{numerical}$ and exact u_i^{exact} solutions of the problem (12)

x_i	$u_i^{numerical}$	u_i^{exact}	$u_i^{numerical} - u_i^{exact}$
0.000000000000E+000	1.0000000000000000	1.0000000000000000	0.00000E+000
5.000000000000E-002	1.00125078157569	1.00125078157562	6.533608E-014
0.1000000000000000	1.00501252085944	1.00501252085940	3.497831E-014
0.1500000000000000	1.01131351922362	1.01131351922361	5.002183E-015
0.2000000000000000	1.02020134002678	1.02020134002676	2.150048E-014
0.2500000000000000	1.03174340749917	1.03174340749910	7.15878E-014
0.3000000000000000	1.04602785990882	1.04602785990872	1.072313E-013
0.3500000000000000	1.06316467213420	1.06316467213410	9.834472E-014
0.4000000000000000	1.08328706767501	1.08328706767496	5.269027E-014
0.4500000000000000	1.10655324549790	1.10655324549789	4.473201E-015
0.5000000000000000	1.13314845306681	1.13314845306683	-1.17629E-014
0.5500000000000000	1.16328744359303	1.16328744359302	1.449849E-014
0.6000000000000000	1.19721736312188	1.19721736312181	6.498762E-014
0.6500000000000000	1.23522112174449	1.23522112174439	1.029619E-013
0.7000000000000000	1.27762131320499	1.27762131320489	1.004986E-013
0.7500000000000000	1.32478475872893	1.32478475872887	6.074600E-014
0.8000000000000000	1.37712776433597	1.37712776433596	1.600000E-014
0.8500000000000000	1.43512219658388	1.43512219658387	5.959208E-015
0.9000000000000000	1.49930250005679	1.49930250005677	2.719775E-014
0.9500000000000000	1.57027380147662	1.57027380147660	1.296022E-014
1.0000000000000000	1.64872127070013	1.64872127070013	4.737963E-017

The numerical solution of the problem (1)–(2) can be brought to the form (17) by transforming formula (4) with Dirichlet boundary conditions [4]:

$$u(x) = \left(\frac{u_a + u_b}{2}\right) + \sum_{j=1}^m \left[\left(\frac{(2x-a-b)^j}{b-a}\right) + \left(\frac{-1+(-1)^{j+1}}{2}\right) \right] D_j^* \tag{17}$$

In (17), the limiting values D_j^* of the decomposition vector of the solution by basis functions are used, and D_j^* is the solution of the system of linear algebraic equations (14) on the last iteration.

Example 2.

$$\begin{cases} 2u \cdot u''(x) + 2u' \cdot u'(x) = x = f(x, u), \\ u(1) = 1, u(2) = 2, x \in [1, 2]. \end{cases} \tag{18}$$

Since

$$\begin{aligned} (u^2(x))' &= 2uu', \quad (u^2(x))'' = 2(u')^2 + 2uu'' = x \Rightarrow u^2(x) = \frac{x^3}{6} + C_1x + C_2 \Leftrightarrow \\ u(x) &= \pm \sqrt{\frac{x^3}{6} + C_1x + C_2}, \quad \begin{cases} u(1) = 1 \Leftrightarrow 1 = \frac{1}{6} + C_1 + C_2 \\ u(2) = 2 \Leftrightarrow 4 = \frac{8}{3} + 2C_1 + C_2 \end{cases} \Leftrightarrow \begin{cases} C_1 + C_2 = \frac{5}{6} \\ 2C_1 + C_2 = \frac{8}{3} \end{cases} \Leftrightarrow C_1 = \frac{11}{6}, C_2 = -1. \end{aligned}$$

it follows that $u(x) = \sqrt{\frac{x^3 + 11x - 6}{6}}$ is the exact solution of the boundary value problem (18).

Note that in this case, the boundary conditions (18) unambiguously choose one branch of the solution; otherwise, additional conditions can be set to select one branch.

The number of intervals for calculating the scalar product of two functions in (18) is $n_1=100$, the number of coordinate functions $m=18$, and the number of iterations $n_1=30$, $g_2(x, u, u', u'') = 2u, g_1(x, u, u') = 2u', g_0(x, u) = 0, f(x, u) = x$.

Table 2

Numerical $u_i^{numerical}$ and exact u_i^{exact} solutions of the problem (18)

x_i	$u_i^{numerical}$	u_i^{exact}	$u_i^{numerical} - u_i^{exact}$
1.0000000000000000	1.0000000000000000	1.0000000000000000	0.0000000000E+000
1.0500000000000000	1.05732563573	1.05732563574331	-9.187983707E-012
1.1000000000000000	1.11287914887	1.1128791488746	3.6390890301E-012
1.1500000000000000	1.16696722317	1.16696722319009	-1.377342684E-011
1.2000000000000000	1.21983605454	1.21983605455815	-1.174038644E-011
1.2500000000000000	1.27168687184	1.27168687183599	4.801492536E-012
1.3000000000000000	1.32268665978	1.32268665979513	-8.256284544E-012
1.3500000000000000	1.37297578272	1.37297578274345	-2,059930004E-011
1.4000000000000000	1.42267353949	1.42267353950230	-5.676792369E-012
1.4500000000000000	1.47188229828	1.47188229828339	5.4383164638E-012
1.5000000000000000	1.52069063256	1.52069063257455	-8.254952277E-012
1.5500000000000000	1.56917573902	1.56917573904264	-1.900479773E-011
1.6000000000000000	1.61740532952	1.61740532953246	-6.780798145E-012
1.6500000000000000	1.66543913128	1.66543913128040	3.2989166953E-012
1.7000000000000000	1.71333009078	1.71333009078811	-7.917888567E-012
1.7500000000000000	1.76112535043	1.76112535045067	-1.482725053E-011
1.8000000000000000	1.80886704873	1.80886704873520	-2.779998453E-012
1.8500000000000000	1.85659298177	1.85659298178141	-1.615374500E-012
1.9000000000000000	1.90433715501	1.90433715502271	-6.362910198E-012
1.9500000000000000	1.95213024668	1.95213024667925	6.6588956570E-012
2.0000000000000000	2.0000000000000000	2.0000000000000000	0.0000000000E+000

The Chebyshev vector norm (absolute and relative norms) of the residual for the problem in Example (18) are:

$$\|u^{num} - u^{exact}\|_c = 2.059930004350008E - 011, \frac{\|u^{num} - u^{exact}\|_c}{\|u^{exact}\|_c} = 1.029965002175004E - 011.$$

Note. If the boundary conditions in Example (18) are chosen as $u(1) = -1, u(2) = -2$, and the exact solution of the problem is $u(x) = -\sqrt{\frac{x^3 + 11x - 6}{6}}$, the program gives the same Chebyshev vector norm of the residual due to the symmetry of Example (18) with respect to the transformation $(x, u) \rightarrow (x, -u)$.

Therefore, the algorithm using formulas (1), (5), (6), (13), (15), (16), (17) for the nonlinear Dirichlet boundary value problem with a second-order equation finds the solution for each branch of the multi-valued function. If the boundary conditions for the branches coincide, an additional condition can be selected, for example, the value of the function at the midpoint of the interval $u(c) = u\left(\frac{a+b}{2}\right)$ and this condition can be included in the system of linear algebraic equations (14), thereby reducing the number of orthogonality conditions for the residual of the ODE with respect to the basis functions by 1.

Example 3.

$$\begin{cases} \cos(u) \cdot u''(x) - \sin(u) u' \cdot u'(x) = 2 = f(x, u), \\ u(0) = 0, u(1) = \pi / 6, x \in [0, 1]. \end{cases} \quad (19)$$

Since

$$(\sin(u))' = \cos(u)u', (\sin(u))'' = \cos(u)u'' - \sin(u)(u')^2 = 2 \Leftrightarrow \sin(u(x)) = x^2 + C_1x + C_2 \Rightarrow$$

$$u(x) = \arcsin\left(x^2 + C_1x + C_2\right), \begin{cases} u(0) = 0 \Leftrightarrow 0 = \arcsin(C_2) \\ u(1) = \pi/6 \Leftrightarrow \frac{1}{2} = 1 + C_1 + C_2 \end{cases} \Leftrightarrow \begin{cases} C_2 = 0 \\ C_1 + C_2 = -\frac{1}{2} \end{cases} \Leftrightarrow C_1 = -\frac{1}{2}, C_2 = 0.$$

The function $u(x) = \arcsin\left(x^2 - \frac{x}{2}\right)$ is the exact solution to the problem (19).

In Example (19) $g_2(x, u, u', u'') = \cos(u)$, $g_1(x, u, u') = -\sin(u)u'$, $g_0(x, u) = 0$, $f(x, u) = 2$. The number of intervals for the scalar product of two functions is $n_1=120$, the number of coordinate functions is $m=17$, and the number of iterations is $n_1=30$.

Table 3

Numerical $u_i^{numerical}$ and exact u_i^{exact} solutions of the problem (19)

x_i	$u_i^{numerical}$	u_i^{exact}	$u_i^{numerical} - u_i^{exact}$
0.0000000E+000	0.0000000000E+000	0.00000000000E+000	0.00000E+000
4.16666666E-002	-1.90983832E-002	-1.9098383217E-002	-3.18418E-013
8.33333333E-002	-3.47292032E-002	-3.47292030514E-002	-2.030325E-010
0.125000000000	-4.68921831E-002	-4.68921831332E-002	-1.491510E-011
0.166666666666	-5.55841730E-002	-5.5584173280E-002	2.1348351E-010
0.208333333333	-6.08013439E-002	-6.08013437340E-002	-2.052915E-010
0.250000000000	-6.25407621E-002	-6.25407617964E-002	-3.182648E-010
0.291666666666	-6.08013435E-002	-6.0801343734E-002	1.7451315E-010
0.333333333333	-5.55841729E-002	-5.5584173280E-002	3.3926163E-010
0.375000000000	-4.68921832E-002	-4.6892183133E-002	-1.666960E-010
0.416666666666	-3.47292035E-002	-3.47292030514E-002	-5.013826E-010
0.458333333333	-1.90983833E-002	-1.90983832179E-002	-8.629465E-011
0.500000000000	4.30824846E-010	0.00000000000E+000	4.3082484E-010
0.541666666666	2.25713611E-002	2.25713609537E-002	2,0268367E-010
0.583333333333	4.86302760E-002	4.86302764989E-002	-4.379981E-010
0.625000000000	7.82046914E-002	7.82046919347E-002	-4.480854E-010
0.666666666666	0.1113410145	0.111341014340964	2.1420220E-010
0.708333333333	0.1481103594	0.148110359030227	3.9991367E-010
0.750000000000	0.1886163853	0.188616386175404	-2.500614E-010
0.791666666666	0.2330054316	0.233005432127055	-4.563276E-010
0.833333333333	0.2814800734	0.281480073230845	2.1672891E-010
0.875000000000	0.3343179941	0.334317994036368	1.4096033E-010
0.916666666666	0.3918993389	0.391899339315036	-3.222679E-010
0.958333333333	0.4547481928	0.454748192610442	2.4028019E-010
1.000000000000	0.523598775598299	0.523598775598299	2.8514517E-017

The Chebyshev vector norm of the residual for the problem in Example (19) is

$$\|u^{num} - u^{exact}\|_c = 5.602360454820782E - 010 .$$

Example 4 (with a nonlinear third-order differential equation).

$$\begin{cases} -\sin(u) \cdot u'''(x) - 3 \cos(u) \cdot u' \cdot u''(x) + \sin(u) \cdot (u')^2 \cdot u' = 6 = f(x, u), \\ u(0) = \pi/3, u(1) = \pi/2, u'(1) = 0, x \in [0, 1] \rightarrow u \in [\pi/3, \pi/2]. \end{cases} \quad (20)$$

Since

$$(\cos(u))' = -\sin(u)u', (\cos(u))'' = -\sin(u)u'' - \cos(u)(u')^2, (\cos(u))''' = -\sin(u)u''' - 3\cos(u)u'u' + \sin(u)(u')^3,$$

$$\cos(u) = x^3 + C_1x^2 + C_2x + C_3, u(x) = \arccos(x^3 + C_1x^2 + C_2x + C_3),$$

$$(\cos(u))' = -\sin(u)u' = 3x^2 + 2C_1x + C_2, u(0) = \pi/3 \Leftrightarrow \cos(\pi/3) = 1/2 = C_3,$$

$$\begin{cases} u(1) = \pi/2 \Leftrightarrow \cos(\pi/2) = 0 = 1 + C_1 + C_2 + 1/2 \\ u'(1) = 0 = \frac{(3x^2 + 2C_1x + C_2)_{x=1}}{-\sin(u = \pi/2)} \Leftrightarrow 3 + 2C_1 + C_2 = 0 \Leftrightarrow \begin{cases} C_1 + C_2 = -3/2 \\ 2C_1 + C_2 = -3 \end{cases} \Leftrightarrow C_1 = -\frac{3}{2}, C_2 = 0. \end{cases}$$

The function $u(x) = \arccos\left(x^3 - \frac{3x^2}{2} + \frac{1}{2}\right) = \arccos\left(\frac{2x^3 - 3x^2 + 1}{2}\right)$ is the exact solution to the problem (20).

The coefficients of the differential equation in Example (20) are $g_3(x, u, u', u'') = -\sin(u)$, $g_2(x, u, u', u'') = -3\cos(u)u'$, $g_1(x, u, u', u'') = \sin(u)(u')^2$, $g_0(x, u) = 0$, $f(x, u) = 6$.

For the third-order equation, the formulas of the algorithm from the work [5] need to be modified, taking into account the iteration index:

$$\sum_{j=1}^m a_{i,j}^s D_j^{s+1} = \overline{f_i^s}, i = \overline{0, m-1}. \tag{21}$$

where the elements of the matrix $a_{i,j}^s, i = \overline{0, m-1}, j = \overline{1, m}, s = 0, 1, 2, \dots$ and the coefficients of the right-hand side $\overline{f_i^s}$ of the system of equations (21), considering the nonlinear form of the differential operator L^s , computed using formula (1), are:

$$L^s[u^s(x)] \equiv \left(\sum_{i=0}^n g_i(x, u^s(x), (u'(x))^s, \dots, (u^{(i)}(x))^s) \frac{d^i}{dx^i} \right) u^s(x),$$

$$L^s[\phi_j] \equiv \left(\sum_{i=0}^n g_i(x, u^s(x), (u'(x))^s, \dots, (u^{(i)}(x))^s) \frac{d^i}{dx^i} \right) \phi_j,$$

$$a_{i,j}^s = \begin{cases} \langle L^s \phi_j, \phi_i \rangle, & \text{if } j \equiv 1 \pmod{2}, i = \overline{0, m-3}, \\ \langle L^s(\phi_j - 1), \phi_i \rangle, & \text{if } j \equiv 0 \pmod{2}, i = \overline{0, m-3}, \\ 1, & \text{if } i = m-2, j \equiv 1 \pmod{2}, \\ 0, & \text{if } i = m-2, j \equiv 0 \pmod{2}, \\ j, & \text{if } i = m-1, \end{cases}$$

$$\overline{f_i^s} = \begin{cases} \left\langle f(x) - L^s\left(\frac{u_0 + u_n}{2}\right), \phi_i(x) \right\rangle, & \text{if } i = \overline{0, m-3}, L^s\left(\frac{u_0 + u_n}{2}\right) = \left(\frac{u_0 + u_n}{2}\right)g_0(x), \\ \frac{u_n - u_0}{2}, & \text{if } i = m-2, \\ 0, & \text{if } i = m-1. \end{cases}$$

The last row of coefficients for a_{ij}^s in (21) is obtained by differentiating formula (4), since at the right end of the interval in Example (20) $u'(b=1) = 0$:

$$(u'(x))^s = \sum_{j=1}^m \phi_j'(x) D_j^s = \sum_{j=1}^m \frac{2j}{(b-a)} \left(\frac{(2x-a-b)}{b-a} \right)_{x=b}^{j-1} D_j^s = 0 \Leftrightarrow D_1^s + 2D_2^s + 3D_3^s + \dots + mD_m^s = 0.$$

The number of intervals for the scalar product of two functions in (20) is $n_1=100$, the number of coordinate functions $m=17$, and the number of iterations $n_1=30$.

Table 4

Numerical $u_i^{numerical}$ and exact u_i^{exact} solutions of the problem (20)

x_i	$u_i^{numerical}$	u_i^{exact}	$u_i^{numerical} - u_i^{exact}$
0.00000000E+000	1.047197551196	1.047197551196	-3.118165448E-016
5.00000000E-002	1.05137830714	1.051378307162	-1.8182033E-011

x_i	$u_i^{numerical}$	u_i^{exact}	$u_i^{numerical} - u_i^{exact}$
0.1000000000000	1.06328930398	1.063289303975	8.411912659E-012
0.1500000000000	1.08193034985	1.081930349812	4.527497062E-011
0.2000000000000	1.10626929727	1.106269297375	-1.03325620E-010
0.2500000000000	1.13528395573	1.135283955730	3.742097994E-012
0.3000000000000	1.16799174328	1.167991743151	1.319257321E-010
0.3500000000000	1.20346614669	1.203466146733	-3.93724372E-011
0.4000000000000	1.24084180881	1.240841808965	-1.47600610E-010
0.4500000000000	1.27931122393	1.279311223897	3.508758333E-011
0.5000000000000	1.31811607179	1.318116071652	1.431814589E-010
0.5500000000000	1.35653572032	1.356535720348	-2.54165034E-011
0.6000000000000	1.39387479319	1.393874793328	-1.33199911E-010
0.6500000000000	1.42945115362	1.429451153606	1.359530738E-011
0.7000000000000	1.46258526518	1.462585265086	1.018387917E-010
0.7500000000000	1.49259163483	1.492591634860	-2.76735182E-011
0.8000000000000	1.51877286350	1.518772863566	-6.40170944E-011
0.8500000000000	1.54041665402	1.540416653986	3.963527726E-011
0.9000000000000	1.55679586942	1.556795869421	-1.078461321E-013
0.9500000000000	1.56717131885	1.567171318855	-3.809447874E-012
1.0000000000000	1.570796326794	1.570796326794	-6.125742274E-017

The Chebyshev vector norm (absolute and relative norms) of the residual for the problem in Example (20) are

$$\|u^{num} - u^{exact}\|_c = 1.522944525480727E - 010, \frac{\|u^{num} - u^{exact}\|_c}{\|u^{exact}\|_c} = 1.454304895709992E - 010.$$

Note 2. It should be noted that in the systems of linear algebraic equations (14) and (21) for the 4 examples, the library of linear algebra msimsl in FORTRAN was used for the computation of D_j^{s+1} .

Note 3. A comparison of the results of numerical solutions of the examples in this paper with the solutions of examples [4], [5] shows that the accuracy of solving boundary value problems is achieved greater than 10^{-13} – 10^{-14} if a small number of intervals were used in the scalar product formula ($n_1=20.50$ in the first example of this paper, $n_1=20$) and the rounding error is not it managed to grow due to fewer calculations. If the number of intervals is large ($n_1=100$) in the second, third and fourth examples of this work, then the accuracy of calculations is low (10^{-10}) due to the increase in rounding error and its effect on the overall error.

Discussion and Conclusion. A numerical solution algorithm for the boundary value problem on the interval with a nonlinear differential equation of order n , modified by the Bubnov-Galerkin method, is proposed. The possibility of decomposing the smooth solution of the nonlinear problem into a system of linearly independent basis functions with a unit Chebyshev norm on the interval $[-1,1]$ is assumed. The number of basis functions m is greater than the order of the differential equation n . Formulas for the elements of the matrix and the coefficients of the right-hand side in the system of linear algebraic equations of the second and third orders are obtained. The systems of linear algebraic equations (14) or (21) are solved sequentially using the simple iteration method, with the number of iterations $n_1=30$. The theorem — sufficient conditions for the existence and uniqueness of the solution of the boundary value problem with the nonlinear ODE using the simple iteration method is proven.

Four nonlinear boundary value problems are solved analytically. The Chebyshev norm of the difference between the exact and numerical solutions in the solved examples has an order of magnitude, 10^{-13} , 10^{-11} , 10^{-10} , 10^{-10} respectively. This accuracy of the solution is intermediate between single 10^{-8} and double precision 10^{-15} , and is also comparable to the accuracy 10^{-11} of the solution of the linear boundary value problem in the work [4].

References

1. Bahvalov N.S., Zhidkov N.P., Kobelkov G.M. *Numerical methods: a textbook for students of physics and mathematics specialties of higher educational institutions*. Binom. lab. Knowledge; 2011. 636 p. (In Russ.)
2. Ershova T.Ya. Boundary value problem for a third-order differential equation with a strong boundary layer. *Bulletin of Moscow University. Episode 15: Computational mathematics and cybernetics*. 2020;1:30–39. (In Russ.) <https://doi.org/10.3103/S0278641920010057>

3. Morozova E.A. Solvability of a boundary value problem for a system of ordinary differential equations. *Bulletin of Perm University. Mathematics. Mechanics. Computer science.* 2010;3(3):46–50. (In Russ.)
4. Volosova N.K. et al. Modified Bubnov-Galerkin method for solving boundary value problems with a linear ordinary differential equation. *Computational Mathematics and Information Technologies.* 2024;8(3):23–33. (In Russ.)
<https://doi.org/10.23947/2587-8999-2024-8-3-23-33>
5. Volosova N.K. et al. Increasing the accuracy of solving boundary value problems with a linear ordinary differential equation using the Bubnov-Galerkin method. *Computational Mathematics and Information Technologies.* 2024;8(4): 7–18. (In Russ.) <https://doi.org/10.23947/2587-8999-2024-8-4-7-18>
6. Bahvalov N.S., Lapin A.V., Chizhonkov E.V. *Numerical methods in problems and exercises.* M.: BINOM. Knowledge laboratory; 2010. 240 p. (in Russ.)
7. Petrov A.G. High-precision numerical schemes for solving plane boundary value problems for a polyharmonic equation and their application to problems of hydrodynamics. *Applied Mathematics and Mechanics.* 2023;87(3):343–368 (In Russ.) <https://doi.org/10.31857/S0032823523030128>
8. Sukhinov A.I. et al. A two-dimensional hydrodynamic model of coastal systems, taking into account evaporation. *Computation Mathematics and Information Technologies.* 2023;7(4):9–21. (In Russ.)
<https://doi.org/10.23947/2587-8999-2023-7-4-9-21>
9. Galaburdin A.V. The application of neural networks to solve the problems of a conductor for regions of regional form. *Computational Mathematics and Information Technologies.* 2024;8(2):68–79. (In Russ.)
<https://doi.org/10.23947/2587-8999-2023-7-4-9-21>
10. Sidoryakina V.V., Solomaha D.A. Symmetrized versions of the Seidel and upper relaxation methods for solving two-dimensional difference problems of elliptic. *Computational Mathematics and Information Technologies.* 2023;7(3):12–19. (In Russ.) <https://doi.org/10.23947/2587-8999-2023-7-3-12-19>
11. Alekseev V.M., Galeev E.M., Tikhomirov V.M. *Collection of optimization problems: Theory. Examples. Problems.* Moscow: Fizmatlit; 2008. 256 p. (In Russ.)
12. Kolmogorov A.N., Fomin S.V. *Elements of the theory of functions and functional analysis. Textbook.* Moscow: Fizmatlit, 2012. 572 p. (In Russ.)

About the Authors:

Natalya K. Volosova, Post-graduate Student of Bauman Moscow State Technical University (2nd Baumanskaya St. 5–1, Moscow, 105005, Russian Federation), [ORCID](#), navalossova@yandex.ru

Konstantin A. Volosov, Doctor of Physical and Mathematical Sciences, Professor of the Department of Applied Mathematics of the Russian University of Transport (Obraztsova St. 9–9, Moscow, GSP-4, 127994, Russian Federation), [ORCID](#), [SPIN-code](#), konstantinvolosov@yandex.ru

Aleksandra K. Volosova, Candidate of Physical and Mathematical Sciences, Chief Analytical Department “Tramplin” LLC, Russian University of Transport (Obraztsova St. 9–9, Moscow, GSP-4, 127994, Russian Federation), [ORCID](#), [SPIN-code](#), alya01@yandex.ru

Mikhail I. Karlov, Candidate of Physical and Mathematical Sciences, Associate Professor of the Department of Mathematics, Moscow Institute of Physics and Technology (9, Institutsky Lane, GSP-4, Dolgoprudny, 141701, Russian Federation), [SPIN-code](#), karlov.mipt@gmail.com

Dmitriy F. Pastukhov, Candidate of Physical and Mathematical Sciences, Associate Professor of Polotsk State University (Blokhin St. 29, Novopolotsk, 211440, Republic of Belarus), [ORCID](#), [SPIN-code](#), dmitrij.pastuhov@mail.ru

Yuriy F. Pastukhov, Candidate of Physical and Mathematical Sciences, Associate Professor of Polotsk State University (Blokhin St. 29, Novopolotsk, 211440, Republic of Belarus), [ORCID](#), [SPIN-code](#), pulsar1900@mail.ru

Contributions of the authors:

N.K. Volosova: ideas; formulation or evolution of overarching research goals and aims.

K.A. Volosov: supervision; methodology.

A.K. Volosova: translation; study of the history of the task; literature.

M.I. Karlov: formal analysis.

D.F. Pastukhov: writing — original draft preparation; visualization; validation.

Yu.F. Pastukhov: software; testing of existing code components.

Conflict of Interest Statement: the authors declare no conflict of interest.

All authors have read and approved the final manuscript.

Об авторах:

Наталья Константиновна Волосова, аспирант Московского государственного технического университета им. Н.Э. Баумана (105005, Российская Федерация, г. Москва, ул. 2-я Бауманская, 5, стр. 1), [ORCID](#), navalossova@yandex.ru

Константин Александрович Волосов, доктор физико-математических наук, профессор кафедры прикладной математики Российского университета транспорта (127994, ГСП-4, Российская Федерация, г. Москва, ул. Образцова, 9, стр. 9), [ORCID](#), [SPIN-код](#), konstantinvolosov@yandex.ru

Александра Константиновна Волосова, кандидат физико-математических наук, начальник аналитического отдела ООО «Трамплин» Российского университета транспорта (127994, ГСП-4, Российская Федерация, г. Москва, ул. Образцова, 9, стр. 9), [ORCID](#), [SPIN-код](#), alya01@yandex.ru

Михаил Иванович Карлов, кандидат физико-математических наук, доцент кафедры математики Московского физико-технического института (141701, ГСП-4, Российская Федерация, г. Долгопрудный, Институтский переулок, 9), [Спин-код](#), karlov.mipt@gmail.com

Дмитрий Феликсович Пастухов, кандидат физико-математических наук, доцент кафедры технологий программирования Полоцкого государственного университета (211440, Республика Беларусь, г. Новополоцк, ул. Блохина, 29), [ORCID](#), [SPIN-код](#), dmitrij.pastuhov@mail.ru

Юрий Феликсович Пастухов, кандидат физико-математических наук, доцент кафедры технологий программирования Полоцкого государственного университета (211440, Республика Беларусь, г. Новополоцк, ул. Блохина, 29), [ORCID](#), [SPIN-код](#), pulsar1900@mail.ru

Заявленный вклад авторов:

Н.К. Волосова: постановка задачи; формулировка идей исследования, целей и задач.

К.А. Волосов: научное руководство; разработка методологии.

А.К. Волосова: перевод; изучение истории задачи; поиск литературы.

М.И. Карлов: формальный анализ.

Д.Ф. Пастухов: написание черновика рукописи; визуализация; валидация.

Ю.Ф. Пастухов: разработка программного обеспечения; тестирование существующих компонентов кода.

Конфликт интересов: авторы заявляют об отсутствии конфликта интересов.

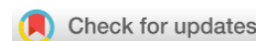
Все авторы прочитали и одобрили окончательный вариант рукописи.

Received / Поступила в редакцию 17.01.2025

Revised / Поступила после рецензирования 14.02.2025

Accepted / Принята к публикации 04.03.2025

COMPUTATIONAL MATHEMATICS ВЫЧИСЛИТЕЛЬНАЯ МАТЕМАТИКА



UDC 519.6

Original Theoretical Research

<https://doi.org/10.23947/2587-8999-2025-9-1-20-30>



Sufficient Conditions for the Convergence of Solutions of the Linearized Problem to the Solution of the Original Nonlinear Problem of Multifractional Sediment Transport in Shallow Water

Valentina V. Sidoryakina 

Don State Technical University, Rostov-on-Don, Russian Federation

✉ cvv9@mail.ru

Abstract

Introduction. This paper examines a two-dimensional spatial model of multifractional sediment transport, specifically focusing on shallow water zones. This process can be described using an initial-boundary value problem for a parabolic equation with nonlinear coefficients. The study employs a temporal grid linearization method with a step size τ , where nonlinear coefficients are calculated with a “lag” at the previous time layer. Previously, the well-posedness conditions for the linearized sediment transport problem were established, and a conservative and stable finite-difference scheme was developed and analyzed, with numerical implementations for both model and real-world problems (the Sea of Azov, the Taganrog Bay, and the Tsimlyansk Reservoir). However, the convergence of solutions of the linearized problem to the solution of the original nonlinear initial-boundary value problem for multifractional sediment transport had not yet been explored. The research results presented in this paper fill this gap. Earlier, the author, together with A.I. Sukhinov, conducted similar studies in the case where sediment fraction composition was not considered. These studies formed the basis for obtaining new results.

Materials and Methods. The derivation of inequalities guaranteeing the convergence of the solutions of a sequence of linearized problems to the solution of the original nonlinear problem is carried out using the method of mathematical induction, with the application of differential equation theory.

Results. The conditions for the convergence of solutions of the linearized multifractional sediment transport problem to the solution of the nonlinear problem in the Banach space L_1 norm at a rate $O(\tau)$ of are determined.

Discussion and Conclusion. The obtained research results can be used for forecasting nonlinear hydrophysical processes, improving their accuracy and reliability due to the new functional capabilities that account for physically significant factors.

Keywords: two-dimensional spatial sediment transport model, multifractional sediment composition, shallow water zone, nonlinear problem, linearized problem

Funding. This research was supported by a grant from the Russian Science Foundation No. 25–11–68060, <https://rscf.ru/project/25-11-68060>

For Citation. Sidoryakina V.V. Sufficient conditions for the convergence of solutions of the linearized problem to the solution of the original nonlinear problem of transport of multifractional sediments in the shallow water zone. *Computational Mathematics and Information Technologies*. 2025;9(1):20–30. <https://doi.org/10.23947/2587-8999-2025-9-1-20-30>

Достаточные условия сходимости решений линейризованной задачи к решению исходной нелинейной задачи транспорта многофракционных наносов в зоне мелководья

В.В. Сидорякина 

Донской государственный технический университет, г. Ростов-на-Дону, Российская Федерация

✉ cvv9@mail.ru

Аннотация

Введение. Рассматривается пространственно-двумерная модель транспорта наносов многофракционного состава, ориентированная на зоны мелководья. Для описания этого процесса может быть использована начально-краевая задача для параболического уравнения с нелинейными коэффициентами. Ее исследование проводится с помощью линейризации на временной сетке с шагом τ , при которой нелинейные коэффициенты рассчитываются «с запаздыванием» на предыдущем временном слое. Для линейризованной задачи транспорта многофракционных наносов ранее были определены условия корректности, построена и исследована консервативная устойчивая разностная схема, численно реализованная для модельных и реальных задач (Азовское море и Таганрогский залив, Цимлянское водохранилище). Однако вопросы сходимости решений линейризованной задачи к решению исходной нелинейной начально-краевой задачи транспорта многофракционных наносов пока оставались не рассмотренными. Результаты исследований, представленные в данной работе, восполняют этот пробел. Ранее автором совместно с А.И. Сухиновым удалось провести аналогичные исследования для случая, когда фракционный состав наносов не учитывается. Эти исследования легли в основу для получения нового результата.

Материалы и методы. Получение неравенств, гарантирующих сходимость решений цепочки линейризованных задач к решению исходных нелинейных задач, проводится методом математической индукции с привлечением теории дифференциальных уравнений.

Результаты исследования. Определены условия сходимости решений линейризованной задачи транспорта наносов многофракционного состава к решению нелинейной задачи в норме банахового пространства L_1 со скоростью $O(\tau)$.

Обсуждение и заключение. Полученные результаты исследования могут быть использованы при прогнозировании нелинейных гидрофизических процессов, повышении их точности и надежности в силу наличия новых функциональных возможностей учета физически важных факторов.

Ключевые слова: пространственно-двумерная модель транспорта наносов, многофракционный состав наносов, зона мелководья, нелинейная задача, линейризованная задача

Финансирование. Исследование выполнено за счет гранта Российского научного фонда № 25–11–68060, <https://rscf.ru/project/25-11-68060>

Для цитирования. Сидорякина В.В. Достаточные условия сходимости решений линейризованной задачи к решению исходной нелинейной задачи транспорта многофракционных наносов в зоне мелководья. *Computational Mathematics and Information Technologies*. 2025;9(1):20–30. <https://doi.org/10.23947/2587-8999-2025-9-1-20-30>

Introduction. One of the important and complex problems in studying sediment transport in shallow water zones is accounting for its fractional composition. The fractional composition of sediments varies significantly depending on the slope and morphological structure of the seabed, depth, flow velocity, bed surface roughness, and other factors. Differences in fractional composition determine the nature of sediment movement and sedimentation processes. Considering particle size in mathematical modeling of sediment transport enables more accurate and reliable predictions of seabed morphodynamics.

This study examines a nonlinear 2D model of sediment transport that takes into account its fractional composition [1–4]. To analyze this model, a linearization is performed on a time grid with step size τ , where nonlinear coefficients are computed with a “lag” from the previous time step. Using the method of mathematical induction and differential equation theory, sufficient conditions for the convergence of solutions of the linearized problem to the solution of the original nonlinear initial-boundary value problem are determined. It is worth noting that previous studies have ensured the well-posedness of this problem.

The existence and uniqueness of solutions to the linearized multifractional sediment transport problem were studied in [3]. The work [4] demonstrated the continuous dependence of the solutions of the linearized multifractional sediment transport problem on the input data. Research on the well-posedness of the linearized sediment transport problem, which does not account for heterogeneous fractional composition, is presented in [5–8].

Materials and Methods. The sediment transport equation, including R fractions, is written as:

$$(1 - \tilde{\varepsilon}) \frac{\partial H}{\partial t} + \sum_{r=1}^R \operatorname{div}(V_r k_r \vec{\tau}_b) = \sum_{r=1}^R \operatorname{div} \left(V_r k_r \frac{\tau_{bc,r}}{\sin \varphi_0} \operatorname{grad} H \right) - \sum_{r=1}^R \frac{w + w_{g,r}}{\rho_r} c_r, \quad r = \overline{1, R}, \quad (1)$$

where $H = H(x, y, t)$ is the water body depth; $\tilde{\varepsilon}$ is the porosity of bottom sediments averaged over all components; t is the time variable, $t \in [0, T]$; V_r volume fraction of the r -th component; $\vec{\tau}_b$ is the vector of tangential shear stress at the bottom of the water body; $\tau_{bc,r}$ is the critical value of tangential stress for the r -th sediment component, $\tau_{bc,r} = a_r \sin \varphi_0$ where a_r is the coefficient for the r -th sediment component, φ_0 is the angle of natural slope of the ground in the water body; w is the vertical component of the velocity vector \vec{U} of the water medium; $w_{g,r}$ is the hydraulic size or settling velocity of the r -th component; ρ_r is the density of the r -th bottom material component; c_r is the concentration of the r -th suspended fraction; k_r is the coefficient determined by the relation:

$$k_r = k_r(H, x, y, t) = \frac{A \tilde{\omega} d_r}{((\rho_r - \rho_0) g d_r)^\beta} \left| \vec{\tau}_b - \frac{\tau_{bc,r}}{\sin \varphi_0} \operatorname{grad} H \right|^{\beta-1},$$

($\tilde{\omega}$ is the average wave frequency; d_r is the characteristic size of the r -th component; g is the gravitational acceleration; ρ_0 is the density of the water medium; A and β are the dimensionless constants),

$$k_r \geq k_{0,r} = \text{const} > 0, \quad \forall (x, y) \in \overline{G}, \quad r = \overline{1, R}, \quad 0 < t \leq T.$$

We assume that $\Pi_T = G \times (0, T)$ is the domain where equation (1) is defined. Let the sediment transport process take place in the domain with the boundary Γ , which represents a piecewise-smooth curve.

The boundary of this cylinder consists of the lateral surface $\Gamma \times [0, T]$ and two bases — $\overline{G} \times \{0\}$ and $\overline{G} \times \{T\}$.

Equation (1) is considered in the domain $G(x, y) = \{0 < x < L_x, 0 < y < L_y\}$ (Fig. 1).

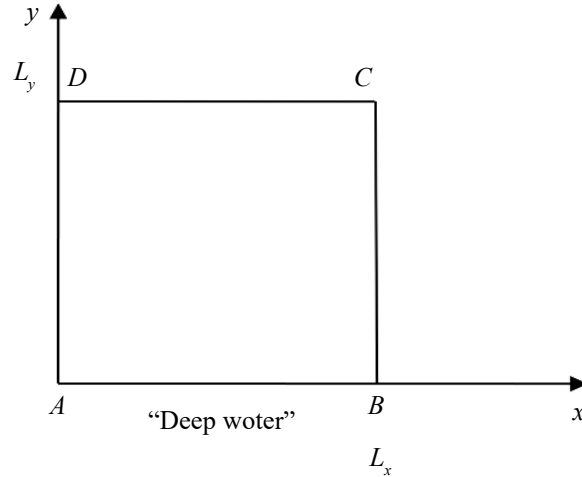


Fig. 1. Computational domain

We supplement equation (1) with initial and boundary conditions:

$$H(x, y, 0) = H_0(x, y), \quad H_0(x, y) \in C^2(G) \cap C(\overline{G}), \quad (2)$$

$$AD: \quad H(0, y, t) = H_1(y, t), \quad (3)$$

$$BC: \quad H(L_x, y, t) = H_2(y, t), \quad (4)$$

$$AB: \quad H(x, 0, t) = H_3(x), \quad (5)$$

$$CD: \quad H(x, L_y, t) = H_4(x, t) \geq c_0 \equiv \text{const} > 0, \quad L'_y < L_y. \quad (6)$$

Additionally, we assume:

$$AB: \quad |\vec{\tau}_b| = 0, \quad (7)$$

$$\operatorname{grad}_{(x,y)} H \in C(\overline{U}_T) \cap C^1(U_T), \quad \operatorname{grad}_{(x,y)} H_0 \in C(\overline{G}), \quad (8)$$

$$\frac{\partial H}{\partial x} \Big|_{x=0} = \frac{\partial H}{\partial x} \Big|_{x=L_x} = 0, \quad (9)$$

$$k_r \geq k_{0,r} = \text{const} > 0, \forall (x, y) \in \bar{G}, \quad (10)$$

$$\vec{\tau}_b = \tau_{bx} \vec{i} + \tau_{by} \vec{j}, |\tau_{bx}| \leq c_1, |\tau_{by}| \leq c_2, c_1 = \text{const}, c_2 = \text{const}. \quad (11)$$

The condition

$$H(x, y, t) \geq c_0 \equiv \text{const} > 0, 0 \leq x \leq L_x, 0 \leq y \leq L'_y, 0 \leq t \leq T. \quad (12)$$

ensures that no drying occurs in the considered domain.

Linearization of problem (1)–(6) is performed on a time grid:

$$\omega_\tau = \{t_n = n\tau, n = 0, 1, \dots, N_t, N_t \tau = T\},$$

using the methods presented in [5–10].

After linearization, equation (1) and the initial conditions (2) are written as:

$$(1 - \tilde{\varepsilon}) \frac{\partial H^{(n)}}{\partial t} = \sum_{r=1}^R \text{div} \left(V_r k_r^{(n-1)} \frac{\tau_{bc,r}}{\sin \varphi_0} \text{grad} H^{(n)} \right) - \sum_{r=1}^R \text{div} (V_r k_r^{(n-1)} \vec{\tau}_b) - \sum_{r=1}^R \frac{w + w_{g,r}}{\rho_r} c_r, \quad (13)$$

$$r = \overline{1, R}, t_{n-1} < t \leq t_n, n = 1, 2, \dots, N_t,$$

$$H^{(1)}(x, y, t_0) = H_0(x, y), H^{(n)}(x, y, t_{n-1}) = H^{(n-1)}(x, y, t_{n-1}), (x, y) \in \bar{G}, n = 2, \dots, N_t. \quad (14)$$

The coefficient $k_r^{(n-1)}$ in equation (14) is determined by the equation:

$$k_r^{(n-1)} = k_r^{(n-1)}(H^{(n-1)}, x, y, t) = \frac{A \tilde{\omega} d_r}{((\rho_r - \rho_0) g d_r)^\beta} \left| \vec{\tau}_b - \frac{\tau_{bc,r}}{\sin \varphi_0} \text{grad} H^{(n-1)}(x, y, t_{n-1}) \right|^{\beta-1}.$$

Results. We will show that the solution of problem (13), (14), (3)–(6) converges to the solution of the nonlinear problem (1)–(6) in the norm of the space $L_1(G \times [0, T])$ as $\tau \rightarrow 0, N_t \tau = T$.

Let us denote the solution of the nonlinear problem as $H_{np}(x, y, t), (x, y) \in \bar{G}$, and the solution of the linearized problem as $H_{lp}(x, y, t), (x, y) \in \bar{G}$. Note that for each time layer, its own solution function $H_{lp} = (x, y, t)$ is defined, and in general, the linearized problem constructs a family of solutions $\{H_{lp}^{(n)}(x, y, t)\}, n = 1, 2, \dots, N_t$, that depends on the parameter τ .

We assume that:

1. The function $H_{np} = (x, y, t)$ is bounded on the interval $0 < t \leq T$;
2. The derivatives exist and are bounded:

$$\frac{\partial}{\partial x} \left(\text{grad} \left(\frac{\partial H_{np}}{\partial t} \right) \right), \frac{\partial}{\partial y} \left(\text{grad} \left(\frac{\partial H_{np}}{\partial t} \right) \right), \frac{\partial}{\partial x} \left(\text{grad} \left(\frac{\partial H_{lp}}{\partial t} \right) \right), \frac{\partial}{\partial y} \left(\text{grad} \left(\frac{\partial H_{lp}}{\partial t} \right) \right);$$

3. The expression $\frac{w + w_{g,r}}{\rho_r} c_r$ is bounded.

Substituting the function $H_{np} = (x, y, t)$ into equation (1) and the function $H_{lp} = (x, y, t)$ into equation (12), we obtain:

$$(1 - \tilde{\varepsilon}) \frac{\partial H_{np}}{\partial t} = \sum_{r=1}^R \text{div} \left(V_r k_{np,r} \frac{\tau_{bc,r}}{\sin \varphi_0} \text{grad} H_{np} \right) - \sum_{r=1}^R \text{div} (V_r k_r \vec{\tau}_b) - \sum_{r=1}^R \frac{w + w_{g,r}}{\rho_r} c_r, r = \overline{1, R}. \quad (15)$$

$$(1 - \tilde{\varepsilon}) \frac{\partial H_{lp}^{(n)}}{\partial t} = \sum_{r=1}^R \text{div} \left(V_r k_{lp,r}^{(n-1)} \frac{\tau_{bc,r}}{\sin \varphi_0} \text{grad} H_{lp}^{(n)} \right) - \sum_{r=1}^R \text{div} (V_r k_{lp,r}^{(n-1)} \vec{\tau}_b) - \sum_{r=1}^R \frac{w + w_{g,r}}{\rho_r} c_r, \quad (16)$$

$$r = \overline{1, R}, t_{n-1} < t \leq t_n, n = 1, 2, \dots, N_t,$$

where

$$k_{np,r} = k_{np,r}(H_{np}, x, y, t) = \frac{A \tilde{\omega} d_r}{((\rho_r - \rho_0) g d_r)^\beta} \left| \vec{\tau}_b - \frac{\tau_{bc,r}}{\sin \varphi_0} \text{grad} H_{np}(x, y, t) \right|^{\beta-1},$$

$$k_{lp,r}^{(n-1)} = k_{lp,r}^{(n-1)}(H_{lp}^{(n-1)}, x, y, t) = \frac{A \tilde{\omega} d_r}{((\rho_r - \rho_0) g d_r)^\beta} \left| \vec{\tau}_b - \frac{\tau_{bc,r}}{\sin \varphi_0} \text{grad} H_{lp}^{(n-1)}(x, y, t) \right|^{\beta-1}.$$

Multiplying both sides of equations (15) and (16) by the functions $H_{np}(x, y, t), H_{lp}^{(n)} = H_{lp}^{(n)}(x, y, t), (x, y) \in \bar{G}$, respectively, and integrating the resulting expressions over the variables $t, 0 < t \leq T$ и (x, y) in the domain G followed by some straightforward transformations, we can write:

$$\frac{1}{2}(1-\tilde{\varepsilon})\iint_G(H_{np}^2(x,y,T)-H_{np}^2(x,y,0))dxdy = \sum_{r=1}^R\int_0^T\left(\iint_G H_{np}\operatorname{div}\left(V_r k_{np,r}\frac{\tau_{bc,r}}{\sin\varphi_0}\operatorname{grad}H_{np}\right)dxdy\right)dt - \sum_{r=1}^R\int_0^T\left(\iint_G H_{np}\operatorname{div}(V_r k_{np,r}\vec{\tau}_b)dxdy\right)dt - \sum_{r=1}^R\int_0^T\left(\iint_G H_{np}\frac{w+w_{g,r}}{\rho_r}c_r\right)dt. \quad (17)$$

$$(1-\tilde{\varepsilon})\int_{t_{n-1}}^{t_n}\left(\iint_G H_{lp}^{(n)}\frac{\partial H_{lp}^{(n)}}{\partial t}dxdy\right)dt = \sum_{r=1}^R\int_{t_{n-1}}^{t_n}\left(\iint_G H_{lp}^{(n)}\operatorname{div}\left(V_r k_{lp,r}^{(n-1)}\frac{\tau_{bc,r}}{\sin\varphi_0}\operatorname{grad}H_{lp}^{(n)}\right)dxdy\right)dt - \sum_{r=1}^R\int_{t_{n-1}}^{t_n}\left(\iint_G H_{lp}^{(n)}\operatorname{div}(V_r k_{lp,r}^{(n-1)}\vec{\tau}_b)dxdy\right)dt - \sum_{r=1}^R\int_0^T\left(\iint_G H_{lp}^{(n)}\frac{w+w_{g,r}}{\rho_r}c_r\right)dt, \quad r = \overline{1, R}. \quad (18)$$

Summing both sides of relation (18) over $n, n = 1, \dots, N$, we obtain:

$$(1-\tilde{\varepsilon})\iint_G\left(\sum_{n=1}^N\int_{t_{n-1}}^{t_n}H_{lp}^{(n)}\frac{\partial H_{lp}^{(n)}}{\partial t}dt\right)dxdy = \sum_{r=1}^R\sum_{n=1}^N\left[\int_{t_{n-1}}^{t_n}\iint_G H_{lp}^{(n)}\operatorname{div}\left(V_r k_{lp,r}^{(n-1)}\frac{\tau_{bc,r}}{\sin\varphi_0}\operatorname{grad}H_{lp}^{(n)}\right)dxdy\right]dt - \int_{t_{n-1}}^{t_n}\left(\iint_G H_{lp}^{(n)}\operatorname{div}(V_r k_{lp,r}^{(n-1)}\vec{\tau}_b)dxdy\right)dt - \int_{t_{n-1}}^{t_n}\left(\iint_G H_{lp}^{(n)}\frac{w+w_{g,r}}{\rho_r}c_r dxdy\right)dt. \quad (19)$$

By transforming the left-hand side of equality (19), we write:

$$\frac{1}{2}(1-\tilde{\varepsilon})\iint_G(H_{lp}^2(x,y,T)-H_{lp}^2(x,y,0))dxdy = \sum_{r=1}^R\sum_{n=1}^N\left[\int_{t_{n-1}}^{t_n}\iint_G H_{lp}^{(n)}\operatorname{div}\left(V_r k_{lp,r}^{(n-1)}\frac{\tau_{bc,r}}{\sin\varphi_0}\operatorname{grad}H_{lp}^{(n)}\right)dxdy\right]dt - \int_{t_{n-1}}^{t_n}\left(\iint_G H_{lp}^{(n)}\operatorname{div}(V_r k_{lp,r}^{(n-1)}\vec{\tau}_b)dxdy\right)dt - \int_{t_{n-1}}^{t_n}\left(\iint_G H_{lp}^{(n)}\frac{w+w_{g,r}}{\rho_r}c_r dxdy\right)dt. \quad (20)$$

Subtracting expression (20) from equality (17) and considering that $H_{np} = (x,y,t) = H_{lp} = (x,y,t), H_{lp} = (x,y,t) = H_{lp}^{(0)}$, we obtain:

$$\begin{aligned} & \frac{1}{2}(1-\tilde{\varepsilon})\iint_G(H_{np}^2(x,y,T)-H_{lp}^2(x,y,T))dxdy = \\ & = \sum_{r=1}^R\int_0^T\left(\iint_G H_{np}\operatorname{div}\left(V_r k_{np,r}\frac{\tau_{bc,r}}{\sin\varphi_0}\operatorname{grad}H_{np}\right)dxdy\right)dt - \sum_{r=1}^R\int_0^T\left(\iint_G H_{np}\operatorname{div}(V_r k_{np,r}\vec{\tau}_b)dxdy\right)dt - \\ & - \sum_{r=1}^R\int_0^T\left(\iint_G H_{np}\frac{w+w_{g,r}}{\rho_r}c_r\right)dt - \sum_{r=1}^R\sum_{n=1}^N\left[\int_{t_{n-1}}^{t_n}\iint_G H_{lp}^{(n)}\operatorname{div}\left(V_r k_{lp,r}^{(n-1)}\frac{\tau_{bc,r}}{\sin\varphi_0}\operatorname{grad}H_{lp}^{(n)}\right)dxdy\right]dt + \\ & + \int_{t_{n-1}}^{t_n}\left(\iint_G H_{lp}^{(n)}\operatorname{div}(V_r k_{lp,r}^{(n-1)}\vec{\tau}_b)dxdy\right)dt + \int_{t_{n-1}}^{t_n}\left(\iint_G H_{lp}^{(n)}\frac{w+w_{g,r}}{\rho_r}c_r dxdy\right)dt. \end{aligned} \quad (21)$$

We perform transformations on the right-hand side of equality (21). To do this, we add and then subtract the expressions $H_{lp}^{(n)}\operatorname{div}\left(V_r k_{np,r}\frac{\tau_{bc,r}}{\sin\varphi_0}\operatorname{grad}H_{np}\right), H_{lp}^{(n)}\operatorname{div}(V_r k_{np,r}\vec{\tau}_b)$ under the integral sign, respectively, in the fourth and fifth terms of the right-hand side of equality (21).

Combining the terms, we obtain:

$$\begin{aligned} & \frac{1}{2}(1-\tilde{\varepsilon})\iint_G(H_{np}^2(x,y,T)-H_{lp}^2(x,y,T))dxdy = \\ & = \sum_{r=1}^R\sum_{n=1}^N\int_{t_{n-1}}^{t_n}\left[\iint_G(H_{np}-H_{lp}^{(n)})\operatorname{div}\left(V_r k_{np,r}\frac{\tau_{bc,r}}{\sin\varphi_0}\operatorname{grad}H_{np}\right)dxdy\right] + \iint_G H_{lp}^{(n)}\operatorname{div}\left(V_r\frac{\tau_{bc,r}}{\sin\varphi_0}\cdot\right. \\ & \cdot(k_{np,r}\operatorname{grad}H_{np}-k_{lp,r}^{(n-1)}\operatorname{grad}H_{lp}^{(n)})dxdy + \iint_G(H_{lp}^{(n)}-H_{np})\operatorname{div}(V_r k_{np,r}\vec{\tau}_b)dxdy + \\ & \left. + \iint_G H_{lp}^{(n)}\operatorname{div}(V_r(k_{lp,r}^{(n-1)}-k_{r,np})\vec{\tau}_b)dxdy + \iint_G(H_{lp}^{(n)}-H_{np})\frac{w+w_{g,r}}{\rho_r}c_r dxdy\right]dt. \end{aligned} \quad (22)$$

We estimate each of the integrals on the right-hand side of equality (22) under the summation sign. For this purpose, we use the reasoning detailed in [9].

Let us introduce the following notation:

$$I_{1,r}^n = \int_{t_{n-1}}^{t_n} \left(\iint_G (H_{np} - H_{lp}^{(n)}) \operatorname{div} \left(V_r k_{np,r} \frac{\tau_{bc,r}}{\sin \varphi_0} \operatorname{grad} H_{np} \right) dx dy \right) dt, \quad (23)$$

$$I_{2,r}^n = \int_{t_{n-1}}^{t_n} \left(\iint_G H_{lp}^{(n)} \operatorname{div} \left(V_r \frac{\tau_{bc,r}}{\sin \varphi_0} (k_{np,r} \operatorname{grad} H_{np} - k_{lp,r}^{(n-1)} \operatorname{grad} H_{lp}^{(n)}) \right) dx dy \right) dt, \quad (24)$$

$$I_{3,r}^n = \int_{t_{n-1}}^{t_n} \left(\iint_G (H_{lp}^{(n)} - H_{np}) \operatorname{div} (V_r k_{np,r} \vec{\tau}_b) dx dy \right) dt, \quad (25)$$

$$I_{4,r}^n = \int_{t_{n-1}}^{t_n} \left(\iint_G H_{lp}^{(n)} \operatorname{div} (V_r (k_{lp,r}^{(n-1)} - k_{np,r}) \vec{\tau}_b) dx dy \right) dt, \quad (26)$$

$$I_{5,r}^n = \int_{t_{n-1}}^{t_n} \left(\iint_G (H_{lp}^{(n)} - H_{np}) \frac{w + w_{g,r}}{\rho_r} c_r dx dy \right) dt, \quad n = 1, \dots, N. \quad (27)$$

For $n = 1$ for integrals (23)–(27), we obtain:

$$\begin{aligned} I_{1,r}^1 &\leq \frac{1}{2} \tau^2 L_x L_y M_{1,r}^1, & I_{2,r}^1 &\leq \frac{1}{2} \tau^2 M_{2,r}^1 L_x L_y, & I_{3,r}^1 &\leq \frac{1}{2} \tau^2 L_x L_y M_{3,r}^1, \\ I_{4,r}^1 &\leq \frac{1}{2} \tau^2 M_{4,r}^1 L_x L_y, & I_{5,r}^1 &\leq \frac{1}{2} \tau^2 L_x L_y M_{5,r}^1, \end{aligned} \quad (28)$$

where

$$\begin{aligned} M_{1,r}^1 &\equiv \max_{t_0 \leq t \leq t_1} \left\{ \max_{(x,y) \in G} \left| \left(\frac{\partial H_{np}}{\partial t}(x,y,\xi_1) - \frac{\partial H_{lp}^{(1)}}{\partial t}(x,y,\xi_2) \right) \operatorname{div} \left(V_r k_{np,r} \frac{\tau_{bc,r}}{\sin \varphi_0} \operatorname{grad} H_{np} \right) \right| \right\}, \\ M_{2,r}^1 &\equiv \max_{t_0 \leq t \leq t_1} \left\{ \max_{(x,y) \in G} \left| \left| H_{lp}^{(1)} \operatorname{div} \left(V_r \frac{\tau_{bc,r}}{\sin \varphi_0} \left(\frac{\partial k_{np,r}}{\partial t}(x,y,\xi_3) \operatorname{grad} H_{np} + k_{lp,r}^{(0)} \operatorname{grad} \frac{\partial H_{np}}{\partial t}(x,y,\xi_4) \right) \right) \right| \right| dx dy \right\}, \\ M_{3,r}^1 &\equiv \max_{t_0 \leq t \leq t_1} \left\{ \max_{(x,y) \in G} \left| \left(\frac{\partial H_{lp}^{(1)}}{\partial t}(x,y,\xi_5) - \frac{\partial H_{np}}{\partial t}(x,y,\xi_6) \right) \operatorname{div} (V_r k_{np,r} \vec{\tau}_b) \right| \right\}, \\ M_{4,r}^1 &\equiv \max_{t_0 \leq t \leq t_1} \left\{ \max_{(x,y) \in G} \left| \left| H_{lp}^{(1)} \operatorname{div} \left(V_r \left(-\frac{\partial k_{np,r}}{\partial t}(x,y,\xi_7) \right) \vec{\tau}_b \right) \right| \right| \right\}, \\ M_{5,r}^1 &\equiv \max_{t_0 \leq t \leq t_1} \left\{ \max_{(x,y) \in G} \left| \left(\frac{\partial H_{lp}^{(1)}}{\partial t}(x,y,\xi_5) - \frac{\partial H_{np}}{\partial t}(x,y,\xi_6) \right) \frac{w + w_{g,r}}{\rho_r} c_r \right| \right\}, \\ &t_0 < \xi_1, \xi_2, \xi_3, \xi_4, \xi_5, \xi_6, \xi_7 \leq t_1, \quad t_0 < t \leq t_1. \end{aligned}$$

Considering the obtained estimates (28) and using the triangle inequality for the magnitudes of the quantities, we obtain an inequality of the form:

$$\iint_G (H_{np}^2(x,y,t_1) - H_{lp}^{(1)2}(x,y,t_1)) dx dy \leq \tau^2 L_x L_y \sum_{r=1}^R M_{1,r}^*, \quad (29)$$

where

$$M_{1,r}^* = \frac{1}{1 - \varepsilon} (M_{1,r}^1 + M_{2,r}^1 + M_{3,r}^1 + M_{4,r}^1 + M_{5,r}^1).$$

By swapping the functions $H_{np}^2(x,y,t_1)$ и $H_{lp}^{(1)2}(x,y,t_1)$ and following reasoning analogous to the one given above, we can obtain an estimate:

$$\iint_G (H_{lp}^{(1)2}(x,y,t_1) - H_{np}^2(x,y,t_1)) dx dy \leq \tau^2 L_x L_y \sum_{r=1}^R M_{1,r}^*. \quad (30)$$

From inequalities (29) and (30), we get the following inequality:

$$\iint_G \left| H_{lp}^{(1)2}(x, y, t_1) - H_{np}^2(x, y, t_1) \right| dx dy \leq \tau^2 L_x L_y \sum_{r=1}^R M_{1,r}^*. \tag{31}$$

We transform the left-hand side of inequality (31):

$$\begin{aligned} \iint_G \left| H_{lp}^{(1)2}(x, y, t_1) - H_{np}^2(x, y, t_1) \right| dx dy &= \iint_G \left| H_{lp}^{(1)}(x, y, t_1) - H_{np}(x, y, t_1) \right| \\ &\cdot \left| H_{lp}^{(1)}(x, y, t_1) + H_{np}(x, y, t_1) \right| dx dy. \end{aligned} \tag{32}$$

Next, we will assume that an inequality of the form (12) holds for the functions $H_{np} = (x, y, t)$ and $H_{lp}^{(1)}$, i. e.

$$H_{np}(x, y, t) \geq c_0 > 0, (x, y) \in \bar{G}, \quad 0 \leq t \leq T, \tag{33}$$

$$H_{lp}^{(1)}(x, y, t) \geq c_0 > 0, (x, y) \in \bar{G}, \quad 0 \leq t \leq T. \tag{34}$$

Considering expressions (33)–(34), we obtain:

$$\iint_G \left| H_{lp}^{(1)2}(x, y, t_1) - H_{np}^2(x, y, t_1) \right| dx dy \geq 2c_0 \iint_G \left| H_{lp}^{(1)}(x, y, t_1) - H_{np}(x, y, t_1) \right| dx dy. \tag{35}$$

From relations (31), (32), and (35), we get the following estimate:

$$\iint_G \left| H_{lp}^{(1)}(x, y, t_1) - H_{np}(x, y, t_1) \right| dx dy \leq \frac{1}{2c_0} \tau^2 L_x L_y \sum_{r=1}^R M_{1,r}^*. \tag{36}$$

The required estimate for $n = 1$ is obtained, since inequality (36) is equivalent to a relation of the form:

$$\left\| H_{lp}^{(1)}(x, y, t_1) - H_{np}(x, y, t_1) \right\|_{L_1(G \times [t_0, t_1])} \leq \frac{1}{2c_0} \tau^2 L_x L_y \sum_{r=1}^R M_{1,r}^*, \tag{37}$$

where

$$\left\| Q(x, y, t) \right\|_{L_1(G \times [t_0, t_1])} \equiv \int_{t_0}^{t_1} \left(\iint_G |Q(x, y, t)| dx dy \right) dt.$$

For $n = 2$ for integrals (23)–(27), we obtain:

$$\begin{aligned} I_{1,r}^2 &\leq \frac{1}{2} \tau^2 L_x L_y \left(\frac{1}{c_0} \tau M_{1,r}^* M_{1,r}^2 + M_{2,r}^2 \right), \quad I_{2,r}^2 \leq \frac{1}{2} \tau^2 L_x L_y M_{3,r}^2 M_{4,r}^2, \quad I_{3,r}^2 \leq \frac{1}{2} \tau^2 L_x L_y \left(\frac{1}{c_0} \tau M_{1,r}^* M_{5,r}^2 + M_{6,r}^2 \right), \\ I_{4,r}^2 &\leq \frac{1}{2} \tau^2 L_x L_y M_{3,r}^2 M_{7,r}^2, \quad I_{5,r}^2 \leq \frac{1}{2} \tau^2 L_x L_y \left(\frac{1}{c_0} \tau M_{1,r}^* M_{8,r}^2 + M_{9,r}^2 \right), \end{aligned} \tag{38}$$

where

$$\begin{aligned} M_{1,r}^2 &\equiv \max_{t_1 \leq t \leq t_2} \left\{ \max_{(x,y) \in \bar{G}} \left| \operatorname{div} \left(V_r k_{np,r} \frac{\tau_{bc,r}}{\sin \varphi_0} \operatorname{grad} H_{np} \right) \right| \right\}, \\ M_{2,r}^2 &\equiv \max_{t_1 \leq t \leq t_2} \left\{ \max_{(x,y) \in \bar{G}} \left| \left(\frac{\partial H_{np}(x, y, \xi_1)}{\partial t} - \frac{\partial H_{lp}^{(2)}(x, y, \xi_2)}{\partial t} \right) \operatorname{div} \left(V_r k_{np,r} \frac{\tau_{bc,r}}{\sin \varphi_0} \operatorname{grad} H_{np} \right) \right| \right\}, \\ M_{3,r}^2 &\equiv \max_{t_1 \leq t \leq t_2} \left\{ \max_{(x,y) \in \bar{G}} \left\{ \left| H_{lp}^{(2)} \right| \right\} \right\}, \\ M_{4,r}^2 &= M_{21,r}^2 + M_{22,r}^2 + M_{23,r}^2 + M_{24,r}^2 + M_{25,r}^2 + M_{26,r}^2, \\ M_{5,r}^2 &\equiv \max_{t_1 \leq t \leq t_2} \left\{ \max_{(x,y) \in \bar{G}} \left| \operatorname{div} (V_r k_{np,r} \vec{\tau}_b) \right| \right\}, \\ M_{6,r}^2 &\equiv \max_{t_1 \leq t \leq t_2} \left\{ \max_{(x,y) \in \bar{G}} \left| \left(\frac{\partial H_{np}(x, y, \xi_1)}{\partial t} - \frac{\partial H_{lp}^{(2)}(x, y, \xi_2)}{\partial t} \right) \operatorname{div} (V_r k_{np,r} \vec{\tau}_b) \right| \right\}, \\ M_{7,r}^2 &= M_{31,r}^2 + M_{32,r}^2 + M_{33,r}^2, \end{aligned}$$

$$M_{8,r}^2 \equiv \max_{t_1 \leq t \leq t_2} \left\{ \max_{(x,y) \in \bar{G}} \left| \frac{w + w_{g,r}}{\rho_r} c_r \right| \right\},$$

$$M_{9,r}^2 \equiv \max_{t_1 \leq t \leq t_2} \left\{ \max_{(x,y) \in \bar{G}} \left| \left(\frac{\partial H_{np}(x,y,\xi_1)}{\partial t} - \frac{\partial H_{lp}^{(2)}(x,y,\xi_2)}{\partial t} \right) \frac{w + w_{g,r}}{\rho_r} c_r \right| \right\},$$

$$M_{7,r}^2 = M_{31,r}^2 + M_{32,r}^2 + M_{33,r}^2,$$

$$M_{11,r}^2 \equiv \max_{t_1 \leq t \leq t_2} \left\{ \max_{x \in BC} \left| \tau_{bx} \frac{\partial H_2(y,t)}{\partial x} + \tau_{bx}^{(1)} \frac{\partial H_2(y,t_1)}{\partial x} \right| \right\}, \quad M_{12,r}^2 \equiv \max_{t_1 \leq t \leq t_2} \left\{ \max_{y \in BC} \left| \tau_{by} \frac{\partial H_2(y,t)}{\partial y} + \tau_{by}^{(1)} \frac{\partial H_2(y,t_1)}{\partial y} \right| \right\},$$

$$M_{13,r}^2 \equiv \max_{t_1 \leq t \leq t_2} \left\{ \max_{x \in CD} \left| \frac{\partial H_4(x,t)}{\partial x} + \frac{\partial H_4(x,t_1)}{\partial x} \right| \right\}, \quad M_{14,r}^2 \equiv \max_{t_1 \leq t \leq t_2} \left\{ \max_{x \in CD} \left| \frac{\partial H_4(x,t)}{\partial y} + \frac{\partial H_4(x,t_1)}{\partial y} \right| \right\},$$

$$M_{15,r}^2 \equiv \max_{t_1 \leq t \leq t_2} \left\{ \max_{x \in AD} \left| \frac{\partial H_1(y,t)}{\partial x} + \frac{\partial H_1(y,t_1)}{\partial x} \right| \right\}, \quad M_{16,r}^2 \equiv \max_{t_1 \leq t \leq t_2} \left\{ \max_{y \in AD} \left| \frac{\partial H_1(y,t)}{\partial y} + \frac{\partial H_1(y,t_1)}{\partial y} \right| \right\},$$

$$M_{21,r}^2 \equiv \max_{t_1 \leq t \leq t_2} \left\{ \max_{y \in BC} \left| V_r \frac{\tau_{bc,r}^2}{\sin^2 \varphi_0} \frac{A\tilde{\omega}d_r}{((\rho_r - \rho_0)gd_r)^3} \left[\frac{\partial}{\partial x} \left(\frac{\partial H_2(y,\xi_4)}{\partial t} \right) \left(\frac{\tau_{bc,r}}{\sin \varphi_0} M_{11,r}^2 - 2\tau_{bx} \right) + \right. \right. \right. \\ \left. \left. \left. + \frac{\partial}{\partial y} \left(\frac{\partial H_2(y,\xi_4)}{\partial t} \right) \left(\frac{\tau_{bc,r}}{\sin \varphi_0} M_{12,r}^2 - 2\tau_{by} \right) \right] \frac{\partial H_2(y,t_1)}{\partial x} \right| \right\},$$

$$M_{22,r}^2 \equiv \max_{t_1 \leq t \leq t_2} \left\{ \max_{y \in BC} \left| k_{np,r} \frac{\partial}{\partial x} \left(\frac{\partial H_2(y,\xi_4)}{\partial t} \right) \right| \right\},$$

$$M_{23,r}^2 \equiv \max_{t_1 \leq t \leq t_2} \left\{ \max_{x \in CD} \left| V_r \frac{\tau_{bc,r}^2}{\sin^2 \varphi_0} \frac{A\tilde{\omega}d_r}{((\rho_r - \rho_0)gd_r)^3} (t - t_1) \left[\frac{\partial}{\partial x} \left(\frac{\partial H_4(x,\xi_5)}{\partial t} \right) \left(\frac{\tau_{bc,r}}{\sin \varphi_0} M_{13,r}^2 - 2\tau_{bx} \right) + \right. \right. \right. \\ \left. \left. \left. + \frac{\partial}{\partial y} \left(\frac{\partial H_4(x,\xi_5)}{\partial t} \right) \left(\frac{\tau_{bc,r}}{\sin \varphi_0} M_{14,r}^2 - 2\tau_{by} \right) \right] \frac{\partial H_4(x,t_1)}{\partial y} \right| \right\},$$

$$M_{24,r}^2 \equiv \max_{t_1 \leq t \leq t_2} \left\{ \max_{x \in CD} \left| k_{np,r} \frac{\partial}{\partial y} \left(\frac{\partial H_4(x,\xi_5)}{\partial t} \right) \right| \right\},$$

$$M_{25,r}^2 \equiv \max_{t_1 \leq t \leq t_2} \left\{ \max_{y \in AD} \left| V_r \frac{\tau_{bc,r}^2}{\sin^2 \varphi_0} \frac{A\tilde{\omega}d_r}{((\rho_r - \rho_0)gd_r)^3} \left[\frac{\partial}{\partial x} \left(\frac{\partial H_1(y,\xi_3)}{\partial t} \right) \left(\frac{\tau_{bc,r}}{\sin \varphi_0} M_{15,r}^2 - 2\tau_{bx} \right) + \right. \right. \right. \\ \left. \left. \left. + \frac{\partial}{\partial y} \left(\frac{\partial H_1(y,\xi_3)}{\partial t} \right) \left(\frac{\tau_{bc,r}}{\sin \varphi_0} M_{16,r}^2 - 2\tau_{by} \right) \right] \frac{\partial H_1(y,t_1)}{\partial x} \right| \right\},$$

$$M_{26,r}^2 \equiv \max_{t_1 \leq t \leq t_2} \left\{ \max_{y \in AD} \left| k_{np,r} \frac{\partial}{\partial x} \left(\frac{\partial H_1(y,\xi_3)}{\partial t} \right) \right| \right\},$$

$$M_{31,r}^2 \equiv \max_{t_1 \leq t \leq t_2} \left\{ \max_{y \in BC} \left| V_r \frac{\tau_{bc,r}}{\sin \varphi_0} \frac{A\tilde{\omega}d_r}{((\rho_r - \rho_0)gd_r)^3} \left[\frac{\partial}{\partial x} \left(\frac{\partial H_2(y,\xi_4)}{\partial t} \right) \left(2\tau_{bx} - \frac{\tau_{bc,r}}{\sin \varphi_0} M_{11,r}^2 \right) + \right. \right. \right. \\ \left. \left. \left. + \frac{\partial}{\partial y} \left(\frac{\partial H_2(y,\xi_4)}{\partial t} \right) \left(2\tau_{by} - \frac{\tau_{bc,r}}{\sin \varphi_0} M_{12,r}^2 \right) \right] \tau_{bx} \right| \right\},$$

$$M_{32,r}^2 \equiv \max_{t_1 \leq t \leq t_2} \left\{ \max_{x \in CD} \left| V_r \frac{\tau_{bc,r}}{\sin \varphi_0} \frac{A\tilde{\omega}d_r}{((\rho_r - \rho_0)gd_r)^3} \left[\frac{\partial}{\partial x} \left(\frac{\partial H_4(x, \xi_5)}{\partial t} \right) \left(2\tau_{bx} - \frac{\tau_{bc,r}}{\sin \varphi_0} M_{13,r}^2 \right) + \frac{\partial}{\partial y} \left(\frac{\partial H_4(x, \xi_5)}{\partial t} \right) \left(2\tau_{by} - \frac{\tau_{bc,r}}{\sin \varphi_0} M_{14,r}^2 \right) \right] \tau_{by} \right\},$$

$$M_{33,r}^2 \equiv \max_{t_1 \leq t \leq t_2} \left\{ \max_{y \in AD} \left| V_r \frac{\tau_{bc,r}}{\sin \varphi_0} \frac{A\tilde{\omega}d_r}{((\rho_r - \rho_0)gd_r)^3} \left[\frac{\partial}{\partial x} \left(\frac{\partial H_1(y, \xi_3)}{\partial t} \right) \left(2\tau_{bx} - \frac{\tau_{bc,r}}{\sin \varphi_0} M_{15,r}^2 \right) + \frac{\partial}{\partial y} \left(\frac{\partial H_1(y, \xi_3)}{\partial t} \right) \left(2\tau_{by} - \frac{\tau_{bc,r}}{\sin \varphi_0} M_{16,r}^2 \right) \right] \tau_{by} \right\},$$

$$t_1 < \xi_1, \xi_2, \xi_3, \xi_4, \xi_5 \leq t_2, t_1 < t \leq t_2.$$

Thus, using the estimates (38), we obtain:

$$\iint_G |H_{np}^2(x, y, t_2) - H_{lp}^{(2)}(x, y, t_2)| dx dy \leq \tau^2 L_x L_y \sum_{r=1}^R (M_{01,r}^2 + \tau M_{02,r}^2), \tag{39}$$

where

$$M_{r,01}^2 = \frac{1}{1 - \tilde{\epsilon}} (M_{r,2}^2 + M_{r,6}^2 + M_{r,9}^2 + M_3^2 (M_{r,4}^2 + M_{r,7}^2)),$$

$$M_{r,02}^2 = \frac{1}{(1 - \tilde{\epsilon})c_0} M_{r,1}^* (M_{r,1}^2 + M_{r,5}^2 + M_{r,8}^2).$$

From inequality (39), we can move to the following estimate:

$$\|H_{lp}^{(2)}(x, y, t_2) - H_{np}(x, y, t_2)\|_{L_1(G \times [t_1, t_2])} \leq \frac{1}{2c_0} \tau^2 L_x L_y (1 + \tau) \sum_{r=1}^R M_{2,r}^*, \tag{40}$$

where

$$M_{2,r}^* = \max_{(x,y) \in G} \{M_{01,r}^2; M_{02,r}^2\},$$

$$\|Q(x, y, t)\|_{L_1(G \times [t_1, t_2])} \equiv \int_{t_1}^{t_2} \left(\iint_G |Q(x, y, t)| dx dy \right) dt.$$

The required estimate for $n = 2$ is obtained. The first step of the induction is completed.

Next, we assume that for $n = s$ the estimate holds:

$$\|H_{lp}^{(s)}(x, y, t_s) - H_{np}(x, y, t_s)\|_{L_1(G \times [t_{s-1}, t_s])} \leq \frac{1}{2c_0} \tau^2 L_x L_y \frac{1 - \tau^s}{1 - \tau} \sum_{r=1}^R M_{s,r}^*, \tag{41}$$

where $M_{s,r}^*$ is some constant function.

For $n = s + 1$ in equations (23)–(27), we consider integrals over the time interval $t_s < t \leq t_{s+1}$. By estimating these integrals with the consideration of (41) on the previous time step, we obtain the inequality:

$$\iint_G |H_{lp}^2(x, y, t_{s+1}) - H_{np}^2(x, y, t_{s+1})| dx dy \leq \tau^2 L_x L_y \sum_{r=1}^R (M_{01,r}^{s+1} + \tau M_{02,r}^{s+1} + \dots + \tau^s M_{0s+1,r}^{s+1}) \tag{42}$$

with constants $M_{01,r}^{s+1}, M_{02,r}^{s+1}, \dots, M_{0s+1,r}^{s+1}$, that depend on the magnitudes of the derivatives.

Using inequality (42), we arrive at the estimate:

$$\|H_{lp}(x, y, t_{s+1}) - H_{np}(x, y, t_{s+1})\|_{L_1(G \times [t_s, t_{s+1}])} \leq \frac{1}{2c_0} \tau^2 L_x L_y \frac{1 - \tau^{s+1}}{1 - \tau} \sum_{r=1}^R M_{s+1,r}^*, \tag{43}$$

where

$$M_{s+1,r}^* = \max_{(x,y) \in G} \{M_{01,r}^{s+1}; M_{02,r}^{s+1}; \dots; M_{0s+1,r}^{s+1}\},$$

$$\|Q(x, y, t)\|_{L_1(G \times [t_s, t_{s+1}])} \equiv \int_{t_s}^{t_{s+1}} \left(\iint_G |Q(x, y, t)| dx dy \right) dt.$$

The inductive step has been completed, allowing us to state the validity of the assertion for any s , $1 < s \leq N$.

Using the estimates (37), (40), and (43) from formula (22), we obtain:

$$\begin{aligned} \|H_{lp}(T) - H_{np}(T)\|_{L_1(G \times [0, T])} &\leq \frac{1}{2c_0(1-\tau)} \tau^2 L_x L_y C \left((1-\tau) + (1-\tau^2) + \dots + (1-\tau^{N+1}) \right) \leq \\ &\leq \frac{1}{2c_0(1-\tau)} \tau^2 L_x L_y C \left[N + 1 - \frac{\tau - \tau^{N+2}}{1-\tau} \right], \end{aligned} \quad (44)$$

where

$$\begin{aligned} C &\equiv \max_{(x,y) \in G} \left\{ \sum_{r=1}^R M_{1,r}^*, \sum_{r=1}^R M_{2,r}^*, \dots, \sum_{r=1}^R M_{s+1,r}^* \right\}, \\ \|Q(x, y, t)\|_{L_1(G \times [0, T])} &\equiv \int_0^T \left(\iint_G |Q(x, y, t)| dx dy \right) dt = \sum_{n=1}^N \int_{t_{n-1}}^{t_n} \left(\iint_G |Q(x, y, t)| dx dy \right) dt. \end{aligned}$$

Since $N\tau \equiv T \equiv const$, inequality (44) leads to

$$\|H_{lp}(T) - H_{np}(T)\|_{L_1(G \times [0, T])} = O(\tau), \quad (45)$$

which completes the study of the convergence of the linearized problem to the solution of the original nonlinear problem.

Discussion and Conclusion. The conditions for the convergence of the solutions of the linearized sediment transport problem with a multicomponent composition to the solution of the nonlinear problem in the Banach space norm L_1 with a rate $O(\tau)$ of convergence have been determined. The obtained research results can be used in the forecasting of nonlinear hydrophysical processes, improving their accuracy and reliability due to the availability of new functional capabilities for accounting for physically significant factors.

References

1. Sukhinov A.I., Chistyakov A.E., Sidoryakina V.V. Parallel Solution of Sediment and Suspension Transportation Problems on the Basis of Explicit Schemes. *Communications in Computer and Information Science*. 2018;910:306–321. https://doi.org/10.1007/978-3-319-99673-8_22
2. Sukhinov A.I., Sidoryakina V.V. Mathematical nonlinear spatial-two-dimensional model of multicomponent sediment transport in shallow water bodies and its linearization. *Bulletin of the Taganrog Institute named after A.P. Chekhov*. 2018;2:242–245. (In Russ.)
3. Sidoryakina V.V. Existence and uniqueness of the solution of the initial-boundary value problem of transport of multicomponent sediments of coastal marine systems. *Computational Mathematics and Information Technologies*. 2023;7(2):73–80. (In Russ.) <https://doi.org/10.23947/2587-8999-2023-7-2-73-80>
4. Sidoryakina V.V. Continuous dependence of solutions of the linearized initial-boundary value problem of multicomponent sediment transport on the input data of the problem. *News of universities. North Caucasian region. Natural sciences*. 2024;1(221):30–37. (In Russ.) <https://doi.org/10.18522/1026-2237-2024-1-30-37>
5. Sidoryakina V.V., Sukhinov A.I. Well-posedness analysis and numerical implementation of a linearized two-dimensional bottom sediment transport problem. *Comput. Math. Math. Phys.* 2017;57(6):978-994. <https://doi.org/10.1134/S0965542517060124>
6. Sukhinov A.I., Sidoryakina V.V., Sukhinov A.A. Sufficient conditions for the convergence of positive solutions of a linearized two-dimensional sediment transport problem. *Bulletin of the Don State Technical University*. 2017;17(1):5–17. (In Russ.) <https://doi.org/10.23947/1992-5980-2017-17-1-5-17>
7. Sukhinov A.I., Sidoryakina V.V. On the uniqueness of the solution of a linearized two-dimensional initial-boundary value problem of sediment transport. *Bulletin of the Taganrog Institute named after A.P. Chekhov*. 2016;2:270–274.
8. Sukhinov A.I., Sidoryakina V.V., Sukhinov A.A. Linearization of a spatially two-dimensional sediment transport problem and its convergence to the original nonlinear problem. In: *Proceedings of the International Conference "Modern Problems of Mathematical Physics and Computational Mathematics"*. Moscow: Publishing Department of the Faculty of Computational Mathematics and Cybernetics, Lomonosov Moscow State University; MAKS Press; 2016. P. 113. (In Russ.)
9. Sukhinov A.I., Sidoryakina V.V. Convergence of linearized sequence tasks to the nonlinear sediment transport task solution. *Mat. Model.* 2017;29(11):19–39.

10. Sukhinov A.I., Protsenko E.A., Chistyakov A.E., Shreter S.A. Comparison of computational efficiencies of explicit and implicit schemes for the problem of sediment transport in coastal water systems. In: *Proceedings of the International Scientific Conference "Parallel Computing Technologies (PaVT'2015)"*. Chelyabinsk: Publishing Center of SUSU; 2015. P. 297–307. (In Russ.)
11. Sukhinov A.I., Chistyakov A.E., Protsenko E.A. Construction of a discrete two-dimensional mathematical model of sediment transport. *Bulletin of SFedU. Engineering sciences*. 2011;8(121): 32–44. (In Russ.)
12. Sukhinov A.I., Chistyakov A.E., Bondarenko Yu.S. Estimation of the error in solving the diffusion equation based on schemes with weights. *Bulletin of SFedU. Engineering sciences*. 2011;8(121):6–13. (In Russ.)
13. Sidoryakina V.V. Efficient algorithms for the numerical solution of the coupled sediment and suspended matter transport problems in coastal systems. *Atlantis Press. Series: Atlantis Highlights in Computer Sciences*. 2019;3:243–248. <https://doi.org/10.2991/csit-19.2019.42>
14. Sukhinov A.I., Chistyakov A.E., Protsenko S.V., Sidoryakina, V.V. Coupled 3D wave and 2D bottom deposit transportation models for the prediction of harmful phenomena in coastal zone. *Trends in the Analysis and Design of Marine Structures*. 2019. P. 597–603. <https://doi.org/10.1201/9780429298875>
15. Sukhinov A., Chistyakov A., Sidoryakina V. Investigation of nonlinear 2D bottom transportation dynamics in coastal zone on optimal curvilinear boundary adaptive grids. *MATEC Web of Conferences*. 2017;132:04003. <https://doi.org/10.1051/mateconf/201713204003>

About the Author:

Valentina V. Sidoryakina, Candidate of Physical and Mathematical Sciences, Associate Professor of the Department of Mathematics and Computer Science, Don State Technical University (1, Gagarin Sq., Rostov-on-Don, 344003, Russian Federation); Associate Professor of the Department of Mathematics and Physics, Taganrog Institute named after A.P. Chekhov (branch) of RSUE (RINH) (48, Initsiativnaya str., Taganrog, 347936, Russian Federation), [ORCID](#), [SPIN-code](#), [ResearcherID](#), [MathSciNet](#), [ScopusID](#), cvv9@mail.ru

Conflict of Interest Statement: the author do not have any conflict of interest.

Author has read and approved the final manuscript.

Об авторе:

Валентина Владимировна Сидорякина, кандидат физико-математических наук, доцент кафедры математики и информатики Донского государственного технического университета (344003, Российская Федерация, г. Ростов-на-Дону, пл. Гагарина, 1); доцент кафедры математики и физики Таганрогского института имени А.П. Чехова (филиал) РГЭУ (РИНХ) (347936, Российская Федерация, г. Таганрог, ул. Инициативная, 48), [ORCID](#), [SPIN-код](#), [ResearcherID](#), [MathSciNet](#), [ScopusID](#), cvv9@mail.ru

Конфликт интересов: автор заявляет об отсутствии конфликта интересов.

Автор прочитал и одобрил окончательный вариант рукописи.

Received / Поступила в редакцию 31.01.2025

Reviewed / Поступила после рецензирования 21.02.2025

Accepted / Принята к публикации 03.03.2025

MATHEMATICAL MODELLING МАТЕМАТИЧЕСКОЕ МОДЕЛИРОВАНИЕ



UDC 519.6

Original Theoretical Research

<https://doi.org/10.23947/2587-8999-2025-9-1-31-38>



Accuracy Assessment of Sentinel-3 Satellite Altimetry in the Coastal Areas of the Azov Sea

Sofya V. Protsenko  , Elena A. Protsenko , Anton V. Kharchenko

Taganrog Institute named after A.P. Chekhov (branch) of RSUE (RINH), Taganrog, Russian Federation

 rab55555@rambler.ru

Abstract

Introduction. The Azov Sea is a shallow semi-enclosed sea where satellite altimetry (SA) faces challenges in ensuring accurate sea level measurements. This study focuses on verifying Sentinel-3 altimetry data in the coastal areas of the Azov Sea using observational platform data and a three-dimensional hydrodynamic model.

Materials and Methods. The study is based on a comparison of sea surface heights (SSH) obtained from the Sentinel-3 radar altimeter with tide gauge data and modelling results. A three-dimensional hydrodynamic model, adapted to the conditions of the Azov Sea, was used, along with satellite data processed considering atmospheric and tidal corrections.

Results. The root mean square error (RMSE) between satellite-derived and reference data was found to be 85 mm. The analysis demonstrated that Sentinel-3 Doppler altimetry in SAR mode provides higher accuracy compared to traditional altimetry, particularly in coastal areas.

Discussion and Conclusion. The assessment of Sentinel-3 data confirms their reliability in modeling water levels in the Azov Sea. The comparative analysis methodology proposed in this study enables the identification of systematic errors in satellite data and facilitates their integration with modelling and in situ observations. The study confirms the effectiveness of Sentinel-3 data in determining sea levels in complex coastal conditions. The developed methodology can be applied to other coastal areas to assess satellite altimetry performance.

Keywords: satellite altimetry, Sentinel-3, Azov Sea, sea level variations, hydrodynamic modeling, three-dimensional hydrodynamic model, satellite data verification

Funding. This research was supported by the Russian Science Foundation, grant No. 25–21–00021, <https://rscf.ru/project/25-21-00021/>.

For Citation. Protsenko S.V., Protsenko E.A., Kharchenko A.V. Accuracy Assessment of Sentinel-3 Satellite Altimetry in the Coastal Areas of the Azov Sea. *Computational Mathematics and Information Technologies*. 2025;9(1):31–38. <https://doi.org/10.23947/2587-8999-2025-9-1-31-38>

Оригинальное теоретическое исследование

Оценка точности спутниковой альтиметрии Sentinel-3 в прибрежных районах Азовского моря

С.В. Проценко  , Е.А. Проценко , А.В. Харченко

Таганрогский институт имени А.П. Чехова (филиал) РГЭУ (РИНХ), г. Таганрог, Российская Федерация

 rab55555@rambler.ru

Аннотация

Введение. Азовское море является мелководным полузамкнутым морем, где спутниковая альтиметрия (SA) сталкивается с трудностями в обеспечении точности измерений уровня моря. Рассматривается верификация данных альтиметрии спутника Sentinel-3 в прибрежных районах Азовского моря с использованием данных платформ наблюдений и трехмерной гидродинамической модели.

Материалы и методы. Исследование основано на сравнении высот поверхности моря (SSH), полученных с радиовысотомера Sentinel-3, с данными мареографов и результатами моделирования. Использована трехмерная гидродинамическая модель, адаптированная к условиям Азовского моря, а также спутниковые данные, обработанные с учетом атмосферных и приливных поправок.

Результаты исследования. Среднеквадратичная ошибка (RMSE) между спутниковыми и эталонными данными составила 85 мм. Анализ показал, что доплеровская альтиметрия Sentinel-3 в SAR-режиме обеспечивает более высокую точность по сравнению с традиционной альтиметрией, особенно в прибрежной зоне.

Обсуждение и заключение. Оценка данных Sentinel-3 демонстрирует их надежность в моделировании уровня воды в Азовском море. Методика сравнительного анализа, предложенная в работе, позволяет учитывать систематические ошибки спутниковых данных и использовать их в сочетании с моделированием и натурными наблюдениями. Исследование подтверждает эффективность данных Sentinel-3 в определении уровня моря в сложных прибрежных условиях. Разработанная методика может быть применена в других прибрежных районах для оценки характеристик спутниковой альтиметрии.

Ключевые слова: спутниковая альтиметрия, Sentinel-3, Азовское море, колебания уровня моря, гидродинамическое моделирование, трехмерная гидродинамическая модель, верификация спутниковых данных

Финансирование. Исследование выполнено за счет гранта Российского научного фонда № 25–21–00021, <https://rscf.ru/project/25-21-00021/>.

Для цитирования. Проценко С.В., Проценко Е.А., Харченко А.В. Оценка точности спутниковой альтиметрии Sentinel-3 в прибрежных районах Азовского моря. *Computational Mathematics and Information Technologies*. 2025;9(1):31–38. <https://doi.org/10.23947/2587-8999-2025-9-1-31-38>

Introduction. The Azov Sea is a shallow semi-enclosed body of water characterized by low salinity, significant seasonal fluctuations in water levels, and intense river discharge. These factors significantly affect the dynamics of water masses and necessitate precise tools for monitoring sea level changes. In recent decades, remote sensing has become one of the key methods for studying marine and coastal processes. In particular, satellite altimetry (SA) enables continuous observation of sea level variations on a global scale.

One of the modern tools for satellite monitoring is the Sentinel-3A satellite, launched by the European Space Agency (ESA) in 2016 as part of the Copernicus program. It is equipped with a synthetic aperture radar (SAR) altimeter, which significantly improves the spatial resolution of data compared to traditional altimetry. However, the application of satellite altimetry methods in coastal zones presents significant challenges due to the influence of the coastline, wave heterogeneity, seabed topography variations, and land-induced interference. This makes the verification of Sentinel-3 data particularly relevant in complex marine areas such as the Azov Sea.

Previous studies have shown that while satellite altimetric data achieve high accuracy in open ocean waters, their precision may decrease in coastal areas due to signal reflections, meteorological effects, and water mass dynamics. Therefore, it is crucial to assess the accuracy of Sentinel-3 data under the specific conditions of the Azov Sea, where shallow depths and the influence of river discharge and seasonal changes significantly affect sea levels [1].

This study conducts a comprehensive verification of Sentinel-3 satellite altimetry data by comparing them with in situ tide gauge measurements installed in the Azov Sea, as well as with numerical modeling results obtained using a three-dimensional hydrodynamic model. The objective of the study is to determine the accuracy of satellite data and analyze their applicability for monitoring sea level in coastal conditions.

To achieve this, the following tasks were carried out:

- collection and processing of Sentinel-3 satellite altimetry data;
- adaptation and application of a three-dimensional hydrodynamic model to calculate sea surface height;
- analysis of discrepancies between satellite, model-based, and in situ data;
- determination of root mean square error (RMSE) and evaluation of the reliability of satellite data for monitoring the Azov Sea.

Thus, this study aims to expand the capabilities of satellite altimetry in coastal areas and enhance methods for evaluating Sentinel-3 data under the complex hydrodynamic conditions of the Azov Sea.

Materials and Methods

Satellite Altimetry Data. Satellite altimetry (SA) is a remote sensing method for measuring sea level based on the use of a radar altimeter, which emits an electromagnetic pulse and records the time it takes to return after reflecting off the water surface. This method enables global measurements of sea surface height (SSH) and provides valuable data for analyzing water level variations in both coastal and open sea areas.

The Sentinel-3 satellite (Fig. 1), launched by the European Space Agency (ESA) as part of the Copernicus program, is equipped with the SRAL (Synthetic Aperture Radar Altimeter), which operates in two modes:

- Low Resolution Mode (LRM) — traditional altimetry with relatively low spatial resolution;
- Synthetic Aperture Radar (SAR) Mode — a synthetic aperture mode that provides enhanced resolution and more accurate sea level measurements, particularly in coastal areas.



Fig. 1. Artistic depiction of Sentinel-3 [2]

This study analyzes data obtained in SAR mode, which minimizes signal reflections from land and improves measurement accuracy under complex hydrodynamic conditions.

The Sentinel-3 satellite follows a sun-synchronous orbit at an altitude of 814 km with an inclination of 98.6° , ensuring global coverage with a repeat cycle of 27 days over the same region (when combined with Sentinel-3B, the repeat period is reduced to 13.5 days) (Fig. 2). The SRAL radar altimeter operates in the Ku/C bands and transmits pulses at a frequency of 1 kHz, allowing sea level measurements with a temporal resolution of 20 Hz (i. e., approximately one measurement every 350 meters along the satellite’s track) (Fig. 3) [2].

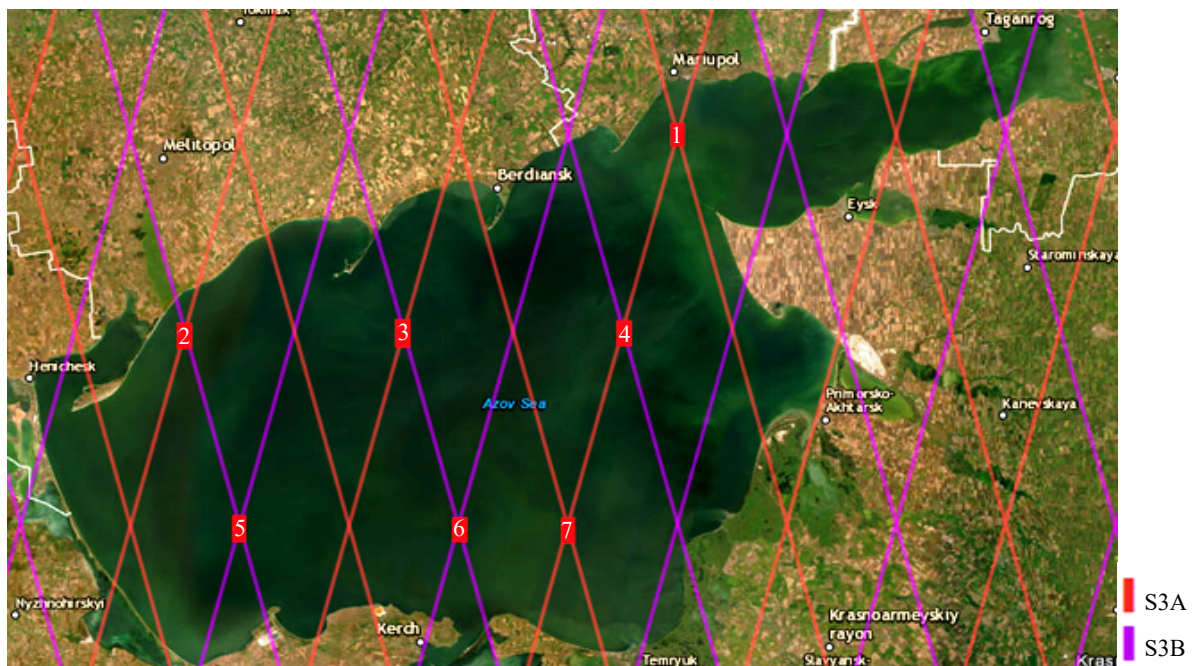


Fig. 2. Study area location, with lines indicating Sentinel-3 passes

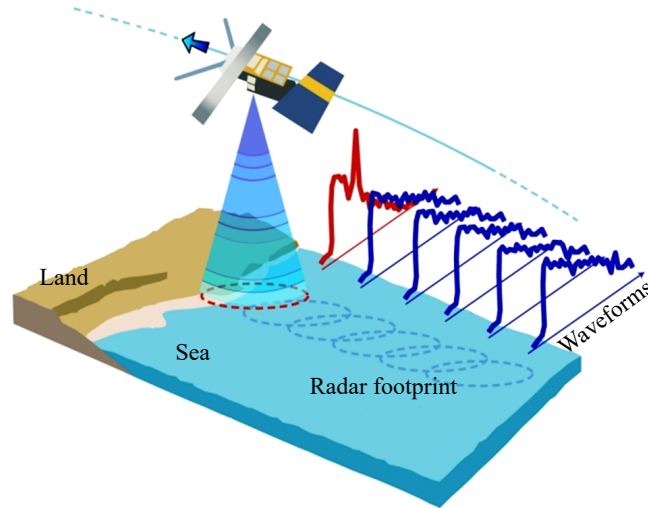


Fig. 3. Changes in signal shape (red) as the satellite altimeter approaches the coastline and enters the radar coverage zone [2]

The altimeter onboard the satellite transmits microwave radiation at two frequencies toward the sea surface and records the time required for the signal to return to the satellite. The initial distance $R(\lambda, \phi, t)$ at a specific coordinate and time t is corrected for atmospheric effects and instrumental errors. The corrected distance R_c is calculated using the formula [3]:

$$R_{corr}(\lambda, \phi, t) = R(\lambda, \phi, t) - C_r,$$

where the corrections C_r , applied to the satellite range include:

- sea state bias correction, which accounts for the influence of waves on radar signal reflection;
- polar tide correction, which compensates for changes in the Earth's shape due to mass movements in polar regions;
- solid Earth tide correction, which considers the deformation of the Earth's crust caused by the gravitational pull of the Moon and the Sun;
- ionospheric correction, which adjusts for the effect of electron density in the ionosphere on radio wave propagation;
- dry and wet tropospheric corrections, which account for the refraction of radio waves in the atmosphere due to the presence of water vapor and other gases.

These corrections are essential to minimize systematic errors and ensure high-precision satellite sea level measurements.

After applying all necessary corrections, the sea surface height determined from satellite data is calculated as follows:

$$SSH_{SA}(\lambda, \phi, t) = h_{sat}(\lambda, \phi, t) - R_{corr}(\lambda, \phi, t),$$

where $SSH_{SA}(\lambda, \phi, t)$ — sea surface height determined from satellite altimetry data; $h_{sat}(\lambda, \phi, t)$ — satellite altitude above the reference ellipsoid; $R_{corr}(\lambda, \phi, t)$ — corrected distance from the satellite to the water surface [4–5].

The verification of Sentinel-3 satellite altimetry data is performed by comparing the sea surface heights obtained from the altimeter SSH_{SA} , with reference data, including measurements from observation platforms in the Azov Sea SSH_{TG} and results from numerical modeling based on a three-dimensional hydrodynamic model SSH_{HDM} .

In this study, Sentinel-3 SSH products obtained from the official Copernicus Data Hub [6] were used. The data were downloaded in NetCDF format and underwent preprocessing, which included:

- selecting Sentinel-3 orbital segments passing over the Azov Sea;
- filtering and removing noisy data with anomalous values;
- interpolating to align with the coordinates of tide gauges and the hydrodynamic model.

To verify the accuracy of Sentinel-3 measurements, SSH data were compared with reference measurements from:

1. Ground-based observation platforms (tide gauges) – sea level height data from the Unified State Information System on the Situation in the World Ocean (ESIMO).
2. Numerical modeling – sea surface height data obtained using a three-dimensional hydrodynamic model (the model description is provided in the next section).

The accuracy assessment of the data was conducted by calculating the root mean square error (RMSE) between SSH values derived from satellite data and tide gauge observations, as well as analyzing the standard deviation (STD) between Sentinel-3 data and numerical modeling results.

Observation Platforms in the Azov Sea. For the verification of Sentinel-3 satellite altimetry data in the coastal zone of the Azov Sea, data from seven observation platforms registered in the Unified State Information System on the Situation in the World Ocean (ESIMO) were used (Fig. 4). These platforms are tide gauge stations equipped with high-precision measuring instruments, enabling real-time sea level recording and providing long-term observation series [7].



Fig. 4. Observation platforms in the AZOV Sea

Tide gauges installed at various locations across the Azov Sea continuously record sea level fluctuations. These stations are strategically positioned near key hydrodynamic nodes where wave action, wind surges, and river discharge effects are most pronounced. This placement ensures the collection of representative data on sea level dynamics across different regions of the Azov Sea.

Coastal tide gauges are used to measure and continuously record fluctuations in the sea level of the Azov Sea. The sea surface height $SSH_{TG}(\lambda_{TG}, \phi_{TG}, t)$ based on tide gauge data can be determined as follows: where $H_{TG}(t)$ — sea level measured by the tide gauge relative to the zero level of the national vertical reference system.

For a proper comparison with satellite data, tide gauges were used, located at varying distances from the shore: from deep-water areas to shallow zones influenced by the shoreline. This distribution allows for the assessment of the accuracy of Sentinel-3 altimetric data depending on the distance from the shore, the identification of the impact of coastal effects on satellite measurements, and consideration of the local hydrodynamic features of the Sea of Azov when analyzing discrepancies in the data. The locations of the tide gauge stations are shown in Fig. 2, with the coordinates of each observation platform marked.

The tide gauge data were standardized to a common reference system for accurate comparison with satellite altimetry and hydrodynamic modeling data. The processing included:

- harmonic analysis of tidal and set-up oscillations of the sea level;
- filtering of high-frequency fluctuations caused by local hydrodynamic processes (e. g., short-term wind effects);
- adjustment of data to a reference level aligned with the geoid used in satellite measurements;
- interpolation of time series to match Sentinel-3 satellite passes.

Additionally, an analysis of statistical characteristics of the measured data was performed, including the mean value, standard deviation (STD), and range of sea level fluctuations for each station.

A spatially inhomogeneous three-dimensional mathematical model of wave hydrodynamics in a shallow water body. The governing equations of the wave hydrodynamics model are [8–12]:

- the equation of motion (Navier-Stokes):

$$\begin{aligned} u'_t + uu'_x + vv'_y + ww'_z &= -\frac{1}{\rho} P'_x + (\mu u'_x)'_x + (\mu v'_y)'_y + (v u'_z)'_z, \\ v'_t + uv'_x + vv'_y + ww'_z &= -\frac{1}{\rho} P'_y + (\mu v'_x)'_x + (\mu v'_y)'_y + (v v'_z)'_z, \\ w'_t + uw'_x + vw'_y + ww'_z &= -\frac{1}{\rho} P'_z + (\mu w'_x)'_x + (\mu w'_y)'_y + (v w'_z)'_z + g; \end{aligned} \quad (1)$$

- the continuity equation in the case of variable density:

$$\rho'_t + (\rho u)'_x + (\rho v)'_y + (\rho w)'_z = 0, \quad (2)$$

where $V = \{u, v, w\}$ is the velocity vector; P is the pressure; ρ is the density; μ, ν are the horizontal and vertical components of the turbulent exchange coefficient; g is the acceleration due to gravity.

The system of equations (1)–(2) is considered with the following boundary conditions:

- at the inlet:

$$u(x, y, z, t) = u(t), \quad v(x, y, z, t) = v(t), \quad P'_n(x, y, z, t) = 0, \quad V'_n(x, y, z, t) = 0,$$

- on the lateral boundary (shore and bottom):

$$\rho \mu (u')_n(x, y, z, t) = -\tau_x(t), \quad \rho \mu (v')_n(x, y, z, t) = -\tau_y(t),$$

- on the upper boundary:

$$V'_n(x, y, z, t) = 0, \quad P'_n(x, y, z, t) = 0,$$

$$\begin{aligned} \rho\mu(u')_n(x, y, z, t) &= -\tau_x(t), \quad \rho\mu(v')_n(x, y, z, t) = -\tau_y(t), \\ w(x, y, t) &= -\omega - P'_t / \rho g, \quad P'_n(x, y, t) = 0, \end{aligned} \quad (3)$$

where ω is the intensity of liquid evaporation; τ_x, τ_y are the tangential stress components.

Tangential stress components for the free surface are given by $\{\tau_x, \tau_y\} = \rho_a C d_s |\vec{w}| \{w_x, w_y\}$, where $C d_s = 0.0026$ is the wind velocity relative to the water, ρ_a is the air density; $C d_s$ is the dimensionless surface drag coefficient, which depends on wind speed and is considered in the range of 0.0016–0.0032.

Tangential stress components for the bottom, accounting for water movement, can be written as $\{\tau_x, \tau_y\} = \rho C d_b |V| \{u, v\}$, $C d_b = g n^2 / h^{1/3}$, where $n = 0.04$ is the roughness group coefficient in the Manning formula (0.025–0.2); $h = H + \eta$ is the depth of the water body; H — is the depth to the undisturbed surface; η is the free surface elevation relative to the geoid (sea level).

The data from the hydrodynamic model on sea level $H_{HDM}(\lambda, \phi, t)$ relative to the geoid will be used in the form of:

$$SSH_{HDM}(\lambda, \phi, t) = H_{HDM}(\lambda, \phi, t) + N(\lambda, \phi).$$

The displacement between the tide gauge data and the three-dimensional wave hydrodynamics model can be determined at a nearby tide gauge location at time t :

$$B_{TG/HDM}(t) = SSH_{TG}(\lambda_{TG}, \phi_{TG}, t) - SSH_{HDM}(\lambda_{TG}, \phi_{TG}, t).$$

The displacement is introduced for each corresponding node of the grid cell in the discrete hydrodynamic model during the computation of SSH_{HD} :

$$SSH_{HDMcorr}(\lambda, \phi, t) = SSH_{HDM}(\lambda, \phi, t) \cdot B_{TG/HDM}(t).$$

To account for the systematic error $SSH_{diff}(\lambda, \phi, t)$ between the satellite data and the hydrodynamic model, the following is introduced:

$$SSH_{diff}(\lambda, \phi, t) = SSH_{SA}(\lambda, \phi, t) - SSH_{HDMcorr}(\lambda, \phi, t).$$

The effectiveness of the Sentinel-3 SRAL altimeter was assessed in the coastal zone of the Sea of Azov. Remote sensing data were obtained from the official Copernicus data center in the standard NetCDF format [1]. Based on these data, SSH_{HDM} was calculated. Observation series from 7 coastal tide gauges were used to calculate $SSH_{TG}(\lambda_{TG}, \phi_{TG}, t)$ [2]. The three-dimensional spatially inhomogeneous model of wave hydrodynamics in shallow water, which includes three equations of motion, was used to obtain $SSH_{HDM}(\lambda, \phi, t)$ [3].

Results

Comparative analysis of Sentinel-3 satellite altimetry data, tide gauge observations, and hydrodynamic modelling. To assess the accuracy of Sentinel-3 satellite data, it was compared with in situ measurements from tide gauges located in the Sea of Azov, as well as with the results of numerical simulations performed using a three-dimensional hydrodynamic model. The analysis is based on the calculation of statistical characteristics of the differences between measured and computed sea surface height values, considering the spatial and temporal alignment of the data.

The study covers the year 2024, during which the satellite passes of Sentinel-3A and Sentinel-3B over the Sea of Azov were analyzed. SAR-mode altimetry products were used, providing higher accuracy compared to traditional methods. For each satellite pass, points of intersection with the tide gauges and the hydrodynamic model grid were identified.

For verification, the following data were used:

- tide gauge data (seven stations), recorded in the Unified Interagency Federal Information System (ESIMO);
- Sentinel-3 SSH satellite measurements, obtained from the Copernicus data center;
- results of a three-dimensional hydrodynamic model, adapted for the conditions of the Sea of Azov.

To quantitatively assess the discrepancies between the SSH values obtained by different methods, the following were calculated:

- Root Mean Square Error (RMSE) — the scatter of satellite data relative to tide gauge and model values;
- Mean Bias (Bias) — the magnitude of the systematic error;
- Standard Deviation (STD) — the degree of scatter of the values.

The results of the calculations showed that the overall RMSE between the Sentinel-3 data and the tide gauges was 85 mm. The mean bias between the satellite data and the tide gauges does not exceed 2–3 cm, indicating the absence of significant systematic deviation. The STD ranged from 6 to 9 cm, depending on the specific satellite pass and its distance from the shore.

Table 1 presents statistical data on the difference in SSH measurements. The overall difference across all fourteen passes was 85 mm.

Data on the difference in SSH measurements

Points	Sentinel-3 Passes	RMSE, mm	Distance from the point to the shore, km	Distance from the point to the platform, km
1	653 S3A	78	16.3	2.3
	270 S3A	106		
2	42 S3A	109	11.6	2.4
	425 S3B	84		
3	539 S3B	43	36.2	2.1
	156 S3A	115		
4	270 S3A	68	48.6	3.2
	653 S3B	102		
5	156 S3B	87	37.8	2.7
	425 S3B	110		
6	270 S3B	63	33.9	3.2
	539 S3B	75		
7	539 S3A	79	28.3	4.4
	270S3A	68		

To assess the impact of coastal effects on the accuracy of Sentinel-3 altimetry, an analysis of the dependence of discrepancies on the distance of the measurement point from the shore was conducted. In deep-water areas (>20 km from the shore), the measurement accuracy is maximal: RMSE does not exceed 6–7 cm, and STD ranges from 5 to 8 cm. In areas 10–20 km from the shore, the errors increase: RMSE reaches 7–9 cm, and STD ranges from 6 to 9 cm. In shallow coastal zones (<10 km from the shore), the accuracy of satellite data deteriorates due to reflection effects and the influence of dynamic processes in the surf zone. In these areas, RMSE reaches 10–12 cm, and STD ranges from 9 to 12 cm. Thus, Sentinel-3 data in SAR mode demonstrate high accuracy in open waters but require correction when analyzing coastal areas.

The three-dimensional hydrodynamic model used in the study allowed for the calculation of SSH with high spatial and temporal resolution, providing an additional means of assessing the accuracy of satellite altimetry. The analysis showed that the average discrepancy between the model and satellite SSH data is 4–6 cm, confirming the high accuracy of the model. In areas with intense river runoff (e. g., the mouths of the Don and Kuban rivers), discrepancies increase to 8–10 cm due to variations in water density and currents. In deep-water areas of the Sea of Azov, model data align with satellite data within ± 5 cm, further confirming their reliability.

Discussion and Conclusion. Sentinel-3 satellite altimetry in SAR mode demonstrates high measurement accuracy in the open waters of the Sea of Azov but is subject to errors in coastal areas (<10 km from the shore). The root mean square error (RMSE) between satellite and tide gauge data is 85 mm, which aligns with the current level of altimetry methods. The hydrodynamic model showed good agreement with Sentinel-3 data (average discrepancy of 4–6 cm), confirming the possibility of jointly using numerical modeling and satellite data. To further improve the accuracy of satellite altimetry in coastal areas, adaptive data filtering and correction algorithms should be applied. Therefore, the results of the study confirm the effectiveness of using Sentinel-3 data for sea level monitoring in the Sea of Azov and underscore the need for continued improvement of satellite measurement correction methods in the coastal zone.

References

1. Arnold D, Montenbruck O, Hackel S, Sosnica K. Satellite laser ranging to low Earth orbiters: orbit and network validation. *J Geodesy*. 2019;93(11):2315–2334. <https://doi.org/10.1007/s00190-018-1140-4>
2. Catalog of spatial and temporal assets of the Copernicus data space ecosystem. URL: <https://dataspace.copernicus.eu/> (accessed: 09.01.2025)
3. Cipollini P., Calafat F.M., Jevrejeva S. Monitoring sea level in the coastal zone with satellite altimetry and tide gauges. *Surv Geophys*. 2017;38:33. <https://doi.org/10.1007/s10712-016-9392-0>
4. EUMETSAT. *Sentinel-3 SRAL Marine User Handbook*. 2017;55.
5. Fernandez J., Peter H., Calero E.J., Berzosa J., Gallardo L.J., Femenias P. Sentinel-3A: Validation of orbit products at the Copernicus POD service. *Fiducial Reference Measurements for Altimetry, International Association of Geodesy Symposia*. 2019;150:75–82. https://doi.org/10.1007/1345_2019_64
6. Montenbruck O., Hackel S., Jaggi A. Precise orbit determination of the Sentinel-3A altimetry satellite using ambiguity-fixed GPS carrier phase observations. *J Geodesy*. 2018;92:711–726. <https://doi.org/10.1007/s00190-017-1090-2>
7. Unified State Information System on the Situation in the World Ocean. URL: <http://portal.esimo.ru/> (accessed: 09.01.2025)

8. Protsenko S., Sukhinova T. Mathematical modeling of wave processes and transport of bottom materials in coastal water areas taking into account coastal structures. *MATEC Web Conf.* 2017;04002. <https://doi.org/10.1051/mateconf/201713204002>
9. Protsenko S.V., Protsenko E.A., Kharchenko A.V. Comparison of hydrodynamic processes modelling results in shallow water bodies based on 3D model and 2D model averaged by depth. *Computational Mathematics and Information Technologies.* 2023;7(3):49–63. (In Russ.) <https://doi.org/10.23947/2587-8999-2023-7-3-49-63>
10. Sukhinov A.I., Protsenko S.V., Panasenko N.D. Mathematical modeling and ecological design of the marine systems taking into account multi-scale turbulence using remote sensing data. *Computational Mathematics and Information Technologies.* 2022;6(3):104–113. (In Russ.) <https://doi.org/10.23947/2587-8999-2022-1-3-104-113>
11. Sukhinov A.I., Protsenko E.A., Chistyakov A.E., Shreter S.A. Comparison of computational efficiency of explicit and implicit schemes for the problem of sediment transport in coastal water systems. *Parallel Computational Technologies (PaVT'2015). Proceedings of the International Scientific Conference.* 2015. P. 297–307. (In Russ.)
12. Sukhinov A.I., Chistyakov A.E., Protsenko E.A. Construction of a discrete two-dimensional mathematical model of sediment transport. *Izvestiya SFedU. Technical Sciences.* 2011;8(121):32–44. (In Russ.)

About the Authors:

Sofia V. Protsenko, Candidate of Physical and Mathematical Sciences, Associate Professor of the Department of Mathematics, Research Fellow, A.P. Chekhov Taganrog Institute (branch) Rostov State University of Economics (48, Initiative St., Taganrog, 347936, Russian Federation), [ORCID](#), [SPIN-code](#), rab5555@rambler.ru

Elena A. Protsenko, Candidate of Physical and Mathematical Sciences, Associate Professor of the Department of Mathematics, Leading Research Fellow, A.P. Chekhov Taganrog Institute (branch) Rostov State University of Economics (48, Initiative St., Taganrog, 347936, Russian Federation), [ORCID](#), [SPIN-code](#), eapros@rambler.ru

Anton V. Kharchenko, Research Fellow at the Taganrog Institute of A.P. Chekhov (branch) of the Rostov State Economic University (48, Initiative St., Taganrog, 347936, Russian Federation), kharch_91@rambler.ru

Contributions of the authors:

S.V. Protsenko: concept development; scientific guidance.

E.A. Protsenko: data management; annotation, data cleaning, and maintaining data integrity; software development; visualization.

A.V. Kharchenko: conducting research; methodology development; result validation.

Conflict of Interest Statement: the authors declare no conflict of interest.

All authors have read and approved the final manuscript.

Об авторах:

Протсенко Софья Владимировна, кандидат физико-математических наук, доцент кафедры математики, научный сотрудник, Таганрогский институт им. А.П. Чехова (филиал) Ростовского государственного экономического университета (347936, Российская Федерация, г. Таганрог, ул. Инициативная, 48), [ORCID](#), [SPIN-код](#), rab5555@rambler.ru

Протсенко Елена Анатольевна, кандидат физико-математических наук, доцент кафедры математики, ведущий научный сотрудник, Таганрогский институт им. А.П. Чехова (филиал) Ростовского государственного экономического университета (347936, Российская Федерация, г. Таганрог, ул. Инициативная, 48), [ORCID](#), [SPIN-код](#), eapros@rambler.ru

Харченко Антон Владимирович, научный сотрудник Таганрогского института им. А.П. Чехова (филиал) Ростовского государственного экономического университета (347936, Российская Федерация, г. Таганрог, ул. Инициативная, 48), kharch_91@rambler.ru

Заявленный вклад авторов:

С.В. Протсенко: разработка концепции; научное руководство.

Е.А. Протсенко: курирование данных; деятельность по аннотированию, очистке данных и поддержанию их целостности; разработка программного обеспечения; визуализация.

А.В. Харченко: проведение исследования; разработка методологии; валидация результатов.

Конфликт интересов: авторы заявляют об отсутствии конфликта интересов.

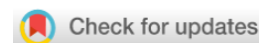
Все авторы прочитали и одобрили окончательный вариант рукописи.

Received / Поступила в редакцию 22.01.2025

Reviewed / Поступила после рецензирования 19.02.2025

Accepted / Принята к публикации 28.02.2025

РАЗДЕЛ МАТЕМАТИЧЕСКОЕ МОДЕЛИРОВАНИЕ



UDC 519.6

Original Theoretical Research

<https://doi.org/10.23947/2587-8999-2025-9-1-39-51>


Estimation of the Unidirectional Traffic Flow Velocity Limit with High Computational Efficiency

Ivan A. Kuteynikov

Moscow Automobile and Road State Technical University (MADI), Moscow, Russian Federation

✉ ivankuteynikov09@gmail.com

Abstract

Introduction. In the modern development of intelligent transportation systems (ITS), an urgent task is the accurate estimation of the velocity limit of traffic flow on a highway. Despite existing solutions to this problem based on statistical mechanics methods and stochastic models, gaps remain in adapting these theories to real road segments of limited length. The traditional thermodynamic limit formula, used to calculate the average velocity of traffic flow, becomes inaccurate for small road segment lengths, limiting its applicability in practical traffic monitoring tasks. The aim of this study is a comparative analysis of various approaches to estimating the average velocity limit of traffic flow.

Materials and Methods. The study was conducted using the method of statistical mechanics and a stochastic model on a one-dimensional finite lattice. Numerical experiments with various parameter values (number of cells, traffic density, and movement probability) were used for analysis.

Results. The study revealed significant discrepancies between the results obtained using the statistical mechanics method and other approaches when the road segment length was small. The efficiency of the second and third approaches was confirmed for limited road segments, where they demonstrated greater accuracy and applicability.

Discussion and Conclusion. The research results have practical significance for the development of intelligent traffic management systems, especially for short road segments. The proposed approaches can be successfully integrated into modern monitoring systems to improve their accuracy. The theoretical significance of this work lies in advancing the methodology for traffic flow estimation while accounting for the specific conditions of real-world environments.

Keywords: traffic flows, thermodynamic limit, exclusion processes, asymptotic behavior of average velocity, stationary solutions, probabilistic traffic model, queuing systems

For Citation. Kuteynikov I.A. Estimation of the unidirectional traffic flow velocity limit with high computational efficiency. *Computational Mathematics and Information Technologies*. 2025;9(1):39–51. <https://doi.org/10.23947/2587-8999-2025-9-1-39-51>

Оригинальное теоретическое исследование

Оценка предельной скорости однонаправленного транспортного потока с высокой вычислительной эффективностью

И.А. Кутейников

Московский автомобильно-дорожный государственный технический университет (МАДИ), г. Москва, Российская Федерация

✉ ivankuteynikov09@gmail.com

Аннотация

Введение. В современных условиях развития интеллектуальных транспортных систем (ITS) возникает актуальная задача точной оценки предельной скорости транспортного потока на магистрали. Несмотря на существующие решения данной проблемы, основанные на методах статистической механики и стохастических моделях, остаются

пробелы в адаптации этих теорий для реальных сегментов дорог с ограниченной протяженностью. Традиционная формула термодинамического предела, используемая для расчета средней скорости транспортного потока, становится некорректной при малых значениях длины дорожной полосы, что ограничивает ее применимость в практических задачах мониторинга транспорта. Целью настоящего исследования является сравнительный анализ различных подходов к оценке средней предельной скорости транспортного потока.

Материалы и методы. Исследование проведено на основе метода статистической механики и стохастической модели на одномерной конечной решетке. Для анализа использовались численные эксперименты с различными значениями параметров (число клеток, плотность потока, вероятность движения).

Результаты исследования. Проведенное исследование показало значительные расхождения между результатами метода статистической механики и другими подходами при малых значениях длины дорожной полосы. Эффективность второго и третьего подходов была подтверждена для ограниченных сегментов дорог, где они демонстрируют большую точность и применимость.

Обсуждение и заключение. Результаты исследования имеют практическое значение для разработки интеллектуальных систем управления транспортными потоками, особенно на коротких участках дорог. Предложенные подходы могут быть успешно интегрированы в современные системы мониторинга для повышения их точности. Теоретическая значимость работы заключается в развитии методологии оценки транспортных потоков с учетом специфики реальных условий.

Ключевые слова: транспортные потоки, термодинамический предел, случайные процессы с запретами, асимптотическое поведение средней скорости, стационарные решения, вероятностная модель трафика, системы массового обслуживания

Для цитирования. Кутейников И.А. Оценка предельной скорости однонаправленного транспортного потока с высокой вычислительной эффективностью. *Computational Mathematics and Information Technologies*. 2025;9(1):39–51. <https://doi.org/10.23947/2587-8999-2025-9-1-39-51>

Introduction. The complexity of traffic flow modeling arises from the need to account for numerous factors, such as driver behavior, weather conditions, and the technical characteristics of vehicles and infrastructure. Despite significant progress in the development of mathematical traffic flow models, existing approaches often face a number of limitations that reduce their applicability in real-world conditions.

Mathematical models based on physical concepts traditionally describe physical media using methods from solid mechanics, hydrodynamics, and gas dynamics. These approaches are formulated as systems of differential equations, which impose smoothness requirements on their solutions. For example, the Navier-Stokes equations in hydrodynamics assume that the velocity and pressure of a fluid change smoothly, allowing for the description of fluid flow across a wide range of conditions. However, such models, based on differential equations, often lack the flexibility needed to describe complex and nonlinear processes, such as traffic flows, where abrupt changes in density and velocity are observed.

One of the fundamental properties of many controlled, interacting many-body systems is the emergence of shocks. A shock in a system of classical flowing particles represents a sudden transition from a low-density region to a high-density region. A well-known example of a shock is the onset of a traffic jam on a highway (Fig. 1), where incoming vehicles (almost freely flowing particles in a low-density regime) must rapidly decelerate over a short distance, subsequently becoming part of a high-density congested area. A remarkable feature of such shocks is their stability over long periods, meaning they remain localized over distances comparable to the size of individual particles. In a certain sense, these shocks can be viewed as soliton-like collective excitations of the particle system.

The difference between fluid (or gas) flow and traffic flow is too significant to employ a continuous approach and accurately describe traffic flow using macroscopic models [1]. Inaccuracies arise in situations where, for example, very few vehicles are present in the region affecting the movement of a given vehicle, compared to the vast number of particles in thermodynamic problems. Unlike mathematical physics, where molecules obey physical laws that are typically simple and constant, drivers exhibit diverse behavior and adapt their actions, introducing a human factor. While molecules move chaotically, drivers share similar goals (same direction, similar desired speeds) and generally prefer to avoid frequent acceleration and deceleration, making their behavior more varied than that of particles in a fluid or gas.

To address these challenges, this study proposes an evaluation of the velocity limit of unidirectional traffic flow based on various modelling approaches.



Fig. 1. Illustration of the Discontinuity (Stepwise Change) in Traffic Flow Density

Lighthill-Whitham-Richards (LWR) Model. One of the most popular approaches to traffic modelling since the mid-1950s has been the network hydrodynamic model and its various modifications, which liken vehicle flow to the motion of a continuous fluid. Hydrodynamic-based models (Payne [2], Kerner-Konhauser [3], Aw-Rascle [4], Zhang [5]) account for additional factors such as driver behavior, flow heterogeneity, phase transitions, and others.

In the 1955 work by Lighthill and Whitham [6] and the 1956 work by Richards [7], the dependence of flow functions on density was likened to fluid flow, where the density $\rho(x,t)$, is defined as the number of vehicles per unit road length, and the flow rate $q(x,t)$, represents the number of vehicles crossing a given section x , where $x \in G$. Considering the law of mass conservation, the number of vehicles remains constant within a closed system. In the case of an open system, we have $q_x + \rho_t = 0$ and $q_x + \rho_t = g(x,t)$. The function $g(x,t)$ represents the rate of vehicles entering or exiting the system. The velocity of traffic flow at a point x at time t is denoted as $v(x,t)$, and in the LWR model, it is assumed that velocity depends only on density. This model corresponded well with real-world observations, particularly at low traffic flow intensities.

Thus:

$$\begin{cases} \frac{\partial \rho}{\partial t} + \frac{\partial(\rho v(\rho))}{\partial x} = 0, \\ v(t, \rho) = F(\rho) \end{cases} \quad (1)$$

where $F(\rho)$ is a non-increasing function, not necessarily convex.

Mathematically, this model is analogous to the equation of motion for a compressible fluid, where the fluid density corresponds to traffic density, and the particle flow $\rho v(\rho)$ is analogous to mass transport flow in hydrodynamics. Although hydrodynamic-type models are widely used to describe traffic flows, they have several limitations that become apparent when analyzing real-world data:

1. *Lack of Discreteness in Vehicle Representation.* Hydrodynamic-type models assume that traffic flow behaves as a continuous medium, whereas in reality, vehicles are discrete entities. This limits the models' ability to describe microscopic phenomena such as gaps or density jumps, which are characteristic of real road conditions.

2. *Inaccurate Representation of Abrupt Density Changes.* The equations of hydrodynamic-type models are based on the assumption of density function smoothness, making it impossible to model discrete or sudden changes, such as unexpected traffic jams.

3. *Limitations in Modelling Complex Vehicle Interactions.* These models assume that a vehicle's speed depends solely on local density, ignoring factors such as individual driver characteristics, perception delays, and long-range interactions.

4. *Limited Adaptability to Real-World Conditions.* The models do not account for external influences such as weather conditions, accidents, or variable speed limits.

5. *Inability to Describe Phase Transitions.* Real traffic flows exhibit phase transitions between free-flowing traffic, stable flow, and congestion. These phenomena are difficult to accurately describe within hydrodynamic-type models without additional assumptions or modifications.

Gas Dynamic Models. Researchers have attempted to address the shortcomings of hydrodynamic models by introducing additional functions into the right-hand side of the equations. One of the most successful models in this regard is the quasi-gas-dynamic (QGD) model, developed under the guidance of Academician B.N. Chetverushkin [8].

The QGD model for traffic flows and its numerical implementation are discussed in detail in [9]. It is based on analogies between vehicle behavior and gas movement, allowing the application of gas dynamics approaches and methods. The

main advantage of this model is that, unlike gases where molecules are distributed in three-dimensional space, in traffic flows, the particles (vehicles) have finite sizes and move along constrained road lanes. In the one-dimensional case, the QGD system of equations for describing vehicular traffic flows takes the following form:

$$\frac{\partial \rho}{\partial t} + \frac{\partial \rho V}{\partial x} = \frac{\partial}{\partial x} \tau \frac{\partial (\rho V^2 + P)}{\partial x} + F_\rho, \quad (2)$$

$$\frac{\partial \rho V}{\partial t} + \frac{\partial \rho V^2}{\partial x} = f - \text{grad}P + \frac{\partial}{\partial x} \tau \frac{\partial (\rho V^3 + PV)}{\partial x} + F_V. \quad (3)$$

In this second-order model $\rho \left[\frac{\text{auto}}{\text{km} \times \text{lane}} \right]$ represents the flow density and $V \left[\frac{\text{km}}{h} \right]$ represents the vehicle speed.

Equation (2) defines the flow density, while equation (3) defines its speed.

For the case of low density, when the distances between vehicles are significant and their interaction is minimal, a simplified model can be used, analogous to incompressible fluid flow. In this case, the density of the traffic flow is considered constant, and changes only occur in the speed and direction of the flow. However, this approach is rarely used in traffic models, as density plays a key role in the formation of traffic jams and other phenomena.

Connection between Microscopic and Macroscopic Models. In more complex microscopic models, where a particle corresponds to a vehicle, the ratio of the number of particles to the number of cells in a section of the grid is a variable quantity. The average speed of the particles and the flow intensity also depend on the location of the grid section. The local state of a section can be characterized by the particle flow density and flow intensity. When the distribution of one of these characteristics is given on the grid, the distribution of the other characteristics is typically studied through simulation modelling.

In a macroscopic model of vehicle traffic flow, the relationship between density, speed, and intensity is described using partial differential equations (equations of mathematical physics). The relationship between the distribution of these characteristics and their dynamics is determined by these differential equations, which are usually solved using numerical methods under given boundary conditions.

Both microscopic and macroscopic traffic models are similar to or directly correspond with statistical physics models. In microscopic models of statistical physics, particles correspond to molecules or elementary particles, while in macroscopic models, distributions of characteristics such as pressure, temperature, flow velocity, and gas or liquid density are defined.

Microscopic models of traffic flows, described by random processes of various types [10], have advantages over macroscopic models as they allow the individual behavior of each vehicle to be considered. This is especially important for analyzing complex situations such as traffic jams, flow merging, or intersections. These models provide a more detailed description of the movement dynamics at the level of individual objects, making them useful in developing real-time traffic management strategies and creating intelligent transportation systems.

Probabilistic Traffic Model on a One-Dimensional Lattice. This work examines the implementation of a microscopic model on a single traffic lane. To obtain stationary solutions, we will investigate it on a closed ring lattice.

Let there be a ring lattice containing N cells, with $M < N$ particles (Fig. 2). Time is discrete. At each moment $t = 0, 1, 2, \dots$ each particle occupies one of the cells. Each cell can contain no more than one particle at a time. The cells are numbered $0, 1, \dots, N-1$ with the numbering directed along the direction of particle movement modulo N .

If at time $t = 0, 1, 2, \dots$ a particle is in cell i and cell $i + 1 \pmod{N}$ is free, then at time $t + 1$ the particle will, with probability $0 < p < 1$ be in cell $i + 1$ and with probability $1 - p$ the particle will remain in cell i . If cell $i + 1$ is occupied, the particle cannot move.

We introduce the concept of the state space of a ring lattice $S = \{s_0, s_1, \dots, s_{C_N^M - 1}\}$, where the total number of possible states C_N^M is the number of combinations of N elements out of M . Each state s_j , $j = 0, 1, \dots, C_N^M - 1$ can be represented by a vector of length $N(x_0, x_1, x_2, \dots, x_{i-1}, x_i, x_{i+1}, \dots, x_{N-1})$, where element $x_i = 1$ if cell i is occupied and $x_i = 0$, if cell i is free.

Thus $\sum_{i=0}^{N-1} x_i = M$.

The transition matrix P has dimensions $C_N^M \times C_N^M$.

Let's consider an example for $N = 4$, $M = 2$.

States of the system:

$$S = \{(1, 1, 0, 0), (1, 0, 1, 0), (1, 0, 0, 1), (0, 1, 1, 0), (0, 1, 0, 1), (0, 0, 1, 1)\}.$$

Let's consider the initial state $s_0 = (1, 1, 0, 0)$. The possible transitions are:

- $(1, 1, 0, 0) \rightarrow (1, 1, 0, 0)$ with probability $1 - p$;
- $(1, 1, 0, 0) \rightarrow (1, 0, 1, 0)$ with probability p .

Now consider the initial state $s_1 = (1,0,1,0)$. The possible transitions are:

- $(1,0,1,0) \rightarrow (1,0,1,0)$ with probability $(1-p)^2$;
- $(1,0,1,0) \rightarrow (0,1,1,0)$ with probability $p(1-p)$;
- $(1,0,1,0) \rightarrow (1,0,0,1)$ with probability $(1-p)p$;
- $(1,0,1,0) \rightarrow (0,1,0,1)$ with probability p^2 .

Next, consider the initial state $s_2 = (1,0,0,1)$. The possible transitions are:

- $(1,0,0,1) \rightarrow (1,0,0,1)$ with probability $1-p$;
- $(1,0,0,1) \rightarrow (0,1,0,1)$ with probability p .

Now consider the initial state $s_3 = (0,1,1,0)$. The possible transitions are:

- $(0,1,1,0) \rightarrow (0,1,1,0)$ with probability $1-p$;
- $(0,1,1,0) \rightarrow (0,1,0,1)$ with probability p .

Consider the initial state $s_4 = (0,1,0,1)$. The possible transitions are:

- $(0,1,0,1) \rightarrow (0,1,0,1)$ with probability $(1-p)^2$;
- $(0,1,0,1) \rightarrow (0,0,1,1)$ with probability $p(1-p)$;
- $(0,1,0,1) \rightarrow (1,1,0,0)$ with probability $(1-p)p$;
- $(0,1,0,1) \rightarrow (1,0,1,0)$ with probability p^2 .

Finally, consider the initial state $s_5 = (0,0,1,1)$. The possible transitions are:

- $(0,0,1,1) \rightarrow (0,0,1,1)$ with probability $1-p$;
- $(0,0,1,1) \rightarrow (1,0,1,0)$ with probability p .

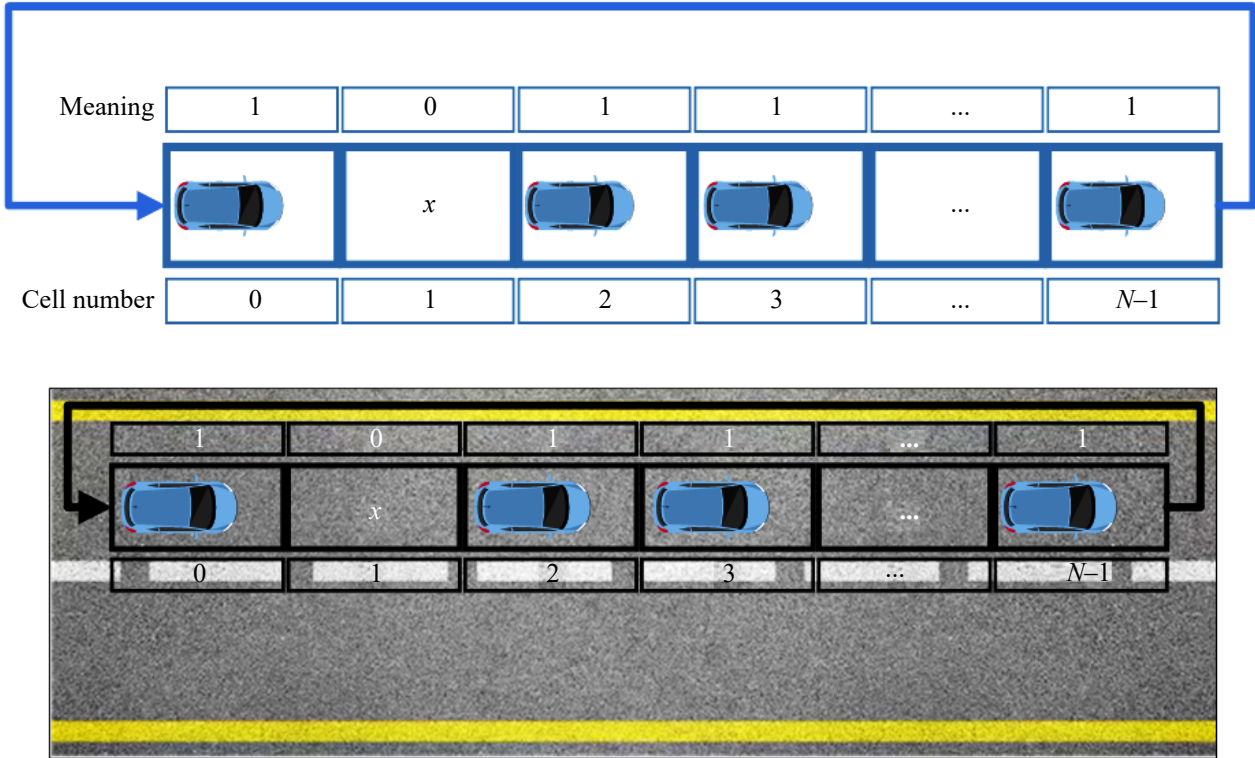


Fig. 2. Visualization of Cell Arrangement on a Ring

Thus, for $N = 4, M = 2$ we get the transition matrix $P_{6 \times 6}$:

$$P_{6 \times 6} = \begin{matrix} & \begin{matrix} s_0 & s_1 & s_2 & s_3 & s_4 & s_5 \end{matrix} \\ \begin{matrix} s_0 \\ s_1 \\ s_2 \\ s_3 \\ s_4 \\ s_5 \end{matrix} & \begin{pmatrix} 1-p & p & 0 & 0 & 0 & 0 \\ 0 & (1-p)^2 & p(1-p) & (1-p)p & p^2 & 0 \\ 0 & 0 & 1-p & 0 & p & 0 \\ 0 & 0 & 0 & 1-p & p & 0 \\ (1-p)p & p^2 & 0 & 0 & (1-p)^2 & p(1-p) \\ 0 & p & 0 & 0 & 0 & 1-p \end{pmatrix} \end{matrix}.$$

Let π_i be the stationary probability of state s_i ; p_{ij} be the probability of transitioning from state s_i to state s_j , $i, j = 0, 1, \dots, C_N^M - 1$.

The stationary probabilities of the states satisfy the system of equations:

$$\pi_i \sum_{j=0}^{C_N^M - 1} p_{ij} = \sum_{j=0}^{C_N^M - 1} \pi_{ij} p_{ji}, \quad i, j = 0, \dots, C_N^M - 1, \quad (4)$$

$$\sum_{i=0}^{C_N^M - 1} \pi_i = 1. \quad (5)$$

Let $k(s_i)$ be the number of “clusters” in the state s_i of the chain. A cluster is defined as a group of neighboring cells occupied by particles, separated from other clusters by free cells. If the chain is in state s_i , the number of particles that can move equals the number of clusters $k(s_i)$, $0 \leq k(s_i) \leq M$. There are $2^{k(s_i)}$ states into which the chain can transition from state s_i . Let the system, starting from state s_i , be able to reach state s_j , $1 < j < C_N^M - 1$ in one time step by moving $l(s_i, s_j)$ particles, $0 \leq l(s_i, s_j) \leq k(s_i)$. Then

$$p_{ij} = p^{l(s_i, s_j)} (1-p)^{k(s_i) - l(s_i, s_j)}, \quad l(s_i, s_i) = 0. \quad (6)$$

The probability that the system remains in state s_i at this step is the probability that none of the $k(s_i)$ particles will move, $p_{ii} = (1-p)^{k(s_i)}$, so

$$\sum_{j=0, j \neq i}^{C_N^M - 1} p_{ij} = 1 - (1-p)^{k(s_i)}. \quad (7)$$

Let $S(k, N, M)$ be the number of states with $0 \leq k \leq M$ clusters for a given number of cells N and particles M .

Lemma 1. The following equality holds:

$$S(k, N, M) = v = \begin{cases} \frac{N}{k} C_{M-1}^{k-1} C_{N-M-1}^{k-1}, & k \leq \min(M, N-M), \\ 0, & k > \min(M, N-M). \end{cases} \quad (8)$$

Proof. Let $R(k, M)$ be the number of ways, taking into account the order, to represent the number M as a sum of k natural summands ($k \leq \min(M, N-M)$). This number is equal to the number of ways to choose $(k-1)$ elements from $M-1$:

$$R(k, M) = C_{M-1}^{k-1}. \quad (9)$$

Next, consider the number $A(k, N, M)$ of states in set A , that contain k clusters and where cell 1 is free, and cell 2 is occupied. This number is the product of the number of ways to distribute M particles among k clusters $R(k, M)$ multiplied by the number of ways to choose the lengths $(k-1)$ of the gaps (intervals between clusters) $R(k, N-M)$. Therefore, if $k \leq \min(M, N-M)$:

$$A(k, N, M) = R(k, M) R(k, N-M). \quad (10)$$

From Equations (9)–(10), we conclude that:

$$A(k, N, M) = C_{M-1}^{k-1} C_{N-M-1}^{k-1}. \quad (11)$$

Let $a = (i_1, \dots, i_N)$ be an arbitrary state from the set A . Define $b(a, d)$ the state corresponding to a by rotating it by d cells, i. e., $b(a, d) = (i_{N-d+1}, i_{N-d+2}, \dots, i_N, i_1, \dots, i_{N-d})$. Any state with k clusters coincides with $b(a, d)$ for k different ordered pairs (a, d) , where a is an element of the set A , and d is one of the numbers $0, 1, \dots, N-1$. The total number of such distinct pairs is $N \cdot A(k, N, M)$. Thus, we have:

$$S(k, N, M) = \frac{N}{k} A(k, N, M). \quad (12)$$

From equations (11) and (12), it follows that equation (9) holds. The lemma is proven.

Theorem 1. The system (4)–(5) has a solution

$$\pi_i = \frac{C}{(1-p)^{k(s_i)-1}}, \quad i = 0, \dots, C_N^M - 1, \quad (13)$$

where the constant is

$$C = \left(\sum_{k=1}^{\min(M, N-M)} \frac{N}{k} \cdot C_{M-1}^{k-1} C_{N-M-1}^{k-1} \frac{1}{(1-p)^{k-1}} \right)^{-1}. \quad (14)$$

Proof. Let's rewrite (4) in the form

$$\sum_{j=0}^{C_N^M-1} \pi_i p_{ij} = \sum_{j=0}^{C_N^M-1} \pi_j p_{ji}, i, j = 0, \dots, C_N^M - 1. \tag{15}$$

Let $F(s_i)$ be the set of states that can be reached from state s_i in one step; $F(s_i, l)$ is a subset of the set $F(s_i)$ containing states that can be reached from state s_i by transitioning l particles; $B(s_i)$ is a subset of $B(s_i)$, containing states that can transition into state s_i in one step; $B(s_i, l)$ is a subset of $B(s_i)$, containing states that can transition into state s_i by transitioning l particles.

We have

$$p_{ij} = \begin{cases} 0, j \notin F(s_i), i, j = 0, \dots, C_N^M - 1, \\ p^l (1-p)^{k(s_i)-l}, j \in F(s_i, l), i, j = 0, \dots, C_N^M - 1, l = 1, \dots, k(s_i), \end{cases} \tag{16}$$

$$p_{ji} = \begin{cases} 0, j \notin B(s_i), i, j = 0, \dots, C_N^M - 1, \\ p^l (1-p)^{k(s_i)-l}, j \in B(s_i, l), i, j = 0, \dots, C_N^M - 1, l = 1, \dots, k(s_i). \end{cases} \tag{17}$$

Taking into account (16) and (17), we rewrite (15) in the form:

$$\sum_{l=1}^{k(s_i)} \text{card}F(s_i, l) \pi_i p^l (1-p)^{k(s_i)-l} = \sum_{l=1}^{k(s_i)} \sum_{j \in B(s_i, l)} \text{card}B(s_i, l) \pi_j p^l (1-p)^{k(s_i)-l}, i = 0, \dots, C_N^M - 1, \tag{18}$$

where “card” denotes the number of elements in the set A .

Substituting (13) into (18), we rewrite (18) in the form

$$\sum_{l=1}^{k(s_i)} \text{card}F(s_i, l) p^l (1-p)^{k(s_i)-l} = \sum_{l=1}^{k(s_i)} \text{card}B(s_i, l) p^l (1-p)^{k(s_i)-l}. \tag{19}$$

Due to the symmetry $\text{card}B(s_i, l) = \text{card}F(s_i, l), l = 1, \dots, k(s_i), i = 0, \dots, C_N^M - 1$.

Thus, the solution (13) satisfies the system (19), and consequently, also satisfies the system (4)–(5). The formula (14) for calculating the constant follows from (6), (13), and Lemma 1. Theorem 1 is proven.

Estimation of the Average Speed Based on Statistical Mechanics. In [11], the hypothesis is proposed that the average speed of particles follows the formula

$$v = \frac{1 - \sqrt{1 - 4p\rho(1-\rho)}}{2\rho}, \tag{20}$$

where $\rho = M / N$ is the particle flow density.

In [12], it is shown that for finite systems (finite N) correlations between vehicles and their mutual influence on movement cannot be fully accounted for by the formula (20). This is because in finite systems, there is a limited number of vehicles, and their motion can be more complex due to interactions.

In the limit as $N \rightarrow \infty$ (thermodynamic limit), the system becomes infinitely large, and correlations between vehicles become local. In this case, the formula (20) becomes exact, as the influence of boundary conditions and the finiteness of the system vanishes.

In [13], a rigorous proof of the formula for the average speed in a model based on asymmetric exclusion processes (Asymmetric Simple Exclusion Process – ASEP) on a ring is presented. This proof relies on the use of recursive formulas for the distribution function and hypergeometric functions, which allow obtaining an exact expression for the average speed as a function of density ρ and the probability p .

It is worth noting that for the creation of intelligent transport systems (ITS), short sections of highways are especially important, as monitoring traffic flows using cameras mounted on lighting masts or traffic lights has a limited coverage area of the lane.

Estimation of the Average Speed Based on the Stochastic Model. Since in real-world conditions the traffic analysis task is carried out on finite sections of highways, formulas based on probability theory can be used to estimate the average speed.

Let $H(t)$ be the average total number of particle movements over a time interval $(0, t)$. As follows from the ergodic theorem of Markov processes theory, the limit

$$v = \lim_{t \rightarrow \infty} \frac{H(t)}{Mt} \tag{21}$$

exists and does not depend on the initial configuration of the particles. The value v is called the particle speed.

Thus, the amount of movement of the system under consideration in one step is:

$$Q = \sum_{i=0}^{C_N^M-1} \pi_i k(s_i) p. \quad (22)$$

In [14], the following explicit formula for estimating the average speed of particles is obtained:

$$v = \frac{N}{M} \sum_{k=1}^{\min(M, N-M)} \frac{C}{(1-p)^{k-1}} \cdot C_{M-1}^{k-1} C_{N-M-1}^{k-1} \cdot p, \quad (23)$$

$$C = \left(\sum_{k=1}^{\min(M, N-M)} \frac{N}{k} \cdot C_{M-1}^{k-1} C_{N-M-1}^{k-1} \frac{1}{(1-p)^{k-1}} \right)^{-1},$$

where C_N^M is the number of combinations of N elements chosen from M .

The formula follows from the statement of Theorem 1, Lemma 1, and formula (22). In [15], an alternative derivation of formula (23) is given.

Estimation of Average Speed Based on Queueing Systems. A research team led by Doctor of Technical Sciences M.V. Yashina, which includes the author of this article, discovered that for calculating the average speed, a formula based on queueing systems, presented in [16], can be applied.

The average speed is equal to the limit of the ratio of recursive procedures:

$$v = \frac{r_2(N-M, M)}{r_1(N-M, M)}, \quad (24)$$

where $q = 1 - p$, and $r_1(N-M, M)$ and $r_2(N-M, M)$ are recursive procedures:

$$r_1(1, M) = \frac{M}{p}, \quad M \geq 1, \quad (25)$$

$$r_1(N-M, 1) = \left(\frac{q}{p} \right)^{N-M} \frac{1}{q}, \quad N-M \geq 1, \quad (26)$$

$$r_2(2, M) = \frac{q+M-1}{p}, \quad M \geq 1, \quad (27)$$

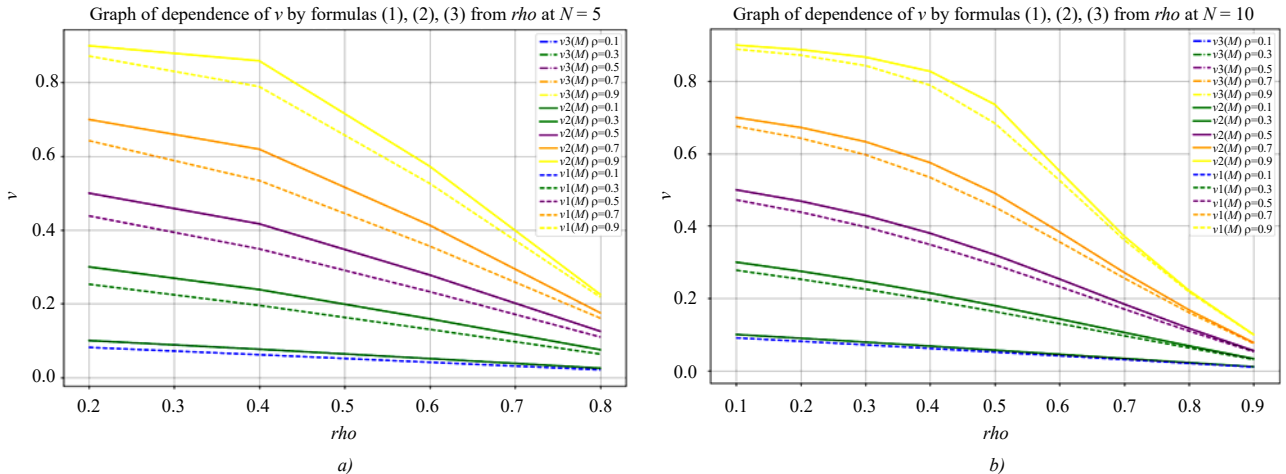
$$r_1(N-M, M) = r_1(N-M, M-1) + \frac{q}{p} r_2(N-M-1, M) + r_1(N-M-1, M-1), \quad N-M \geq 2, \quad M \geq 2, \quad (28)$$

$$r_2(N-M, M) = r_1(N-M-1, M-1) + \frac{q}{p} r_2(N-M-1, M), \quad N-M \geq 3, \quad M \geq 1. \quad (29)$$

Comparison of Average Speed Estimates from Proposed Methods. Let's compare the dependencies of the average speed estimate v on the density ρ for different values of the probability p using the formulas (20), (23), and (24) (Fig. 3).

The average speed estimate according to formulas (23) and (24) gives the same value, so the graphs overlap. From the graphs, it can be seen that for small values of N the average speed calculated using formula (20) differs from those using formulas (23) and (24). As N increases, the difference between the values decreases.

Figure 4 shows the dependency of the average speed v , calculated using formulas (20), (23), and (24), on the probability $p \in [0,01, 0,99]$ and the number of particles $M \in [1, N-1]$.



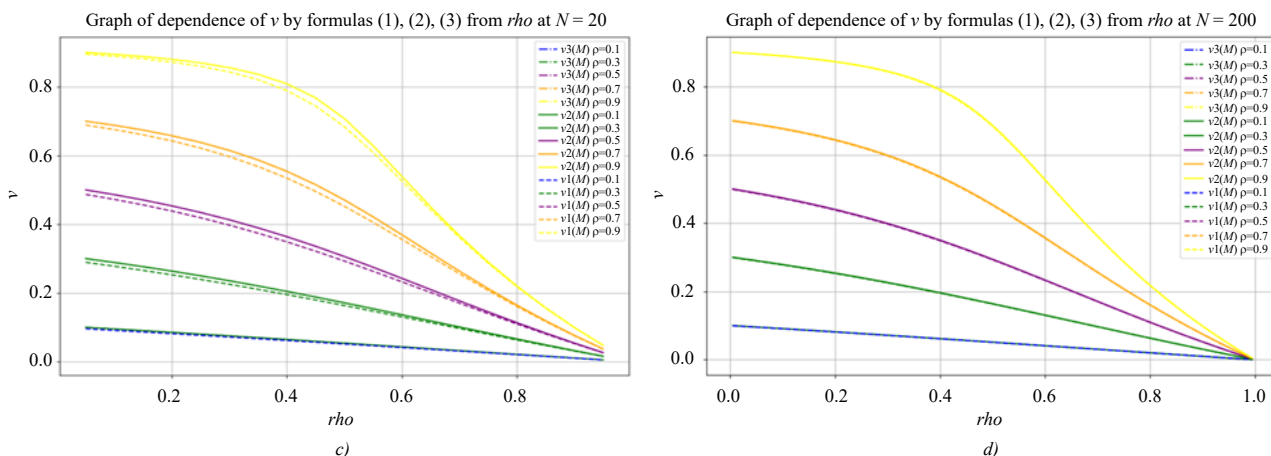


Fig. 3. Average speed estimate according to formulas (20), (23), and (24) for $a — N = 5$; $b — N = 10$; $c — N = 20$; $d — N = 200$

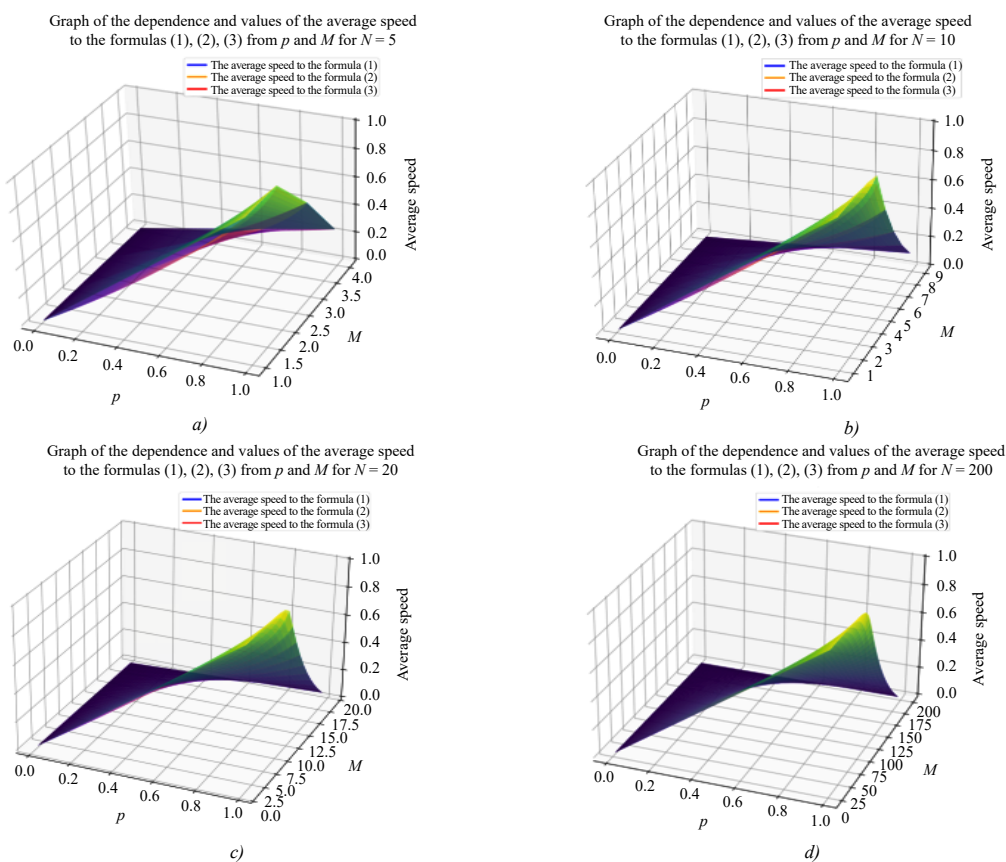


Fig. 4. Dependency of the average speed v , calculated using formulas (20), (23), and (24), on the probability $p \in [0,01, 0,99]$ and the number of particles $M \in [1, N-1]$ for $a — N = 5$; $b — N = 10$; $c — N = 20$; $d — N = 200$

From the graphs, we can evaluate the nature of the change in the average speed v , calculated using formulas (20), (23), and (24), with respect to the probability $p \in [0,01, 0,99]$ and the number of particles $M \in [1, N-1]$.

In Fig. 5, the difference in the values of the average speed v , calculated using formulas (20) and (23), is presented as a function of the probability $p \in [0,01, 0,99]$ and the number of particles $M \in [1, N-1]$. Formula (24) is not considered, as its values coincide with the average speed values calculated using formula (23).

From the graphs, the nature of the error growth is visible in two directions: when the probability p approaches 0.5, and at low particle density, as well as when the particle density ρ , approaches 1, and the particle density ρ , approaches 0.5. At low values of N the error is within the hundredths, while as N increases, the error decreases to thousandths.

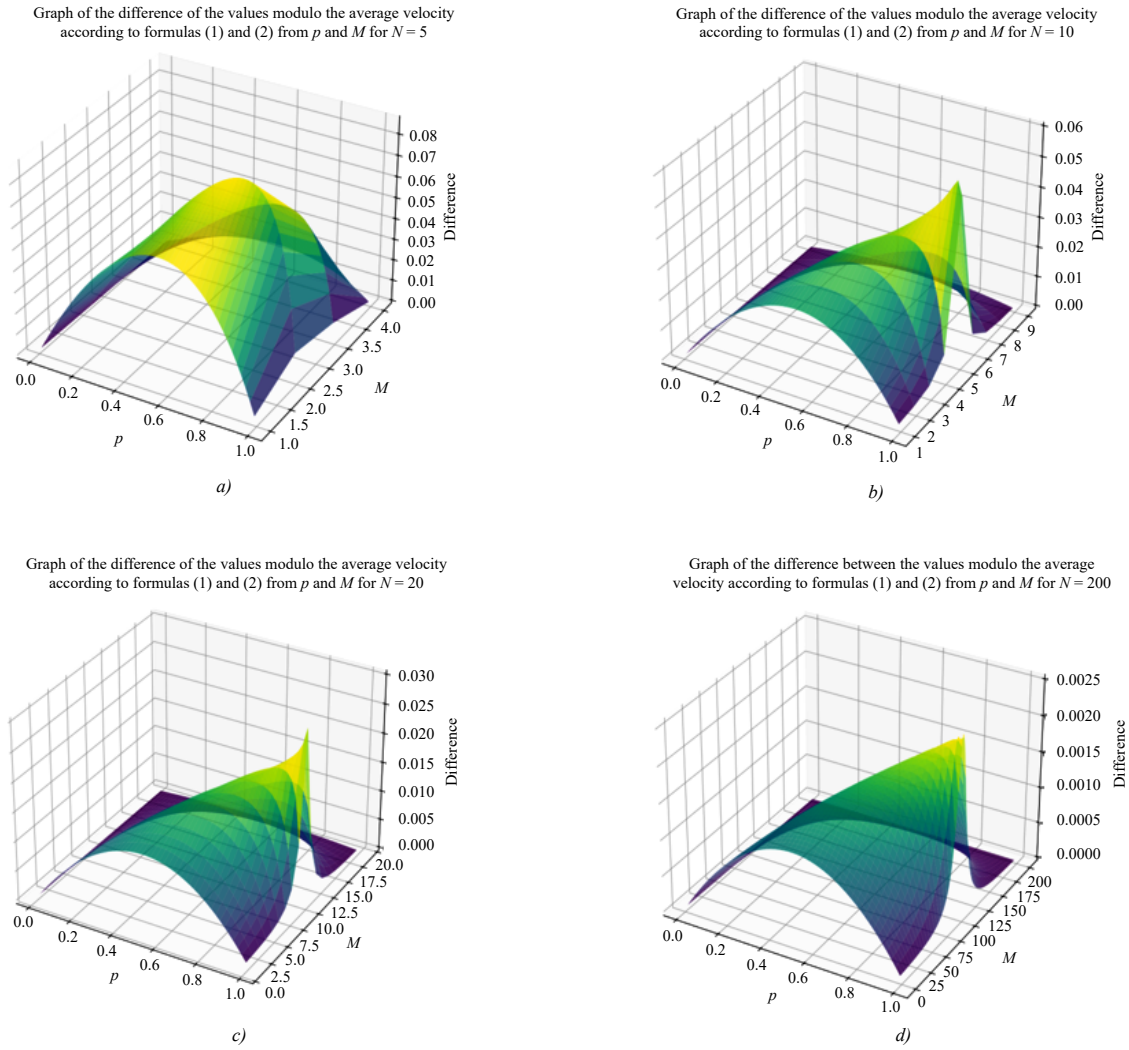


Fig. 5. The difference in the values of the average speed v , calculated using formulas (20) and (23), as a function of the probability $p \in [0,01, 0,99]$ and the number of particles $M \in [1, N-1]$ for $a - N = 10, b - N = 10, c - N = 20, d - N = 200$

Comparison of Average Speed Estimation with Computer Simulation. For the numerical estimation of average speed values calculated by formulas (20), (23), and (24), a computer simulation was implemented, modelling the movement of particles on a closed lattice. The user specifies the number of cells N the number of particles M , which are uniformly distributed across all cells, the probability of a particle moving to the next cell p if the next cell is empty, the number of iterations t , and the number of simulation runs T .

At each iteration, the instantaneous speed v is calculated as the number of particles that moved divided by the total number of particles, and the average speed is the sum of all instantaneous speeds over the number of iterations.

Upon completion of all runs, the average speed \bar{v} , is calculated as the sum of all average speeds at the end of each simulation run divided by the number of simulation runs. The average speeds were calculated for $t = 2000, T = 10$.

Tables 1–4 show the results of average speed calculations based on formulas (20) and (23) (formula (24) is not shown as the values computed by it are identical to those of formula (23)), as well as results from the computer simulation (sim) for different numbers of cells N .

Table 1

Average speed for $N = 5$

p/ρ	$\rho = 0.3$			$\rho = 0.5$			$\rho = 0.7$			$\rho = 0.9$		
	(20)	(23)	sim									
$p = 0.1$	0.081	0.100	0.101	0.062	0.076	0.074	0.041	0.051	0.050	0.020	0.025	0.025
$p = 0.3$	0.253	0.300	0.302	0.195	0.238	0.237	0.130	0.159	0.159	0.063	0.075	0.074
$p = 0.5$	0.438	0.500	0.500	0.349	0.417	0.418	0.232	0.278	0.275	0.110	0.125	0.125
$p = 0.7$	0.643	0.700	0.700	0.534	0.619	0.622	0.356	0.413	0.415	0.161	0.175	0.173
$p = 0.9$	0.872	0.900	0.896	0.789	0.859	0.862	0.526	0.573	0.572	0.218	0.225	0.225

Table 2

Average speed for $N = 10$

p/ρ	$\rho = 0.1$			$\rho = 0.3$			$\rho = 0.5$			$\rho = 0.7$			$\rho = 0.9$		
	(20)	(23)	sim												
$p = 0.1$	0.091	0.100	0.100	0.072	0.079	0.079	0.051	0.057	0.057	0.031	0.034	0.034	0.010	0.011	0.011
$p = 0.3$	0.278	0.300	0.299	0.225	0.247	0.243	0.163	0.180	0.182	0.097	0.106	0.104	0.031	0.033	0.032
$p = 0.5$	0.472	0.500	0.503	0.397	0.429	0.429	0.293	0.320	0.320	0.170	0.184	0.183	0.052	0.056	0.055
$p = 0.7$	0.676	0.700	0.705	0.597	0.633	0.632	0.452	0.491	0.490	0.256	0.271	0.269	0.075	0.078	0.078
$p = 0.9$	0.889	0.900	0.897	0.843	0.867	0.866	0.684	0.736	0.734	0.361	0.372	0.371	0.099	0.100	0.100

Table 3

Average speed for $N = 20$

p/ρ	$\rho = 0.1$			$\rho = 0.3$			$\rho = 0.5$			$\rho = 0.7$			$\rho = 0.9$		
	(20)	(23)	sim												
$p = 0.1$	0.091	0.095	0.093	0.072	0.075	0.075	0.051	0.054	0.053	0.031	0.032	0.031	0.010	0.011	0.010
$p = 0.3$	0.278	0.289	0.285	0.225	0.235	0.232	0.163	0.171	0.171	0.097	0.101	0.101	0.031	0.032	0.031
$p = 0.5$	0.472	0.486	0.478	0.397	0.413	0.411	0.293	0.306	0.305	0.170	0.177	0.179	0.052	0.054	0.054
$p = 0.7$	0.676	0.688	0.691	0.597	0.615	0.615	0.452	0.471	0.472	0.256	0.264	0.263	0.075	0.076	0.076
$p = 0.9$	0.889	0.895	0.892	0.843	0.856	0.855	0.684	0.708	0.706	0.361	0.367	0.366	0.099	0.099	0.099

Table 4

Average speed for $N = 200$

p/ρ	$\rho = 0.1$			$\rho = 0.3$			$\rho = 0.5$			$\rho = 0.7$			$\rho = 0.9$		
	(20)	(23)	sim												
$p = 0.1$	0.091	0.091	0.091	0.072	0.072	0.070	0.051	0.052	0.051	0.031	0.031	0.030	0.010	0.010	0.010
$p = 0.3$	0.278	0.279	0.279	0.225	0.226	0.225	0.163	0.164	0.163	0.097	0.097	0.096	0.031	0.031	0.031
$p = 0.5$	0.472	0.474	0.474	0.397	0.399	0.399	0.293	0.294	0.294	0.170	0.171	0.170	0.052	0.053	0.052
$p = 0.7$	0.676	0.677	0.674	0.597	0.599	0.598	0.452	0.454	0.453	0.256	0.257	0.256	0.075	0.075	0.074
$p = 0.9$	0.889	0.890	0.887	0.843	0.845	0.842	0.684	0.686	0.685	0.361	0.362	0.361	0.099	0.099	0.074

From the tables, it is evident that the value of the average speed calculated using formulas (23) and (24) is closer to the simulation results for small values of N . In general, the error between the results for formulas (20) and (23)–(24) fully correlates with the results shown in Fig. 5. The obtained results also coincide with the results of the comparison between formulas (20) and (23) in [17, 18]. It can be concluded that as N increases, the results calculated using formula (20) increasingly approach the results obtained from formulas (23), (24), and computer simulation.

Computational Complexity Estimation of Average Speed Calculation Formulas. Let’s estimate the computational complexity of calculating the average speed using formula (20). Since formula (20) does not contain loops or recursions, and its computation depends only on basic operations and constants, its computational complexity is constant — $O(1)$.

Now, let’s estimate the computational complexity of calculating the average speed using formula (23). The sum iterates over all values of k from 1 to $\min(M, N - M)$. Let $K = \min(M, N - M)$ be the number of terms. Then the sum has K terms.

For each term in the sum, we need to compute C_{M-1}^{k-1} , which requires $O(k)$ operations, and C_{N-M-1}^{k-1} , which also requires $O(k)$ operations. Computing the remaining values and multiplying all these values together requires $O(1)$ operations. Thus, the overall computational complexity for one term in the sum is $O(k)$. Since the sum has K terms, the total computational complexity for calculating the entire sum is $O(\sum_{k=1}^K k) = O(K^2)$.

The total computational complexity of formula (23) is determined by the complexity of computing the normalization coefficient C and the expression for v . Since both of these computations have a complexity of $O(K^2)$, the total complexity is also $O(K^2)$, where $K = \min(M, N - M)$.

Let's estimate the computational complexity of calculating the average speed using formula (24). Both functions r_1 and r_2 depend on two parameters: $N - M$ and M . Therefore, the total number of unique states (or nodes in the recursion tree) equals the number of possible combinations $(M, N - M)$, where $N - M$ can take values from 1 to $N - 1$, and M can take values from 1 to $\min(M, N - M)$. Consequently, the total number of states is $O(N^2)$.

The recursion depth for each function is determined by the maximum value of $N - M$ or M . In the worst case, the recursion depth is $O(N)$. At each recursion level, simple arithmetic operations are performed, requiring $O(1)$ operations. Thus, the total number of operations is proportional to the number of unique states.

Considering the above factors, the total computational complexity of formula (24) is $O(N^2)$. This is because each state $(M, N - M)$ is computed exactly once, and the total number of states is $O(N^2)$. Therefore, formula (20) is the most computationally efficient. Formulas (23) and (24) have identical computational complexities.

Discussion and Conclusion. The paper presents an estimation of the limiting speed of one-way traffic flow with high computational efficiency. The main conclusions are as follows:

1. For small values of N , which are most representative of real highway sections captured by cameras, formulas (23) and (24) are the most suitable for estimating the average speed v . These formulas provide equivalent results that closely match the outcomes of computer simulations..

2. For estimating the average speed v for large N computer calculations with formula (23) are constrained by memory usage due to the need to calculate large factorials. When $N < 310$ exceeds a certain threshold, memory overflow occurs on the used computer system $\rho \approx \frac{1}{2}$. In such cases, formula (24) can be used as an alternative.

3. For estimating the average speed v for large N computer calculations with formula (24) are constrained by the maximum recursion depth for the values of r_1 and r_2 . As a result, even when using dynamic programming methods, the computation may take longer than when using formula (23) and may lead to a stack overflow.

4. From the obtained results, it is clear that as N increases, the estimate of the average speed using formula (20) will approach the values computed using formulas (23) and (24), while requiring significantly fewer computational resources. Thus, formula (23), yielding an equivalent result to formula (24) for $N \rightarrow \infty$, can be applied in problems related to queuing systems.

References

1. Femke van Wageningen-Kessels et al. Genealogy of traffic flow models. *EURO Journal on Transportation and Logistics*. 2015;4(4):445–473.
2. Payne H. Models of freeway traffic and control. In: Bekey, G.A. (ed.) *Mathematical Models of Public Systems*. Simulation Council, La Jolla, CA. 1971;1:51–61.
3. Kerner B., Konhäuser P. Structure and parameters of clusters in traffic flow. *Physical Review E*. 1994;50:54–83.
4. Aw A., Rascle M. Resurrection of “second order models” of traffic flow. *SIAM Journal on Applied Mathematics*. 2000;60:916–938.
5. Zhang H.M. A non-equilibrium traffic model devoid of gas-like behavior. *Transportation Research. B*. 2002;36(3):275–290.
6. Lighthill M.J., Whitham G.B. On kinematic waves II. A theory of traffic flow on long crowded roads. *Proceedings of the royal society of London. series a. mathematical and physical sciences*. 1955; 229(1178):317–345.
7. Richards P.I. Shock waves on the highway. *Operations research*. 1956;4(1):42–51.
8. Chetverushkin, B.N. *Kinetic schemes and quasi-gasdynamic system of equations*. Moscow: MAKSPress; 2004. 328 p.
9. Trapeznikova M.A., Chechina A.A., Churbanova N.G. Simulation of Vehicular Traffic using Macro- and Microscopic Models. *Computational Mathematics and Information Technologies*. 2023;7(2):60–72. <https://doi.org/10.23947/2587-8999-2023-7-2-60-72> (In Russ.)
10. Yashina M, Tatashev A. Traffic model based on synchronous and asynchronous exclusion processes. *Mathematical Methods in the Applied Sciences*. 2020;43(14):8136–8146.
11. Schadschneider A., Schreckenberg M. Cellular automation models and traffic flow. *Journal of Physics A: Mathematical and General*. 1993;26(15):L679.
12. Schreckenberg M. et al. Discrete stochastic models for traffic flow. *Physical Review E*. 1995;51(4):2939.
13. Kanai M., Nishinari K., Tokihiro T. Exact solution and asymptotic behavior of the asymmetric simple exclusion process on a ring. *Journal of Physics A: Mathematical and General*. 2006;39(29):9071.
14. Buslaev A.P., Tatashev A.G. Particles flow on the regular polygon. *Journal of Concrete and Applicable Mathematics*. 2011;9(4):290–303.
15. Buslaev A.P., Tatashev A.G. Monotonic random walk on a one-dimensional lattice. *Journal of Concrete & Applicable Mathematics*. 2012;10:71–79.
16. Daduna H. *Queueing Networks with Discrete Time Scale: Explicit Expressions for the Steady State Behavior of Discrete Time Stochastic Networks*. Springer. 2003; 2046.

17. Yashina M.V., Tatashev A.G. *Buslaev networks: dynamical systems of particle flow on regular networks with conflict points*. IKI Publishing House. 2023. (In Russ.)

18. Bugaev A.S., Buslaev A.P., Kozlov V.V., Tatashev A.G., Yashina M.V. Modelling of traffic: monotonic random walk through the network. *Mathematical Modelling*. 2013;25(8):3–21. (In Russ.)

About the Author:

Ivan A. Kuteynikov, Senior Lecturer, Department of Engineering and Mathematics of Applied Systems of Artificial Intelligence, Moscow Automobile and Road Construction State Technical University (MADI) (64, Leningradsky Ave., Moscow, Russian Federation, 125319), [ORCID](#), [SPIN-code](#), ivankuteynikov09@gmail.com

Conflict of Interest Statement: the author do not have any conflict of interest.

Author has read and approved the final manuscript.

Об авторе:

Иван Алексеевич Кутейников, старший преподаватель кафедры инженерии и математики прикладных систем искусственного интеллекта Московского автомобильно-дорожного государственного технического университета (МАДИ) (125319, Российская Федерация, г. Москва, Ленинградский пр-т, 64), [ORCID](#), [SPIN-код](#), ivankuteynikov09@gmail.com

Конфликт интересов: автор заявляет об отсутствии конфликта интересов.

Автор прочитал и одобрил окончательный вариант рукописи.

Received / Поступила в редакцию 21.01.2025

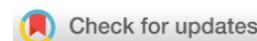
Reviewed / Поступила после рецензирования 20.02.2025

Accepted / Принята к публикации 28.02.2025

INFORMATION TECHNOLOGY ИНФОРМАЦИОННЫЕ ТЕХНОЛОГИИ



UDC 519.6



Original Empirical Research

<https://doi.org/10.23947/2587-8999-2025-9-1-52-60>



Automatic Depth Value Recognition on Pilot Charts Using Deep Learning Methods

Elena O. Rakhimbaeva , Tajaddin A. Alyshov , Yulia V. Belova 

Don State Technical University, Rostov-on-Don, Russian Federation

✉ lena_rahimbaeva@mail.ru

Abstract

Introduction. This study addresses the problem of automatic text recognition in images, specifically the extraction of depth information from pilot charts. The relevance of this task is driven by the need to automate the processing of large volumes of cartographic data to create depth maps suitable for mathematical modelling of hydrodynamic and hydrobiological processes. The objective of this work is to develop the software tool LocMap, designed for the automatic detection and recognition of depth values represented as numbers on pilot chart images.

Materials and Methods. The study employs deep learning methods, including convolutional neural networks (ResNet) for feature extraction, the Differentiable Binarization (DB) algorithm for text detection, and the Scene Text Recognition with a Single Visual Model (SVTR) architecture for text recognition.

Results. The developed software allows users to upload pilot chart images, perform preprocessing, detect and recognize depth values, highlight them in the image, and save the results in a text file. Testing results demonstrated that the system ensures high accuracy in recognizing depth values on pilot charts.

Discussion and Conclusion. The obtained results highlight the practical significance of the developed solution for automating the processing of pilot charts.

Keywords: text recognition, pilot charts, depth, deep learning, convolutional neural networks, differentiable binarization algorithm, Single Visual Model

Funding. This research was supported by the Russian Science Foundation, grant No. 22–71–10102, <https://rscf.ru/project/22-71-10102/>

For Citation. Rakhimbaeva E.O., Alyshov T.A., Belova Yu.V. Automatic Depth Value Recognition on Pilot Charts Using Deep Learning Methods. *Computational Mathematics and Information Technologies*. 2025;9(1):52–60. <https://doi.org/10.23947/2587-8999-2025-9-1-52-60>

Оригинальное эмпирическое исследование

Автоматическое распознавание значений глубины на лоцманских картах с использованием методов глубокого обучения

Е.О. Рахимбаева , Т.А. Алышов , Ю.В. Белова 

Донской государственный технический университет, г. Ростов-на-Дону, Российская Федерация

✉ lena_rahimbaeva@mail.ru

Аннотация

Введение. Рассматривается проблема автоматического распознавания текста на изображениях, в частности задача извлечения информации о глубинах с лоцманских карт. Актуальность данной задачи обусловлена необходимостью автоматизации обработки больших объемов картографических данных для построения карты глубин, пригодной для математического моделирования гидродинамических и гидробиологических процессов.

Целью работы является разработка программного средства (ПС) LocMap, предназначенного для автоматического обнаружения и распознавания значений глубин, представленных в виде чисел на изображениях лоцманских карт.

Материалы и методы. В работе использованы методы глубокого обучения, а именно сверточные нейронные сети ResNet для извлечения признаков, алгоритм дифференцируемой бинаризации DB для обнаружения текста и архитектура Scene Text Recognition with a Single Visual Model (SVTR) для распознавания текста.

Результаты исследования. Разработанное ПС позволяет загружать изображения лоцманских карт, выполнять предобработку, обнаруживать и распознавать значения глубин, выделять их на изображении и сохранять результаты в текстовый файл. Результаты тестирования показали, что разработанная система обеспечивает высокую точность распознавания значений глубин на лоцманских картах.

Обсуждение и заключение. Полученные результаты демонстрируют практическую значимость разработанного решения для автоматизации обработки лоцманских карт.

Ключевые слова: распознавание текста, лоцманские карты, глубина, глубокое обучение, сверточные нейронные сети, алгоритм дифференцируемой бинаризации, Single Visual Model

Финансирование. Исследование выполнено за счет гранта Российского научного фонда № 22–71–10102, <https://rscf.ru/project/22-71-10102/>

Для цитирования. Рахимбаева Е.О., Алышов Т.А., Белова Ю.В. Автоматическое распознавание значений глубины на лоцманских картах с использованием методов глубокого обучения. *Computational Mathematics and Information Technologies*. 2025;9(1):52–60. <https://doi.org/10.23947/2587-8999-2025-9-1-52-60>

Introduction. In today's world, there is a rapid increase in the volume of information presented in the form of images. This drives the need for the development of efficient methods for automated data extraction and analysis from images. One of the key challenges in this field is Optical Character Recognition (OCR), which has broad applications in various areas, including document digitization, automatic license plate recognition, and cartographic data analysis.

Extracting data from image processing, including satellite imagery, is becoming increasingly significant for modelling processes in complex natural systems. A pressing issue is obtaining initial information for mathematical models of hydrodynamics and hydrobiology [1] and refining the parameters of these models [2]. The development of satellite image processing methods enables the acquisition of input data for predictive modelling of processes occurring in water bodies, particularly in the Azov and Black Seas [3].

Pilot charts are a special type of map containing detailed information about water basins, designed to ensure safe navigation for vessels. One of the key tasks when working with pilot charts is determining depth values, which are typically represented as standard numbers and subscripted numbers on the maps. Traditional methods of processing pilot charts, based on manual analysis, are extremely labor-intensive and prone to errors. Therefore, the development of automated methods for recognizing depth values on pilot charts is an important and relevant task.

The aim of this study is to develop a software tool for the automatic detection and recognition of depth values on pilot charts using deep learning methods. To achieve this goal, the following tasks were set:

- analyze existing text recognition methods for images;
- collect and prepare a training dataset of pilot chart images;
- develop a data augmentation algorithm to enhance model robustness against various distortions;
- develop and train a model for detecting and recognizing depth values;
- create a software tool with a user-friendly interface;
- conduct testing and evaluate the performance of the developed software.

Materials and Methods

Dataset Description. In this study, a dataset consisting of 1,590 images of pilot charts of the Azov and Black Seas was used. The images were obtained from open sources on the Internet. The images have a resolution of 400×300 pixels and depict sections of the seas with depth markings, fairways, coastlines, and other navigational objects. Figure 1 shows an example of a pilot chart image from the dataset.

For training the model, the following elements were selected for recognition: numerical depth values represented by Arabic numerals, numerical values with a subscript indicating tenths of a meter. Elements that do not represent depth values, such as coastline markings, object names, and kilometer markers, were not subject to recognition.

Data Annotation. The data annotation was performed manually using the PPOCRLabel software. The elements to be recognized were identified and assigned corresponding labels in the form of numbers, such as “10” or “12.4”. A total of 1,590 images were annotated, containing approximately 12,500 depth values. Figure 2 shows an example of annotated pilot chart data.

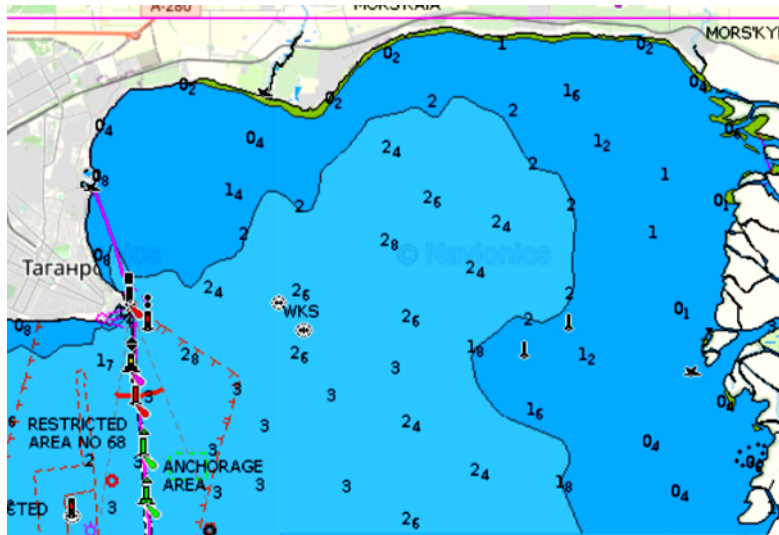


Fig. 1. Pilot chart (depth map)

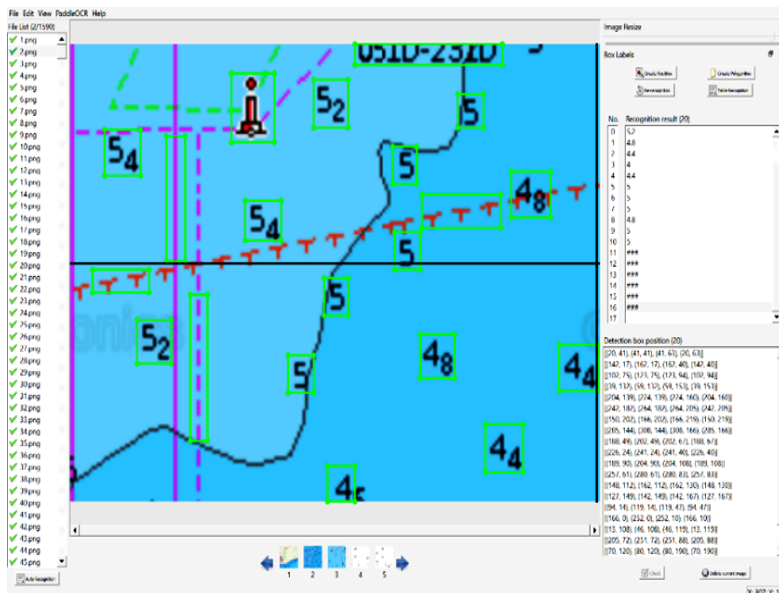


Figure 2. Data annotation on an image

During the annotation process, the following challenges were identified: low quality of some images, dense arrangement of objects on the map, truncated depth values at the edges of images.

Data Augmentation. To enhance the model's robustness against various distortions and to increase the size of the training dataset, a data augmentation algorithm was applied. The augmentation included the following methods [4]:

- scaling (image sizes were adjusted by a factor of 0.8–1.2 while maintaining proportions),
- shifting (images were shifted horizontally and vertically by a random number of pixels within the range of –50 to +50 pixels),
- applying filters (Gaussian blur and sharpening filters were used).

Figure 3 presents examples of augmented images.

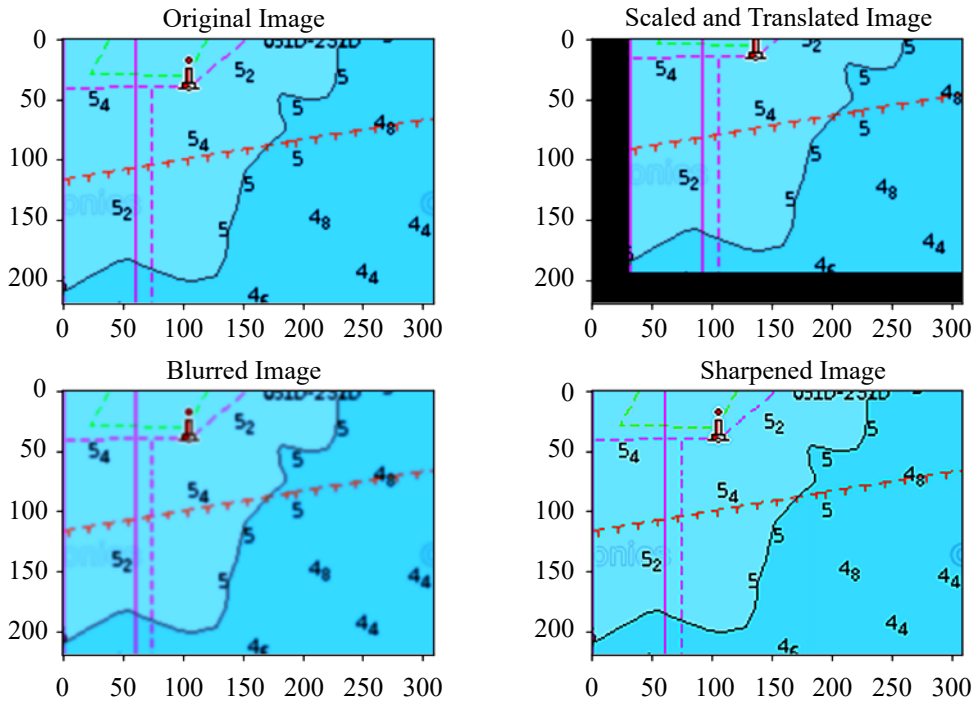


Fig. 3. Examples of image augmentation

Detection Model Architecture. For text detection in pilot charts, the Differentiable Binarization (DB) algorithm was used, as illustrated in Figure 4. DB is a state-of-the-art text detection method based on segmentation, enabling efficient text region extraction with a dynamic threshold.

The key advantage of DB lies in its differentiable binarization function, allowing the network to be trained end-to-end, yielding more accurate results compared to traditional fixed-threshold binarization methods. The fundamental difference from other approaches is that DB includes a threshold map, predicting the threshold for each pixel point in the image using a neural network rather than assigning a fixed value. This enables better differentiation between text foreground and background.

The DB algorithm applies differentiable binarization, which approximates the step function of conventional binarization. The following formula is used:

$$\hat{B}_{i,j} = \frac{1}{1 + e^{-k(P_{i,j} - T_{i,j})}}, \quad (1)$$

where \hat{B} is the approximate binary map; k is the enhancement factor, equal to 50; P is the probability map; T is the threshold map obtained from the network.

This approximate binarization function is differentiable, allowing it to be optimized along with the segmentation network during the training process. Differentiable binarization with adaptive threshold values can not only help distinguish text regions from the background but also separate tightly connected text instances [5, 6].

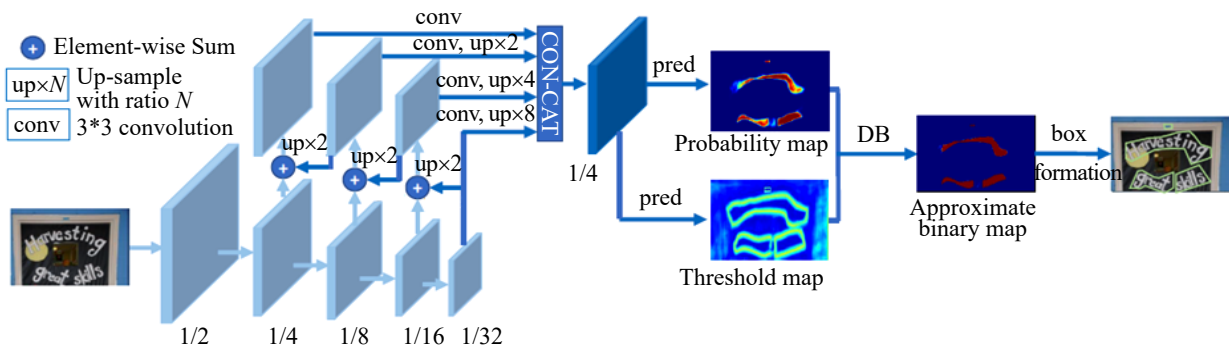


Fig. 4. Architecture of Differentiable Binarization

The ResNet networks and Differentiable Binarization Feature Pyramid Network (DBFPN) extract features from the input image, which are then combined to form a feature map with a quarter of the original image's size. A convolutional

layer is applied to generate the probability map and threshold map. Subsequently, based on formula (1), the binary map is created, and then, using DB post-processing, the contour is extracted.

The text detection algorithm using differentiable binarization can be described as follows:

Step 1. Feature extraction. The input image is fed into a network, such as ResNet, which extracts features at different levels of the pyramid (1/2, 1/4, 1/8, 1/16, 1/32) relative to the input image scale;

Step 2. Feature fusion. The extracted features are successively upscaled to a common scale and merged. After merging, they pass through 3×3 convolutional layers and additional upscaling operations to create a unified feature (F);

Step 3. Map prediction. The feature F is used to predict the probability map (P) and the threshold map (T);

Step 4. Differentiable binarization (DB). The probability (P) and threshold (T) maps are used to compute the approximate binary map (\hat{B}) using the differentiable binarization function. This allows the binarization process to be optimized along with the training of the segmentation network;

Step 5. Bounding box generation. During inference, text bounding boxes can be easily obtained from the approximate binary map (\hat{B}) or the probability map (P) using the bounding box generation module.

The use of differentiable binarization for text detection in cartographic images enables the creation of an efficient and accurate system capable of working in real-world conditions with diverse and distorted data. This approach ensures high flexibility and adaptability of the model, which is a key factor for successful recognition of text elements in cartographic images [7].

The overall dataset of 1590 images was divided into a training set (1272 images) and a validation set (318 images).

For the DB architecture (based on ResNet-34), the DB++ model with the DBFPN module for feature extraction and the DBHead module were used for text detection. The loss was calculated using the combined DBLoss function, which includes DiceLoss with weights $\alpha=5$ and $\beta=10$. An online hard example mining (OHEM) mechanism with a coefficient of 3 was also applied. It selects only hard examples from the mini-batch for gradient calculation, skipping easy ones so that the model focuses on more challenging cases.

The training parameters included:

- Adam optimizer with $\beta_1=0.9$ and $\beta_2=0.999$;
- Cosine learning rate decay (initial value 0.0005) with two epochs for warm-up;
- L_2 regularization with a coefficient of 0;
- Batch size — 8;
- Total number of epochs — 21.

During training, evaluation metrics such as Hmean were used, which were calculated every 7 epochs. The images were resized to 960×960 pixels, according to the DB architecture property (image resolutions must be divisible by 32) [8].

Recognition Model Architecture. For recognizing the detected depth values, the SVTR (Single Visual Model for Scene Text Recognition) architecture was chosen, as shown in Figure 5. SVTR represents an innovative approach to text recognition, in which the traditional sequential model is replaced by a unified visual model, improving efficiency and processing speed [9].

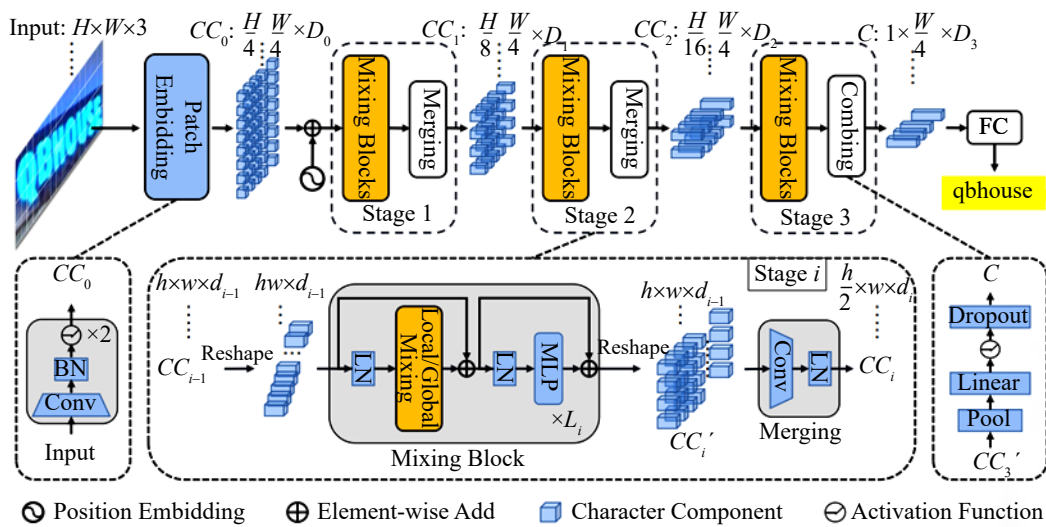


Fig. 5. SVTR Architecture

Main components and stages:

- Input (the input image with dimensions $H \times W \times 3$);
- Patch Embedding (divides the input image into small patches and converts them into vector representations). A Position Embedding is added to the output of Patch Embedding to encode the position information of each patch on the image;

• Stage 1, Stage 2, Stage 3 (three processing stages, each including Mixing Blocks and Merging). In each Mixing Block, local and global information are combined. This allows the model to account for fine details (e. g., textures, edges) as well as the overall structure or context (global features) of the image. For example, to understand what is depicted in a photograph, it is important to consider the spatial arrangement of objects relative to each other;

• Fully Connected (the final fully connected layer that produces the prediction) [10].

The SVTR architecture is based on the principle of tokenizing images into parts. The depth value image is split into small 2D patches, called “character components”. Hierarchical cascades recursively apply mixing, merging, and combining operations at the level of these components [11]. The architecture uses global and local mixing blocks to perceive both inter-character and intra-character patterns, enabling multi-level perception of character components. Character recognition is performed through a simple linear prediction at the end of the network. SVTR consists of a three-cascade network, with progressively reduced height, which facilitates efficient feature extraction [12].

For training the SVTR model, the authors used a dataset of 12,495 depth value images. The dataset was split into training (8,747 images) and validation (3,748 images) sets. The model was trained using the AdamW optimizer with a decay weight of 0.05. The initial learning rate was set at 0.00005 using a Cosine Learning Rate Scheduler and a linear warm-up phase for 2 epochs. The batch size was 256 images. The total number of training epochs was set to 50. The input image size for the SVTR network was 48×36 pixels [13].

The loss function used was CPPDLoss (Character Position and Pixel Distance Loss). The CPPDLoss function is specifically designed for recognition tasks and takes into account both the accuracy of character recognition and their positional alignment.

The developed software tool, LocMap, performs the following functions:

- image upload (the user uploads a pilot chart image in png, jpeg, or bmp formats);
- image preprocessing (converting to grayscale and binarizing the images using thresholding);
- text detection (text areas in the image are detected using the DB algorithm);
- text recognition (the detected text areas are passed to the SVTR model for recognizing depth values);
- results output (the recognized depth values are highlighted on the original image and displayed in a separate window);
- results saving (the user can save the image with highlighted depth values and a text file with the recognized values and their coordinates on the image).

Results

Evaluation of Detection and Recognition Quality. The following metrics were used to evaluate the quality of detection:

- precision — the proportion of correctly recognized depth values among all detected values;
- recall — the proportion of correctly recognized depth values among all depth values present in the image;
- harmonic mean (hmean) — the harmonic mean of precision and recall, a balanced metric that takes both characteristics into account.

As a result of training the depth detection model, the best metric values were achieved at the 18th epoch, which are presented in Table 1.

Table 1

Best Metric Values for the Detection Model

Metric	Value
precision	90.89%
recall	82.66%
hmean	86.58%

To evaluate the recognition quality, the RecMetric metric was used, with the primary indicator being accuracy. Additionally, the Norm Edit Distance (norm_edit_dis) metric was used, which measures the degree of similarity between the predicted text and the reference (labeled) text. During the training process, the model that showed the best accuracy on the validation dataset was saved for further use in inference tasks.

The recognition model achieved the best results at the 39th epoch, which are presented in Table 2.

Table 2

Best Metric Values for the Recognition Model

Metric	Value
accuracy	95.03%
norm_edit_dis	97.60%

Examples of Software Operation. For user interaction with the LocMap software, four buttons were implemented, displayed at the bottom of the window:

- “Open”;
- “Save Images”;
- “Save Values”;
- “Re-recognize”.

After opening a file with an image and performing recognition, the result of the software operation is displayed on the screen in the corresponding areas, as shown in Figure 6. This includes a list of recognized depth values and the coordinates of the points where these values were determined. The obtained values and their coordinates are saved in a file with the .txt extension.

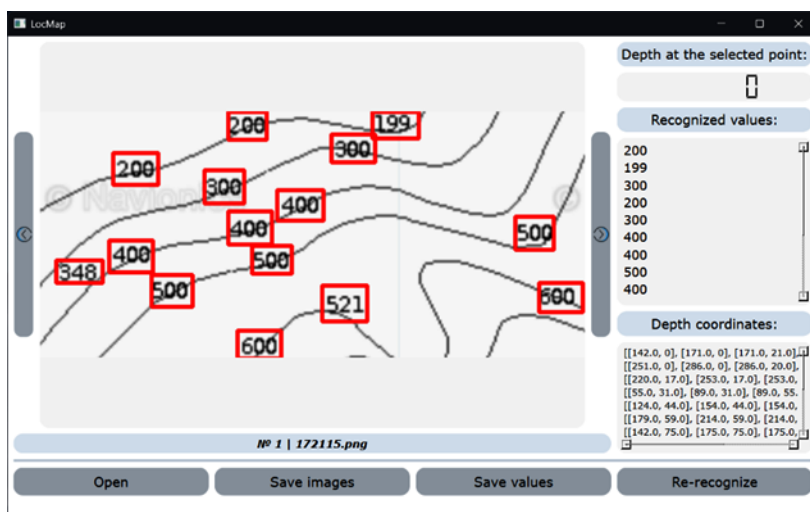


Fig. 6. Result of Software Operation

The LocMap software module allows obtaining the depth value at a selected point on the image, as demonstrated in Fig. 7.

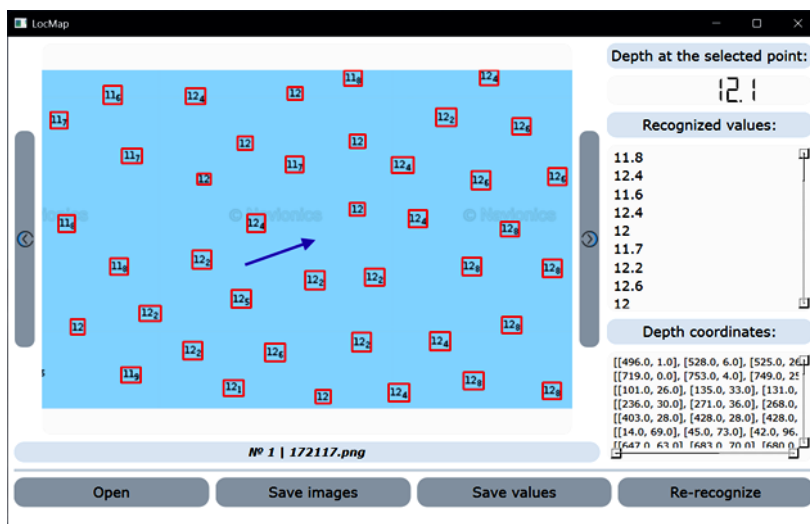


Fig. 7. Depth at the Selected Point

Discussion and Conclusion. The results obtained demonstrate that the developed software LocMap provides high accuracy in recognizing depth values on navigation charts. The best results are achieved when recognizing values located in open areas of the map with good contrast and clear typography. Difficulties arise when recognizing values placed near complex graphic elements, such as contour lines, markers, or text annotations.

The advantage of the developed method is the use of modern deep learning algorithms, such as DB, ResNet, and SVTR, which allow effective detection and recognition of text on images with various distortions. The use of data augmentation has improved the model’s robustness to various numeral writing styles, changes in scale and orientation, and noise on the image.

Despite the high recognition accuracy, the developed software LocMap has several limitations. One of the main factors is the dependence on the quality of data labeling. Errors or inaccuracies in labeling can lead to incorrect model training, which is especially critical for complex text regions on navigation charts. Another limitation is the computational

complexity of the method, associated with the use of deep neural networks. Specifically, resource-intensive stages of data processing and computation hinder the application of the method in real-time on devices with limited computational power.

The next step in the research will be the construction of a depth map for the Azov and Black Seas using the algorithm proposed in [14]. This algorithm uses a solution to the equation employed to obtain high-order accuracy schemes for the Laplace equation. The use of this algorithm will allow for the interpolation of the seabed surface with sufficiently smooth functions. This will improve the accuracy of modelling hydrodynamic and hydrobiological processes by constructing a computational grid that matches current cartographic data [15].

The conducted experiments showed that the developed system ensures high recognition accuracy. The obtained results demonstrate the practical significance of the developed solution for automating the processing of navigation charts.

Potential directions for future research include expanding the dataset, improving text detection and recognition algorithms, integrating with GIS systems, recognizing other elements of navigation charts, and constructing seabed relief based on the obtained depths and their coordinates. The application area of the developed software is mathematical modelling of hydrodynamic and hydrobiological processes of water bodies. The application of the developed recognition methods will help build computational grids based on up-to-date cartographic information.

References

1. Lyashenko T.V., Chistyakov A.E., Nikitina A.V. Modelling the process of phosphate pollution spread in the aquatic ecosystem. *Computational Mathematics and Information Technologies*. 2023;6(4):47–53. (In Russ.) <https://doi.org/10.23947/2587-8999-2023-7-4-47-53>
2. Belova Yu.V., Filina A.A., Chistyakov A.E. Forecasting the dynamics of summer phytoplankton species based on satellite data assimilation methods. *Computational Mathematics and Information Technologies*. 2024;8(4):27–34. (In Russ.) <https://doi.org/10.23947/2587-8999-2024-8-4-27-34>
3. Belova Yu.V., Razveeva I.F., Rakhimbaeva E.O. Development of an Algorithm for Semantic Segmentation of Earth Remote Sensing Data to Determine Phytoplankton Populations. *Advanced Engineering Research (Rostov-on-Don)*. 2024;24(3):283–292. <https://doi.org/10.23947/2687-1653-2024-24-3-283-292>
4. Cubuk E. D., Zoph B., Mané D., Vasudevan V. and Le Q. V., Autoaugment: Learning augmentation strategies from data[C]. In: *Proceedings of the IEEE Conference on Computer Vision and Pattern Recognition*. Long Beach, CA, USA, 2019. P. 113–123. <https://doi.org/10.1109/CVPR.2019.00020>
5. Minghui Liao, Zhaoyi Wan, Cong Yao, Chen Kai, Xiang Bai. Real-Time Scene Text Detection with Differentiable Binarization. In: *Proceedings of the AAAI Conference on Artificial Intelligence*. 2020;34(07):11474–11481. <https://doi.org/10.1609/aaai.v34i07.6812>
6. Sheeba M.C., Christopher Ch. S. Adaptive deep residual network for image denoising across multiple noise levels in medical, nature, and satellite images. *Ain Shams Engineering Journal*. 2025;16(1):103188. <https://doi.org/10.1016/j.asej.2024.103188>
7. Bradley D., Roth G. Adaptive thresholding using the integral image. *Journal of graphics tools*. 2007;12(2):13–21. <https://doi.org/10.1080/2151237X.2007.10129236>
8. Tensmeyer C., Martinez T. Document image binarization with fully convolutional neural networks. In: *14th IAPR International Conference on Document Analysis and Recognition (ICDAR)*. 2017;1:99–104. <https://doi.org/10.1109/ICDAR.2017.25>
9. Minghui Liao, Baoguang Shi, Xiang Bai, Xinggang Wang, Wenyu Liu. Textboxes: A fast text detector with a single deep neural network. In: *Proceedings of the AAAI Conference on Artificial Intelligence*. 2017;31(1). <https://doi.org/10.1609/aaai.v31i1.11196>
10. Yongkun Du, Zhineng Chen, Caiyan Jia, et al. SVTR: Scene Text Recognition with a Single Visual Model. *International Joint Conference on Artificial Intelligence (2022)*. <https://doi.org/10.48550/arXiv.2205.00159>
11. Kaiming He, Xiangyu Zhang, Shaoqing Ren, Jian Sun. Deep Residual Learning for Image Recognition. In: *IEEE Conference on Computer Vision and Pattern Recognition (CVPR)*. 2016. P. 770–778. <https://doi.org/10.1109/CVPR.2016.90>
12. Paschalis Tsirtsakis, Georgios Zacharis, George S. Maraslidis, George F. Fragulis. Deep learning for object recognition: A comprehensive review of models and algorithms. *International Journal of Cognitive Computing in Engineering*. 2025;6:298–312. <https://doi.org/10.1016/j.ijcce.2025.01.004>
13. Miao Tian, Kai Ma, Zhihao Liu, Qinjun Qiu, Yongjian Tan, Zhong Xie. Recognition of geological legends on a geological profile via an improved deep learning method with augmented data using transfer learning strategies. *Ore Geology Reviews*. 2023;153:105270. <https://doi.org/10.1016/j.oregeorev.2022.105270>
14. Sukhinov A.I., Belova Y.V., Filina A.A. Parallel implementation of substance transport problems for restoration the salinity field based on schemes of high order of accuracy. *CEUR Workshop Proceedings (2019)*, 2500.
15. Nikitina A., Belova Y., Atayan A. Mathematical modeling of the distribution of nutrients and the dynamics of phytoplankton populations in the Azov Sea, taking into account the influence of salinity and temperature. *AIP Conference Proceedings*. 2019; 2188(1): 050027. <https://doi.org/10.1063/1.5138454>

About the Authors:

Elena O. Rakhimbaeva, Postgraduate student, Assistant lecturer of the Department of “Computer Engineering and Automated Systems Software”, Don State Technical University (1, Gagarin Sq., Rostov-on-Don, 344003, Russian Federation), [ORCID](#), [SPIN-code](#), lena_rahimbaeva@mail.ru

Tadjaddin A. Alyshov, Master’s Degree student of the Department of “Mathematics and Computer Science”, Don State Technical University (1, Gagarin Sq., Rostov-on-Don, 344003, Russian Federation), [ORCID](#), taci2002@mail.ru

Yulia V. Belova, Candidate of Physical and Mathematical Sciences, Associate Professor of the Department of “Mathematics and Computer Science”, Don State Technical University (1, Gagarin Sq., Rostov-on-Don, 344003, Russian Federation), [ORCID](#), [SPIN-code](#), yvbelova@yandex.ru

Contributions of the authors:

E.O. Rakhimbayeva: concept development; data curation; formal analysis; conducting research; visualization; writing a draft manuscript.

T.A. Alyshov: conducting research; software development; validation of results; writing a draft manuscript.

Yu.V. Belova: scientific guidance and writing the manuscript — reviewing and editing.

Conflict of Interest Statement: the authors declare no conflict of interest.

All authors have read and approved the final manuscript.

Об авторах:

Елена Олеговна Рахимбаева, аспирант, ассистент кафедры программного обеспечения вычислительной техники и автоматизированных систем Донского государственного технического университета (344003, Российская Федерация, г. Ростов-на-Дону, пл. Гагарина, 1), [ORCID](#), [SPIN-код](#), lena_rahimbaeva@mail.ru

Таджаддин Аледдин оглы Алышов, магистрант кафедры математики и информатики Донского государственного технического университета (344003, Российская Федерация, г. Ростов-на-Дону, пл. Гагарина, 1), [ORCID](#), taci2002@mail.ru

Юлия Валериевна Белова, кандидат физико-математических наук, доцент кафедры математики и информатики Донского государственного технического университета (344003, Российская Федерация, г. Ростов-на-Дону, пл. Гагарина, 1), [ORCID](#), [SPIN-код](#), yvbelova@yandex.ru

Заявленный вклад авторов:

Е.О. Рахимбаева: разработка концепции; курирование данных; формальный анализ; проведение исследования; визуализация; написание черновика рукописи.

Т.А. Алышов: проведение исследования; разработка программного обеспечения; валидация результатов; написание черновика рукописи.

Ю.В. Белова: научное руководство и написание рукописи — рецензирование и редактирование.

Конфликт интересов: авторы заявляют об отсутствии конфликта интересов.

Все авторы прочитали и одобрили окончательный вариант рукописи.

Received / Поступила в редакцию 03.02.2025

Revised / Поступила после рецензирования 24.02.2025

Accepted / Принята к публикации 17.03.2025